Adsorption of group-V elements on III–V(1 1 0) surfaces

W. Gero Schmidt and Friedhelm Bechstedt

Institut für Festkörpertheorie und Theoretische Optik, Friedrich-Schiller Universität Jena, Max-Wien-Platz 1, 07743 Jena, Germany

and

Gyaneshwar P. Srivastava

Semiconductor Physics Group, Physics Department, University of Exeter, Exeter EX4 4QL, UK

ELSEVIER

Amsterdam–Lausanne–New York–Oxford–Shannon–Tokyo

Contents

ELSEVIER

Surface Science Reports 25 (1996) 141–223

surface science reports

Adsorption of group-V elements on III–V (1 1 0) surfaces

W. Gero Schmidt [a,*], Friedhelm Bechstedt [a], Gyaneshwar P. Srivastava [b]

[a] *Institut für Festkörpertheorie und Theoretische Optik, Friedrich-Schiller Universität Jena, Max-Wien-Platz 1, 07743 Jena, Germany*

[b] *Semiconductor Physics Group, Physics Department, University of Exeter, Exeter EX4 4QL, UK*

Manuscript received in final form 6 May 1996

Abstract

Adsorption of group-V elements on III–V (1 1 0) surfaces has led to one of the most extensively investigated overlayer systems. Sb and Bi grow epitaxially on the (1 1 0) surfaces of several III–V semiconductors and show in general a (1 × 1) symmetry for one adsorbed monolayer. The resulting interfaces are atomically sharp and therefore suitable model systems for experimental and theoretical studies of the Schottky barrier formation.

In this paper we discuss the present stage of understanding of group-V covered III–V (1 1 0) surfaces. We provide a review of experimental techniques and results, and theoretical approaches applied to these systems. In particular state-of-the-art calculations based on density-functional theory are used to develop a comprehensive picture of the atomic structure, electronic states, vibrational properties, and their accompanying chemical trends. Different stages of the interface formation, from submonolayer coverages to thick overlayers, are considered.

Keywords: Chemisorption; Gallium phosphide; Gallium arsenide; Indium phosphide; Indium arsenide; Adatoms; Arsenic; Antimony; Bismuth; Density functional calculations; Surface electronic phenomena; Phonons; Low index single crystal surfaces

1. Introduction

1.1. Motivation

Surface and interface characteristics of semiconductors play a decisive role in many device technologies. Modifications of surfaces and interfaces have attracted much interest as technological steps themselves. Remarkable examples in this direction are the surface passivation and metallization. Among all semiconductors, these surface adsorbate processes are most interesting for III–V compounds crystallizing in zinc-blende structure, e.g., for GaP, GaAs, GaSb, InP, InAs, and InSb.

* Corresponding author. Fax: +49 3641 635182; e-mail: w.g.schmidt@ifto.physik.uni-jena.de.

PII: S0167-5729 (96)00006-4

In silicon device technology, the formation of insulating native-oxide layers on a silicon substrate is essential for metal–insulator–semiconductor devices having low densities of interface states. On the contrary, native oxides of III–V compounds, in particular of GaAs, do not exhibit passivating properties similar to those of silicon oxide, and thus obstruct the performance and reliability of III–V-compound-based devices. While GaAs appears to be an excellent candidate for a variety of electronic devices, commercial development of the GaAs technology has been hampered by the existence of a high number of surface and interfacial states that pin the Fermi level near midgap. The passivation of the surfaces of GaAs and other III–V compounds is therefore a crucial problem in the development of the technology.

The understanding and control of electrical barriers at metal–semiconductor interfaces is important for their application in Schottky diodes and, hence, has been a major challenge in surface physics for several decades. The issue of the Schottky barrier formation at surfaces of III–V-compound semiconductors, especially of GaAs, has been the subject of a significant amount of research and controversy over practically five decades. A variety of experimental and theoretical studies have been carried out to understand in particular the Fermi level pinning. All techniques of surface science have been attempted to correlate barrier height with properties (e.g., orientation, stoichiometry, and geometry) of the semiconductor surface, properties of the deposited metal, and heats of formation of compounds resulting from intermixing of the metal and substrate.

In the case of III–V-compound semiconductors crystallizing in the zinc-blende structure the polar (1 0 0) surfaces are the technologically relevant faces for the development of sophisticated devices. Nevertheless, the most widely studied and perhaps best understood compound semiconductor surfaces are the (1 1 0) cleavage surfaces, in particular those of GaAs and InP. Nowadays, they may be widely prepared without cleavage-induced defects. Thus, they are excellent model surfaces to investigate adsorption processes as initial stages of passivating or metallic overlayers. Apart from their perfectness the (1 1 0) surfaces are non-polar, with a cation and an anion occurring in the surface unit cell. Strong electrostatic forces that could push the reconstruction process are not present and, hence, the bulk-terminated (1 × 1) translational symmetry is conserved. Furthermore, the (1 1 0) planes contain only weakly interacting zigzag chains of bonded group-III and group-V atoms, where each atom possesses a dangling bond.

Among all possible adsorbates on III–V (1 1 0) surface, the group-V elements take an outstanding position. Firstly, the atoms As, Sb, and Bi (cf. Fig. 1) strongly bind to (1 1 0) surfaces. Consequently there is a chance for the formation of unreactive, non-disruptive, and ordered interfaces which constitute useful prototypes for investigations of issues related to surface chemical bonding, electronic structure, and growth. Secondly, within bulk crystalline modifications of the group-V elements a transition from the semiconducting (As) to semimetallic (Sb, Bi) behaviour appears. Thirdly, the five valence electrons of the adsorbate atoms indicate the possibility of pairing all surface electrons during the monolayer or submonolayer growth of the overlayers. On the other hand, during the growth of thicker overlayers bulk-like character with either semiconducting or semimetallic behaviour may occur.

1.2. Growth and preparation of overlayers

At room temperature, most metal adsorbates react disruptively with III–V (1 1 0) surfaces, e.g., GaAs (1 1 0) [1], and consequently few form epitaxial monolayer systems. Therefore, although

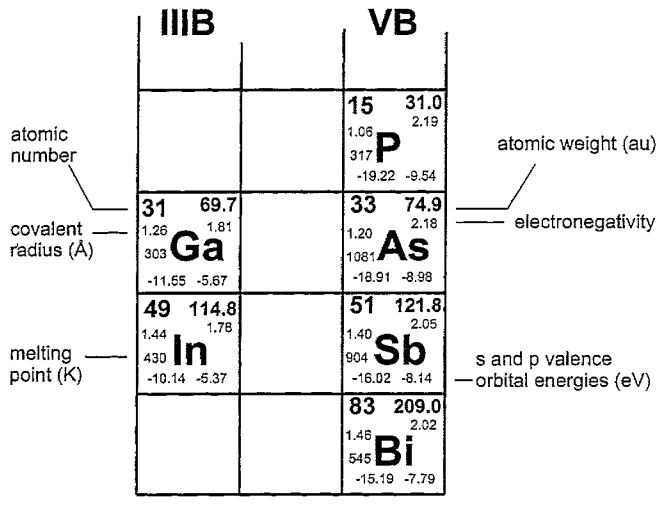

Fig. 1. Important properties of the relevant group-III and group-V elements discussed in this work. Values are taken from [199]. Orbital energies for valence electrons are taken from Hartree–Fock calculations [246].

GaAs (1 1 0) is one of the most thoroughly characterized compound semiconductor surfaces [2,3], there are only few adsorbates which produce overlayers that can be considered to be prototype or model systems. The notable exceptions to the above observation appear to be elements from group V of the periodic table of which Sb is the best-known example [4–15]. Bi also forms an ordered (1 × 1) overlayer on GaAs (1 1 0), and several experimental studies have been performed [16–24] on this system. In contrast to the semimetallic column-V elements Sb and Bi, only a few studies exist concerning As adsorbates [25–34]. Moreover, the resulting overlayers and interfaces are generally not well ordered. Therefore, we focus our attention on group-V semimetal overlayers on the (1 1 0) cleavage surfaces of III–V semiconductors.

Room-temperature (RT) deposition of one monolayer (1 ML) of Sb on clean GaAs (1 1 0) results in a stable and ordered (1 × 1) adsorbate structure [4–6]. Thereby, 1 ML corresponds to two Sb atoms per surface unit cell with an area $a^2/\sqrt{2}$ (a – bulk cubic lattice constant), i.e., 8.85×10^{14} atoms/cm^2. The Sb overlayer is formed through a lateral growth of ordered 1 ML high islands [7,8]. At low coverages (about 0.02 ML) the antimony can be seen in scanning-tunneling microscopy experiments [9,10] as separated protrusions of varying shapes and sizes (Fig. 2(a)). At 0.2 ML (cf. Fig. 2(b)) the Sb clusters start to grow together, forming flat terraces. Increasing the coverage to 0.7 ML (Fig. 2(c)), the Sb terraces coalesce, forming a continuous network extending over the entire GaAs (1 1 0) surface. However, even for about 1 ML coverage (Fig. 2(d)) some bare GaAs patches remain due to excess Sb. The excess Sb is already present at low coverages on small terraces. Since it is predominantly located at terrace edges, most of it is consumed during the growth process. Desorption experiments show that the ordered Sb overlayer is stable up to temperatures of ~ 550°C, whereas any Sb in excess of 1 ML desorbs at temperatures as low as ~ 250°C [7]. In general, the Sb monolayers 'as-deposited' are not ideally ordered. An effective method for preparing a highly ordered single Sb monolayer on GaAs (1 1 0) that exhibits a (1 × 1) LEED pattern is to start with the deposition of a few ML Sb on GaAs. After completion of the rather well ordered first Sb layer, the growth changes over into the

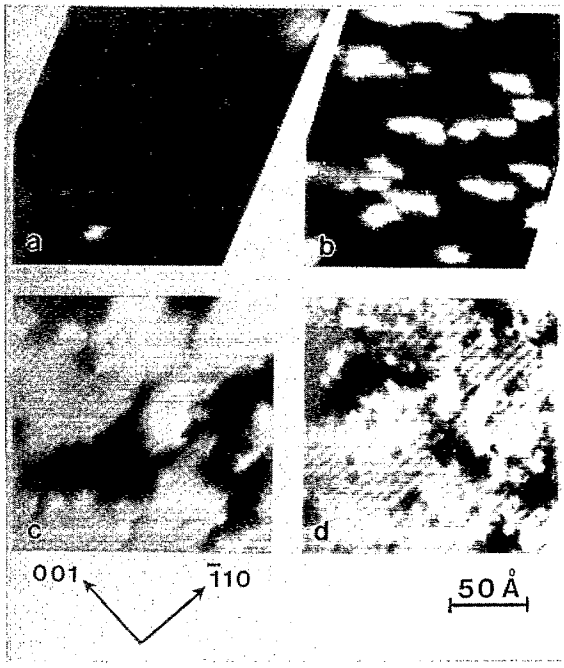

Fig. 2. STM images of GaAs (1 1 0) surfaces with increasing amounts of Sb. The coverages Θ are (a) 0.03, (b) 0.2, (c) 0.7, and (d) 1.0 ML. The sample voltage is -2.5 V for images (a)–(c) and -2.0 V for image (d). The topographic height is displayed by a grey scale, ranging from 0 (black) to 6.5 Å (white). From [10].

Stranski–Krastanov mode. The long-range order disappears [7], which is correlated to the simultaneous growth of multiple layers on top of the first layer [12,15]. After a subsequent annealing at about 600 K a sharp (1 × 1) LEED pattern can be reconstructed. The resulting monolayer is more regular at long-range scale than the as-deposited overlayer [7,14,35]. Betti and co-workers [36] found that antimony adsorption has even an ordering effect on the GaAs (1 1 0) surface, enlarging the coherent domain size in their study from ~ 600 to ~ 800 Å. We mention for the Sb/GaAs (1 1 0) case that the low temperature deposition at about 150 and 80 K does not essentially change the growth picture [13]. This holds at least in the submonolayer case.

The annealing procedure results into a desorption of all antimony with the exception of that in the first monolayer [7,14,35]. The adsorption of Sb on the (1 1 0) face of other III–V semiconductors is also known to provide stable (1 × 1) ordered overlayers of about 1 ML [8]. This holds especially for the RT deposition of Sb onto InP (1 1 0) [37–43] and onto GaP (1 1 0) [41,44]. The (1 × 1) ordered overlayer may be prepared in a similar way as for GaAs (1 1 0) by annealing an excess deposit of ~ 3–5 ML. Some characteristic preparation conditions are summarized in Table 1. The overlayer growth with excess Sb and subsequent annealing is also important for other systems. Antimony deposition on InAs (1 1 0) at RT does not lead to perfectly ordered growth of the first monolayer. Subsequent annealing, however, results in a highly ordered first monolayer which is stable up to 620 K [45]. In contrast there are some indications that for Sb/GaP the long-range order of the first monolayer is somewhat inferior to other Sb/III–V systems [46,47].

Table 1
Typical conditions for the preparation of ordered Sb and Bi overlayers on III–V(1 1 0) surfaces

System	Excess deposit	Annealing procedure	Resulting symmetry	Resulting thickness	Refs.
Sb					
GaP	≥ 1 ML	10 min, 230–350°C	1 × 1	1 ML	[47,217]
GaAs	≥ 1...5 ML	10–15 min, 200–350°C	1 × 1	1 ML	[7,14,35,36,64,48]
InP	3–5 ML	200–400°C	1 × 1	1 ML	[42,48]
InAs		5 min, 250°C	1 × 1	1 ML	[218]
Bi					
GaAs	4 ML	< 270°C	irregular 6 × 1	~ 1 ML	[18,23,70,224]
GaSb	1...8 ML	200–350°C	1 × 2	0.6 ± 0.1 ML	[52,58,59]
InP	3–5 ML	< 200°C	1 × 1	1 ML	[56]
InAs		5 min at 130°C	1 × 1	1 ML	[57]
InSb	1.5 ML	≤ 230°C	1 × 2	0.6 ML	[52]
		> 230°C	1 × 3	0.4 ML	[52]

The Sb monolayers on GaAs and InP (1 1 0) surfaces exhibit a remarkable thermal as well as chemical stability. Whereas excess layers of antimony desorb above 475 K, the ordered Sb monolayer is stable up to more than 800 K on GaAs [7] and to about 500 K on InP [48]. The different thermal stability of the two monolayer systems is, however, not too surprising. Strong Sb–As bonds are observed, for example, in Sb_xAs_{1-x} alloys, whereas Sb–P bonds are essentially unknown in either molecules or solids. The chemical stability of the ordered Sb monolayers on GaAs and InP has been investigated by exposure to oxygen [6] and hydrogen radicals [49]. Ordered Sb monolayers on GaAs are found to be more stable against oxidation than bulk Sb. In agreement with the different thermal desorption thresholds the Sb/GaAs system has been found to be more resistive against hydrogen etching than Sb/InP.

The preparation of Bi overlayers on GaAs (1 1 0) is similar to that of Sb ones, since Bi and Sb are isoelectronic (cf. Table 1). They are formed by evaporating Bi typically from an effusion cell onto a freshly cleaved surface, which is maintained at RT during deposition. It is well established that one monolayer of bismuth forms a regular epitaxial (1 × 1) structure on the (1 1 0) surface of GaAs [16–21]. However, in contrast to Sb the Bi/GaAs (1 1 0) system exhibits regular dislocations with missing adatoms every six unit cells. In particular, scanning tunneling microscopy (STM) [16,17,50,51] reveals that one monolayer of Bi is not a fairly well commensurate adlayer system on GaAs (1 1 0). In the direction of the atomic chains periodic series of Bi atoms are missing. The average separation of these rows of dislocations is about 25 Å. The vacancies have been attributed to strain induced in the adsorbed Bi chains resulting from the poor lattice match between the Bi chains and the GaAs (1 1 0) substrate. However, no preparation scheme has led to the complete development of a (6 × 1) pattern [52]. While the chain vacancies along $[1\,\bar{1}\,0]$ tend to be periodically arranged, the relative placement of the vacancies on neighbouring chains is not, which leads to disorder in the [0 0 1] direction [19,52]. In addition there are other differences from the Sb overlayers. Excess deposit of Bi also desorbs during annealing, but the resulting monolayer is not much more ordered than the as-deposited one [18,53]. It has been observed that the annealing

effects are less pronounced for Bi/III–V systems compared to antimony overlayers [16,54]. This is however not surprising since bulk Bi has a lower melting point (271°C) than Sb (631°C). From their LEED and AES analysis Ford et al. [52] conclude that the ordering temperature for Bi/GaAs is about 100°C.

The covalent radius of Bi adatoms is 1.46 Å and therefore about 4% larger than that of antimony (cf. Fig. 1). Hence, the deposition of Bi on substrates with more extended bonds is of particular interest. InP, InAs, and GaSb have lattice constants of 5.869, 6.058, and 6.096 Å, respectively [55], which are significantly larger than that of GaAs (5.653 Å), and thus should be able to accomodate the Bi overlayer more easily. In a favoured model for a Bi monolayer [43], the Bi atoms form zigzag chains along the surface taking up positions similar to those of the respective cations and anions in the bulk. The validity of this model is shown for Bi/InP [56] by annealing a Bi deposit of $\sim$ 3–5 ML to 500 K. However, LEED experiments by Resch et al. [22] indicate some distortions in the [1 $\bar{1}$ 0] direction. These distortions are presumably not periodic as observed for Bi/GaAs (1 1 0). The Bi/InAs (1 1 0) interface seems to form a perfect structure without defects and dislocations [52,57]. It is also shown [52,58] that Bi films grown at RT on the GaSb (1 1 0) surface form (1 × 1) epitaxial overlayers. For thicker films the growth changes again over into a Stranski–Krastanov mode [59]. However, after annealing of the thicker overlayers, the Bi/GaSb (1 1 0) interface forms a very stable (1 × 2) reconstruction phase [52,58–60].

There are only few experimental studies in which As is deposited on GaAs (1 1 0) surfaces cleaved in the ultrahigh vacuum (UHV) and held at RT. Under arsenic-rich conditions surfaces with a (1 × 1) LEED pattern are observed [25]. Other authors [26] reported that the LEED pattern obtained on such a surface is (1 × 1), but with a diffuse background. This could indicate that the deposited arsenic does not order when the substrate is held at RT. In a further study [27] it has been observed that the As saturation coverage is about 1 ML, and that annealing the surface at 300°C drives off the excess As. In any case, under extreme As-rich conditions theory [28] predicts an As-covered (1 × 1) 1ML structure which is more stable than the clean GaAs (1 1 0) surface plus bulk As clusters. Recently, there has been a renewal of interest in growth of As on GaAs (1 1 0) by means of molecular-beam epitaxy (MBE) [29,30], but there are apparently no experimental attempts for a detailed characterization of such a surface. However, a dramatic development concerning the understanding of As deposition on GaAs (1 1 0) is expected as an accompanying process of the preparation of quantum-well-wire laser structures by cleaved edge overgrowth [31,32]. The basic idea of their preparation is the cleavage of GaAs/GaAlAs superlattices and the overgrowth of the resulting cleavage face in the same MBE machine. The knowledge of the properties of adsorbed As on InP (1 1 0) is even more scarce than in case of the As/GaAs interface [61,62]. At RT a saturated As layer consisting of two differently bonded As species is stable for temperatures up to 250°C. Annealing to higher temperatures is accompanied by both a significant loss of arsenic from the surface due to desorption and partial incorporation into surface sites of the substrate [62]. The resulting structure is characterized by an As–P exchange in the uppermost substrate layer as concluded from a comparison of measured and calculated surface optical properties [34].

The monolayer properties discussed in Section 4 refer to ordered, ideal overlayers if not stated otherwise. The atomic and electronic properties of the monolayer systems, in particular for antimony overlayers, depend strongly on the degree of order as has been shown in many studies (see, e.g., the work by Schäffler et al. [14,35]). As discussed above, well ordered overlayer monolayers are usually produced by an annealing process.

1.3. Experimental techniques

The relatively strong interaction of low-energy electrons with the electronic shells of atoms results not only in a small penetration depth into the material because of inelastic collisions but also in strong elastic scattering. The electrons which are elastically backscattered from the surface regions of the crystal are detected in low energy electron diffraction (LEED). Because of its surface sensitivity LEED is one of the most powerful tools to study the geometry of a surface and corresponding thin overlayers by analysing the position and the intensity of diffraction maxima. The inspection of the pattern of diffraction spots immediately gives information about the ordering of the surface region and, if there is any ordering, the two-dimensional translational symmetry of the surface. Random defects and crystallographic imperfections will broaden the spots and increase the background intensity due to scattering from these statistically distributed centres. This 'static' type of LEED investigations is normally combined with preparation and other analytical techniques. However, from LEED measurements [7,8,39,43,52,63] also the atomic geometry of an overlayer with a certain translational symmetry, in our case usually (1×1), can be extracted by measuring the spot intensities as a function of the kinetic energy of the electrons in the range of 40–300 eV and modelling the resulting $I-V$ curves. The experimental intensity profiles are analysed by means of a dynamical multiple-scattering model in which energy-dependent scattering phase shifts and energy-dependent electron inelastic mean free path are utilized. The experimental results are compared with such multiple-scattering simulations for a sequence of trial atomic geometries. The reliability factor is optimized and the resulting best-fit atomic positions are considered as the true surface geometry. Such dynamical LEED studies have been applied to determine the structure of the systems Sb/GaAs (1 1 0)(1×1) [7,8,178], Sb/InP (1 1 0)(1×1) [39,43], Bi/GaAs (1 1 0)(1×1) [43], and Bi/InP (1 1 0)(1×1) [43] (cf. Table 2).

Another powerful diffraction method for exploring the atomic structure of the column-V overlayers on III–V (1 1 0) surfaces is the X-ray standing wave (XSW) technique [47,64,65]. It allows direct determination of the positions of adsorbed atoms relative to a selected subset of substrate planes. This information is of particular importance since precise information on vertical distances from surface planes is not readily available from STM, and LEED involves a complex model-dependent analysis. On the other hand, XSW requires synchrotron radiation. As the angle or photon energy is swept through a Bragg condition, a standing wave is formed within and in front of the substrate. The change of the phase within the total reflection width causes the spatial movement of the nodes and antinodes of the electric field intensity relative to the diffracting planes. Since photoabsorption is proportional to the electric field intensity at the atom core, this spatial movement of the standing wave produces a modulation in the absorption of the overlayer atoms. Analysis of the variation in absorption allows a precise determination of the vertical adatom position. This has been done for the systems Sb/GaAs (1 1 0)(1×1) [64], Bi/GaAs (1 1 0)(1×1) [65], and Sb/GaP (1 1 0)(1×1) [47].

Another X-ray diffraction method is the grazing-incidence X-ray diffraction (GIXD). It gives similar information as LEED by inspecting a set of independent diffracted beams. The peak intensities are again calculated for certain trial geometries. The GIXD technique is extremely sensitive to the in-plane surface coordinates. It therefore allows to discriminate between different proposed geometrical arrangements of the adatoms with respect to the substrate positions. The method has been applied to monolayers of Sb [36] and Bi [66] on GaAs (1 1 0).

Table 2
Experimental techniques related to the determination of structural, electronic, and vibrational properties of Sb and Bi monolayers on III–V (1 1 0) surfaces

Experiment	Property	System	Refs.
LEED	Geometry	Sb/GaAs	[7,8,178]
		Sb/InP	[39,43]
		Bi/GaAs	[178]
		Bi/InP	[43]
XSW	Geometry	Sb/GaP	[47]
		Sb/GaAs	[64]
		Bi/GaAs	[65]
GIXD	Geometry	Sb/GaAs	[36]
		Bi/GaAs	[66]
PED	Geometry	Sb/GaP	[72]
		Sb/GaAs	[73]
		Sb/InP	[72]
		Sb/InAs	[74]
ARPES/ARUPS	Occupied states	As/GaAs	[33]
		Sb/GaP	[44,217]
		Sb/GaAs	[44,183,214]
		Sb/InP	[37,42,174]
		Sb/InAs	[218]
		Bi/GaAs	[16,17,21]
		Bi/GaSb	[152]
		Bi/InP	[56]
		Bi/InAs	[57]
ARIPS	Empty states	Sb/GaAs	[40,76]
		Sb/InP	[40,76]
		Bi/GaAs	[77,78]
HREELS, EELS, RAS, RRS, Ellipsometry, STM	Interband transitions	Sb/GaP	[80,81]
		Sb/GaAs	[15,23,68,80,81,186,201,210,228]
		Sb/InP	[80,81,185,201,250]
		Sb/InAs	[80,81]
		Bi/GaAs	[224,250]
		Bi/GaSb	[60,153]
RRS	Interface phonons	Sb/GaP	[41,81]
		Sb/GaAs	[41,81,83,202]
		Sb/InP	[41,81]
		Sb/InAs	[81]

The diffraction methods yield structural information. There is another wide class of experimental techniques providing electronic information. With the development of the STM, we have a tool which combines these two types of measurements in a single experiment. Atomic resolution imaging, together with spatially resolved spectroscopy, enables one to observe directly the electronic density of states within a few eV on either side of the Fermi level induced by the semimetal adsorbates, and to determine the origin of the states in terms of the geometric structure of the surface. In the case of adsorption of group-V elements Sb and Bi on GaAs (1 1 0) STM is used to control the submonolayer growth, the geometric structure of the 1 ML overlayer, as well as the corresponding electronic states,

in particular the Fermi level pinning [9–11,16,17,67]. Properties of Sb metal films with thicknesses in the range 1–10 ML have also been studied [68].

Among all experimental methods the photoemission spectroscopy (PES) in its various modifications is the most powerful tool to investigate the electronic structure of the column-V overlayers on III–V (1 1 0) surfaces. High resolution soft X-ray photoemission spectroscopy (SXPS) from the core levels is a standard method to monitor the formation of interfaces of Sb and Bi with the III–V compounds. As an example, the emission from the Sb 4d and Bi 5d core levels of the adsorbates and, respectively, Ga 3d and As 3d (Sb 4d) levels of the GaAs (GaSb) substrate is studied in [4–6,13,14,58,69,70]. The line positions and line shapes of the emission intensities are investigated with dependence on the overlayer thickness for different interface preparations, such as substrate (room or low) temperature [13], annealing steps [13,14,58,69], and additional surface species [6]. The surface band bending can be derived from the energy shifts of the substrate core-level emission lines with respect to the Fermi level. Conclusions about the chemical bonding and order at the surface can be drawn from the surface core-level line shapes. When the overlayer and substrate core-level emissions are recorded as a function of polar angles and photon energy and compared with theoretical models for the surface, structural information can be gained. The photoelectron diffraction (PED) has been applied to several Sb/III–V (1 1 0) interfaces [71]. Explicit structural optimizations based on PED are available for Sb/GaP [72], Sb/GaAs [73], Sb/InP [72] and Sb/InAs [74].

The investigation of the photoelectron emission from the valence bands can be combined with variations of the azimuthal as well as polar angle of the detected electrons. The angle-resolved photoemission electron spectroscopy (ARPES) or angle-resolved ultraviolet photoelectron spectroscopy (ARUPS) allows to measure the occupied surface electronic band structure along high symmetry lines in the surface Brillouin zone (SBZ) for ordered overlayers. Such measurements have been done extensively for a series of V/III–V (1 1 0) interfaces (cf. Table 2). The application of ARPES/ARUPS also increases the surface sensitivity and allows to detect the overlayer anisotropy. It is useful in the case of submonolayer coverages and other overlayer structures that do not give rise to sharp LEED patterns [6]. The results allow conclusions with respect to the bonding behaviour of column-V atoms on GaAs (1 1 0) and the other surfaces considered [15,75].

The measurements of the occupied bands are complemented by studies of unoccupied surfaces bands by means of the angle-resolved inverse photoemission spectroscopy (ARIPS). Results of such studies are available for Sb and Bi overlayers on GaAs (1 1 0) or InP (1 1 0) surfaces [40,76–78].

Important information about the electronic structure of the overlayers and their interfaces also results from spectroscopies which give the spectral behaviour of the inverse dielectric function, the dielectric function, or a derivation of the dielectric function in the energy range of electronic interband transitions. These are the high resolution electron-energy-loss spectroscopy (HREELS), optical methods like reflectance-anisotropy spectroscopy (RAS) and spectroscopic ellipsometry, and the resonance Raman spectroscopy (RRS). EELS is a convenient method to follow the development of certain peaks with the overlayer thickness, in particular the formation of certain semimetal-induced electronic states within the fundamental gap of the semiconductor but also in the range of the bulk valence-band–conduction-band transitions. Such studies have been published for a wide range of V/III–V (1 1 0) interfaces (cf. Table 2). In the RAS the signal originates from the difference in normal-incidence reflectivity for linear polarized light of two perpendicular polarizations. In the case of the considered zinc-blende semiconductors, which are to a good approximation isotropic in the

bulk, the RAS signal is mainly generated by surface related anisotropies. This technique has been applied to ordered Sb overlayers on (1 1 0) surfaces of GaP, GaAs, InP, and InAs in the spectral range 1.5–5.5 eV [79–81]. The ellipsometric spectroscopy also gives direct information about the surface region. It allows a derivation of the real as well as imaginary part of the effective dielectric function for the overlayer as has been shown for Sb on GaAs and InP (1 1 0) surfaces [12,82]. Usually RRS is an optical technique that is not surface sensitive because of the large penetration depth of the photons. However, by detecting the Raman scattering intensities from vibrational modes of the overlayer, electron–hole-pair states coupled to the overlayer or interface modes can be investigated as shown in the case of Sb monolayers on GaAs, InP, and InAs (1 1 0) surfaces [81,83,84].

Techniques like HREELS and RRS also allow to study the vibrational and collective excitations in the group-V/III–V (1 1 0) systems in a large spectral region and for a wide range of overlayer thicknesses. The elementary excitations are substrate–overlayer (interface) vibrations [41,82], bulk phonons when the scattering by them is surface electric-field-induced [85,86], substrate's Fuchs–Kliewer optical phonons [24,87–89], dopant-induced free-carrier plasmons [24,87–89], coupled plasmon–phonon modes and narrow interband transitions [24]. Measurements of such low energy excitations have been made for the systems Sb/GaAs (1 1 0) [24,41,82,85–88], Sb/GaP (1 1 0) [41], Sb/InP (1 1 0) [41], and Bi/GaAs (1 1 0) [24,89]. The electric field-induced Raman scattering (EFIRS) is also an efficient method to determine the eletric field at semiconductor surfaces. Bulk polar optical phonons, which couple to the electrons via the Fröhlich mechanism, give rise to forbidden Raman lines under electric field. The measured Raman intensity is proportional to the square of the surface electric field related to the band bending (see, e.g., [90,91]).

2. Theoretical method

Growth and experimental studies of ordered stable overlayers on semiconductor surfaces have been complemented with theoretical studies on such systems. In this section we outline the basic concepts of presently available successful theoretical techniques together with their strengths and limitations.

Theoretical modelling of ordered overlayers on semiconductor surfaces has been studied at two levels of sophistication. On the one hand, an empirical tight-binding total-energy approach has been applied. On the other, it has become possible to use ab initio methods for accurate calculation of equilibrium atomic structure, electronic states, and phonon frequencies without using any fit parameters. After briefly discussing the empirical method in this section we describe in some detail the ab initio pseudopotential theory.

2.1. Empirical approach

One of the successful empirical approaches to study surface atomic geometry and surface electronic states is based on an empirical tight-binding total-energy method. Chadi's original tight-binding total-energy work [92] for clean surfaces was based on only interactions of s and p orbitals on nearest-neighbour atoms, as proposed by Slater and Koster [93]. The sp^3 tight-binding model is usually inadequate for describing even the lowest conduction band of indirect band gap semiconductors. This deficiency can be remedied by using an sp^3s^* basis [94]. The sp^3s^* band-

structure model has been developed by Mailhiot et al. [63], LaFemina et al. [95], and McCoy and LaFemina [96] for atomic geometry determination for Sb covered III–V (1 1 0) surfaces by using the tight-binding total-energy scheme. In both versions of the scheme the tight-binding interaction parameters are fitted to reproduce reasonably good bulk band structures. A compilation of these parameters is given in the works by Vogl et al. [94], Mailhiot et al. [63], LaFemina et al. [95], and McCoy and LaFemina [96]. The application of this theoretical method to clean and covered III–V (1 1 0) surfaces has been reviewed by LaFemina [97].

In the tight-binding total-energy scheme, the total energy is expressed as

$$E_{\mathrm{tot}} = E_{\mathrm{bs}} + U. \tag{1}$$

The first term on the right hand side of Eq. (1) represents the contribution due to the band-structure energy E_{bs}, and the second term is an empirical correction U for the double counting of electron–electron interactions in the band-structure energy and includes the ion–ion interaction energy. Atomic structural determination at clean and adsorbate-covered semiconductor surfaces is made by examining the variation of the total energy associated with atomic displacements, given in the explicit form by the following expression:

$$\Delta E_{\mathrm{tot}} = \sum_{nk}^{\mathrm{occ}} \Delta\varepsilon_n(\boldsymbol{k}) + \sum_{i \neq j} \sum_{m} U_m \eta_{ij}^m. \tag{2}$$

Here η_{ij} denotes the fractional change in bond length between atoms labelled i and j with respect to the bulk value. U_m are empirical elastic constants, adjusted to fit bulk elastic moduli and phonon frequencies and requiring that ΔE_{tot} has no contribution from linear terms in atomic displacements. Only $m = 1, 2$ are considered, making U_1 and U_2 two elastic constant parameters for each surface material. The variation in the electronic eigenvalues $\varepsilon_n(\boldsymbol{k})$ resulting from atomic displacements is calculated by assuming a d^{-2} dependence of the transfer tight-binding interactions on first nearest-neighbour distance d according to Harrison [98].

McCoy and LaFemina [96] have presented a Monte Carlo computer-simulation study, based on the tight-binding total-energy scheme, of the growth of submonolayer coverages of Sb atoms on the GaAs (1 1 0) surface. This simulation includes diffusion of Sb atoms and surface configuration dependent dissociative chemisorption of molecular Sb.

There is some uncertainty in determining the parameters of this theory, especially for the tight-binding transfer matrix elements between the overlayer Sb atoms and between the Sb atoms and the column-V element of the substrate. Due to the somewhat arbitrary nature of the scaling procedure for interaction parameters used in this theory, the results of surface structure determinations and the Monte Carlo simulations cannot be regarded as quantitative predictions.

2.2. *Ab initio approach*

In order to make theoretical predictions for the equilibrium atomic geometry, electronic states, and atomic vibrations on clean and covered semiconductor surfaces beyond the empirical nature of the type discussed in Section 2.1, one must attempt a parameter-free, i.e., an ab initio, approach. Such an attempt, of course, would require far more computational effort than is needed for the application of the empirical tight-binding total-energy approach. In essence, three main ingredients are required

for an ab initio modelling of clean and covered semiconductor surfaces of the type under consideration: (i) electron–ion potential energy obtained from first-principles, (ii) a fundamental but practical scheme for electron–electron interaction, and (iii) an accurate and efficient numerical scheme for solving the appropriate quantum mechanical problem.

The interaction between ion cores and chemically active valence electrons can be accurately described by norm-conserving pseudopotentials. The Density Functional Theory (DFT) in Local Density Approximation (LDA) provides an accurate and practical approach for treating electron–electron interaction when dealing with ground state properties such as atomic geometry, occupied electronic states, and vibrational frequencies. Physical properties related to unoccupied electronic states, such as band gap and optical properties, can be studied by allowing for self-energy correction to the DFT. With the ingredients (i) and (ii) available, an appropriate equation of motion for electronic degrees of freedom can be set up, which must then be solved numerically. This can be done either by solving a matrix eigenvalue equation (Hamiltonian approach) or a differential equation (Lagrangian approach). It is also possible to simultaneously relax electronic as well as ionic degrees of freedom within the Born–Oppenheimer approximation. In the following sections we will briefly describe some of the concepts underlying the above mentioned three aspects of the theory.

2.2.1. Density functional theory

The DFT was proposed in mid sixties by Hohenberg and Kohn [99], and Kohn and Sham [100]. It basically postulates that the total electronic energy of a condensed matter can be obtained from the knowledge of the correct electronic charge density. The theory is based on two basic principles:

(i) The complete many-electron ground state wave function ψ is a unique functional $\psi[n(\boldsymbol{r})]$ of the ground state electronic charge density $n(\boldsymbol{r})$.

(ii) The total electronic energy obeys a variational principle in the charge density $n(\boldsymbol{r})$. Based on these principles, the total electronic energy E_{ee} can be expressed as

$$E_{ee}[V_{ext}, n] = \int d\boldsymbol{r}\, V_{ext}(\boldsymbol{r}) n(\boldsymbol{r}) + \mathcal{F}[n], \tag{3}$$

where V_{ext} is an external potential to which the electronic system is subjected, and $\mathcal{F}[n]$ is an unknown functional defined as

$$\mathcal{F}[n] = \langle \psi | (T + V_{ee}) | \psi \rangle \tag{4}$$

with T and V_{ee} as the kinetic and electron–electron interaction energy operators, respectively. Using principle (i) Hohenberg and Kohn [99] proposed to express $\mathcal{F}[n]$ as

$$\mathcal{F}[n] = T_s[n] + \frac{e^2}{2} \int d\boldsymbol{r} \int d\boldsymbol{r}' \frac{n(\boldsymbol{r}) n(\boldsymbol{r}')}{|\boldsymbol{r} - \boldsymbol{r}'|} + E_{xc}[n], \tag{5}$$

where the first two quantities on the right hand side represent the kinetic energy and classical mean-field interelectronic Coulomb energy (Hartree term) of a gas of independent fictitious particles with density $n(\boldsymbol{r})$. The third term, $E_{xc}[n]$, is considered as a universal functional of $n(\boldsymbol{r})$ to represent all corrections to the independent particle picture, i.e., to the kinetic energy and the non-classical many-body effects of exchange and correlation (xc), but remains unknown. Using principle (ii) we

can express the ground state energy of a many-electron system in a given external potential $V_{ext}(r)$ as

$$E_{ee}[V_{ext}, n] = T_s[n] + \int dr\, V_{ext}(r)n(r) + \frac{e^2}{2}\int dr \int dr' \frac{n(r)n(r')}{|r-r'|} + E_{xc}[n], \tag{6}$$

where $n(r)$ is the ground state charge density.

The approach to determine the correct charge density $n(r)$ and to evaluate $T_s[n]$ was suggested by Kohn and Sham [100]. Consider the following set of single-particle equations:

$$\left\{\frac{-\hbar^2\nabla^2}{2m} + V_{KS}[n]\right\}\phi_j(r) = \varepsilon_j\phi_j(r). \tag{7}$$

Here ϕ_j and ε_j are wave functions and eigenvalues, respectively, of non-interacting fictitious single particles such that the correct electron density is obtained as

$$n(r) = \sum_j^{occ} |\phi_j(r)|^2, \tag{8}$$

where the sum is over occupied states. The effective Kohn–Sham potential is then defined as

$$V_{KS}[n(r)] \equiv V_{ext}(r) + e^2\int dr' \frac{n(r')}{|r-r'|} + \frac{\delta E_{xc}[n]}{\delta n(r)} \tag{9}$$

$$= V_{ext}(r) + V_H[n(r)] + V_{xc}[n(r)] \tag{10}$$

with V_H and V_{xc} as the Hartree and exchange–correlation potentials, respectively. With n determined, $T_s[n]$ can be evaluated as

$$T_s[n] = \sum_j^{occ} \langle\phi_j|\varepsilon_j - V_{KS}|\phi_j\rangle. \tag{11}$$

The unknown part of the energy, E_{xc}, is approximated by applying the LDA. It is assumed that $n(r)$ is sufficiently slowly varying so that

$$E_{xc}[n] \approx \int dr\, n(r)\varepsilon_{xc}(n(r)), \tag{12}$$

where $\varepsilon_{xc}(n(r))$ is the exchange–correlation energy per electron of a uniform electron gas of density n. The corresponding potential is given by

$$V_{xc}[n(r)] = \frac{\delta E_{xc}[n(r)]}{\delta n} \approx \frac{d}{dn(r)}\{n(r)\varepsilon_{xc}(n(r))\}. \tag{13}$$

For surfaces of III–V materials and V/III–V interfaces, which are characterized by strong covalent bonds, the LDA seems still to be a reasonable approximation. However, straightforward application of the LDA may not be appropriate for physisorbed states with atoms at distances from surfaces much larger than typical bond lengths. Several expressions are available for ε_{xc}, but the scheme due to Ceperley and Alder [101] is considered to provide the most accurate expression for an unpolarized homogeneous electron gas. It has been parametrized by Perdew and Zunger [102]. A simpler form of the combined exchange–correlation functional is the so-called X_α method, advocated by Slater [103].

2.2.2. Plane wave pseudopotential scheme

For simulating interaction between chemically active (valence) electrons and ion cores the concept of pseudopotentials has proved successful. That means that V_{ext} in Eqs. (3), (6) and (10) can be replaced by crystal pseudopotential V_{ps}. In order to guarantee that the pseudopotential for a particular ion can be transferred to various 'environments' (i.e., different geometries or crystal structures) it is necessary to use a norm-conserving criterion during its construction. Various schemes have recently become available to generate norm-conserving pseudopotentials. The first successful attempt was made by Hamann et al. [104]. That work was extended by Bachelet et al. [105], who have published pseudopotentials in an analytical form for a whole range of ions in the periodic table. Some more recent schemes are capable of generating much softer pseudopotentials than those published by Bachelet et al. [105]. Particularly impressive schemes are due to Troullier and Martins [106] and Vanderbilt [107].

Applications of pseudopotentials can be made either in the semi-local (SL) form or in the truly non-local form. In the semi-local (non-relativistic) form a pseudopotential is expressed as local in radial coordinate but non-local in angular coordinates

$$v^{SL} = \sum_l \mathscr{P}_l v_l(r) \mathscr{P}_l, \tag{14}$$

where $\mathscr{P}_l$ is a projection operator which projects out the lth angular momentum from ionic core, and $v_l(r)$ is the corresponding radial pseudopotential. The truly non-local form of a pseudopotential can be expressed in the form suggested by Kleinman and Bylander [108]:

$$v^{KB} = \sum_{lm} v_l(r) R_l(r) Y_{lm}(\hat{r}) \langle v_l \rangle^{-1} Y^*_{lm}(\hat{r}') R_l(r') v_l(r') \tag{15}$$

with R_{lm} as the radial part of the pseudo-orbital and Y_{lm} as the usual spherical harmonics part. The normalizing constant in the above equation is given by

$$\langle v_l \rangle = \int \mathrm{d}\boldsymbol{r}\, R_l(r)\, Y^*_{lm}(\hat{r}) v_l(r)\, Y_{lm}(\hat{r}) R_l(r). \tag{16}$$

The two forms of pseudopotential produce an identical effect on a pseudo-orbital.

The success of the pseudopotential approach is based on two assumptions. Firstly, that the overlap between core and valence electron wave function be negligible. Secondly, there should be a clear separation between core and valence electron energy levels. In the case of the Ga compounds studied in this work, both these conditions are well satisfied. The second condition, however, is unlikely to be fulfilled for heavier atoms in the same column of the periodic table, due to energetically higher lying d electrons. Additionally, spin–orbit interactions, which have not been considered here, become important for heavier atoms. This holds in particular for the description of the electronic properties.

The single-particle wave function ϕ can be expressed in terms of a plane wave basis set

$$\phi_n(\boldsymbol{k}, \boldsymbol{r}) = \frac{1}{v} \sum_{\boldsymbol{G}} A_n(\boldsymbol{k} + \boldsymbol{G}) \exp[\mathrm{i}(\boldsymbol{k} + \boldsymbol{G})\boldsymbol{r}], \tag{17}$$

where v is normalization volume (e.g., crystal volume), $\boldsymbol{G}$ are reciprocal-lattice vectors, n is the band index, and the electronic wave vector $\boldsymbol{k}$ lies within the first Brillouin zone. The size of basis set (i.e., the

number of plane waves) is usually considered by imposing an upper cutoff to the kinetic energy

$$\frac{\hbar^2}{2m}(\boldsymbol{k}+\boldsymbol{G})^2 \leq E_{\mathrm{cut}}. \tag{18}$$

In order to obtain well converged results, the calculations reported in this work have been performed with $E_{\mathrm{cut}} = 15$ Ryd. Convergency tests for such systems as studied here have been reported in [109,110]. The geometries and bond lengths are converged within an uncertainty of about 0.02 Å. The uncertainty in the band structure amounts to approximately 0.1 eV.

The total crystal pseudopotential follows as sum of non-overlapping ionic pseudopotentials

$$V_{\mathrm{ps}}(\boldsymbol{r}) = \sum_{R}\sum_{b}\hat{v}_b(\boldsymbol{r}-\boldsymbol{R}-\tau_b) \tag{19}$$

with $\boldsymbol{R}$ as a Bravais lattice vector, τ_b as an ionic position in a unit cell, and $\hat{v}_b$ as the pseudopotential due to the bth ion. A matrix element of a non-local pseudopotential can be expressed as

$$V(\boldsymbol{k}+\boldsymbol{G},\boldsymbol{k}+\boldsymbol{G}') = \frac{1}{B}\sum_{b} S_b(\boldsymbol{G}-\boldsymbol{G}')v_b(\boldsymbol{k}+\boldsymbol{G},\boldsymbol{k}+\boldsymbol{G}'), \tag{20}$$

where there are B ions in the unit cell, and $S_b(\boldsymbol{G}-\boldsymbol{G}')$ is the structure factor for atoms of type b

$$S_b(\boldsymbol{G}) = \exp\left[\mathrm{i}\,\boldsymbol{G}\cdot\tau_b\right]. \tag{21}$$

$v_b(\boldsymbol{q},\boldsymbol{q}')$ is an ionic form factor, which for the semi-local form of the pseudopotential has the form

$$v_b^{\mathrm{SL}}(\boldsymbol{q},\boldsymbol{q}') = \frac{4\pi}{\Omega_{\mathrm{at}}}\sum_{l}(2l+1)v_{b,l}^{\mathrm{SL}}(q,q')P_l(\hat{q}\cdot\hat{q}') \tag{22}$$

with

$$v_{b,l}^{\mathrm{SL}}(q,q') = \int_0^\infty \mathrm{d}r\, r^2 v_{b,l}(r) j_l(q'r), \tag{23}$$

where $j_l(qr)$ is spherical Bessel function, P_l is Legendre function, and Ω_{at} is atomic volume. Numerically more convenient is the ionic form factor in Kleinman–Bylander form

$$v_b^{\mathrm{KB}}(\boldsymbol{q},\boldsymbol{q}') = \frac{4\pi}{\Omega_{\mathrm{at}}}\sum_{l}(2l+1)v_{b,l}^{\mathrm{KB}}(q,q')P_l(\hat{q}\cdot\hat{q}') \tag{24}$$

with

$$v_{b,l}^{\mathrm{KB}}(q,q') = \frac{1}{\langle v_{b,l}\rangle}\left[\int_0^\infty R_l(r)v_l(r)j_l(qr)r^2\,\mathrm{d}r\right]\left[\int_0^\infty R_l(r)v_l(r)j_l(q'r)r^2\,\mathrm{d}r\right], \tag{25}$$

$$\langle v_{b,l}\rangle = \int_0^\infty v_{b,l}(r)R_l^2(r)r^2\,\mathrm{d}r. \tag{26}$$

Here $R_l(r)$ is the radial pseudo-wave function for the ionic reference configuration with angular momentum l. It can be appreciated from Eqs. (23) and (25) that calculation of matrix elements, with N plane waves in the basis, scales as N^2 in the semi-local case and as N in the KB case. This therefore brings in a great deal of computational saving with the KB form. Consequently, the KB form is usually used in calculations on interface systems such as V/III–V (1 1 0).

Within the plane wave pseudopotential scheme it is fairly straightforward to obtain expressions for the total energy and forces acting on atoms within the unit cell. Following Ihm et al. [111], Yin and Cohen [112], and Srivastava and Weaire [113], total energy per unit cell, i.e., the electronic energy E_{ee} and the ion–ion Coulomb interaction $E_{ion-ion}$, can be written as

$$E_{tot} = \sum_{j}^{occ} \varepsilon_j - E'_H + \Delta E_{xc} + \gamma_E + E_0, \tag{27}$$

where

$$E'_H = \frac{1}{2} \sum_{G \neq 0} \frac{4\pi e^2}{G^2} |n(G)|^2, \tag{28}$$

$$\Delta E_{xc} = \sum_{G} n^*(G) [\varepsilon_{xc}(G) - V_{xc}(G)], \tag{29}$$

$$\gamma_E = E_{ion-ion} - \frac{1}{2} \frac{1}{\Omega_{at}} \sum_{b} \int dr \frac{z_b^2 e^2}{r}, \tag{30}$$

$$E_0 = \bar{z} \frac{1}{\Omega_{at}} \sum_{b} \int dr \left(v_b(r) + \frac{z_b e^2}{r} \right). \tag{31}$$

In the above $z_b e$ is the charge on bth ion and

$$\bar{z} = \frac{1}{B} \sum_{b} z_b, \qquad V_H(G=0) = v_b(G=0) = 0. \tag{32}$$

The forces on the atoms can be calculated via the gradient of the total energy using Feynman's Theorem [114]. The Hellmann–Feynman force on bth atom comprises one part due to the Coulomb interaction with other ions and one part determined by the electronic wave functions:

$$F_b = F_b^{ion-ion} + F_b^{el}. \tag{33}$$

The ionic contribution $F_b^{ion-ion}$ can be evaluated, as $E_{ion-ion}$ can be, using Ewald's method (see, e.g., [115]). The electronic part of the force can be expressed analytically

$$F_b^{el} = -\mathrm{Re} \left\{ \frac{i}{B} \sum_{k,n}^{occ} w(k) \sum_{G,G'} A_n^*(k+G') A_n(k+G)(G-G') \times S_b(G-G') \sum_{l} v_{b,l}(k+G, k+G') \right\}. \tag{34}$$

An evaluation of the electronic charge density, the key variable of the theory, requires performing a k-space integration over Brillouin zone volume. For non-metallic systems it is most expedient to achieve this by employing symmetry and using a finite number of 'special k-points' with weights $w(k)$ within the irreducible part of the Brillouin zone. For studies of clean and covered (1 1 0) surface of III–V semiconductors it is found that four special k-points [116] in the irreducible part of the (1 × 1) two-dimensional SBZ provide adequately converged results. Extensive tests [117] have shown that even for metallic surfaces a larger k-point set induces changes of the bond lengths by typically less

than 0.01 Å. A detailed discussion of calculation of symmetrized charge density using special $\boldsymbol{k}$-points scheme has been given by Pickett [118] and will not be repeated here.

2.2.3. Molecular dynamics, or Car–Parrinello method

Appropriate wave equations must be solved in an attempt to determine equilibrium atomic geometry and in the calculation of the corresponding electronic states and vibrational frequencies localized at the interface between an overlayer and a semiconductor surface. This can be done either by following a static approach (based on the Kohn–Sham theory – see, e.g., [119,120]) or a dynamic approach (based on the Car–Parrinello theory [121,122]).

In the molecular dynamics – density functional (MD–DF) scheme one considers a fictitious dynamical system whose Lagrangian is constructed in a configuration space spanned by the ionic coordinates $\{\boldsymbol{R}_b = \boldsymbol{R} + \tau_b\}$ and the single-particle orbitals $\{\phi_i(\boldsymbol{r})\}$ of the DFT. If μ is an adjustable parameter appropriate for the fictitious single-particle (electronic) dynamics, M_b denotes ionic masses, λ_{ij} are Lagrange multipliers used to satisfy the orthonormality of the ϕ_i's, and $E_{\text{tot}}[\{\boldsymbol{R}_b\}, \{\phi_i\}]$ acts as the potential energy of the fictitious dynamical system, then using generalised coordinates $q = \{\boldsymbol{R}_b, \phi_i\}$ and generalised velocities $\dot{q} = \{\dot{\boldsymbol{R}}_b, \dot{\phi}_i\}$ the Lagrangian is expressed as

$$L(q, \dot{q}) = \frac{1}{2}\mu \sum_i \int \mathrm{d}\boldsymbol{r} |\dot{\phi}_i|^2 + \frac{1}{2}\sum_b M_b \dot{\boldsymbol{R}}_b^2 - E[\{\boldsymbol{R}_b\}, \{\phi_i\}] + \sum_{i,j} \lambda_{ij} \left[\int \mathrm{d}\boldsymbol{r}\, \phi_i^* \phi_j - \delta_{ij} \right]. \tag{35}$$

The minimum of E_{tot} with respect to the single-particle degrees of freedom $\{\phi_i\}$ is the Born–Oppenheimer potential $\mathscr{U}$ for the ions:

$$\mathscr{U}(\{\boldsymbol{R}_b\}) = \min_{\{\phi_i\}} E_{\text{tot}}[\{\boldsymbol{R}_b\}, \{\phi_i\}]. \tag{36}$$

Simultaneous relaxation of the ionic and electronic coordinates towards their equilibrium on the Born–Oppenheimer surface is achieved by solving the Lagrange equations of motion

$$\frac{\mathrm{d}}{\mathrm{d}t}\frac{\partial L}{\partial \dot{q}} = \frac{\partial L}{\partial q}. \tag{37}$$

With Eq. (35) this yields

$$\mu \ddot{\phi}_i = -\frac{\delta E}{\delta \phi_i^*} + \sum_j \lambda_{ij}\phi_j = -H\phi_i + \sum_j \lambda_{ij}\phi_j \tag{38}$$

$$M_b \ddot{\boldsymbol{R}}_b = -\frac{\partial E}{\partial \boldsymbol{R}_b}. \tag{39}$$

In above H is the Kohn–Sham Hamiltonian $H[n(\boldsymbol{r})]$. In the electronic ground state $\ddot{\phi}_i = 0$, and Eq. (38) reduces to the Kohn–Sham eigenvalue equation $H\phi_i = \varepsilon_i \phi_i$ with λ_{ij} replaced by the energy eigenvalues ε_i of state i.

Eqs. (38) and (39) can in principle be solved by several numerical techniques. One approach is to solve the electronic equations of motion in Eq. (38) by using the scheme of Payne et al. [123], and the ionic equations of motion in Eq. (39) by using a damped steepest descent method, as detailed below.

In order to set up the dynamical equations of motion for a surface or overlayer system using the pseudopotential approach we consider an artificially defined periodic geometry along the surface

normal. For example, for an ordered (1 × 1) single monolayer deposition of Sb on a III–V (1 1 0) substrate, a super unit cell may be constructed which along growth direction includes a few (typically 7–10) atomic layers of substrate semiconductor, a single monolayer of the overlayer Sb on each side of the substrate slab, and a vacuum region equivalent of a few (typically 5–7) substrate atomic layers. With slabs constructed in such a way a coupling between the two surfaces either through the substrate or via the vacuum region can be nearly excluded. Electron–ion interaction in the form of fully separable norm-conserving ab initio KB pseudopotentials may be generated from first-principles or taken from the work of Gonze et al. [124].

For a plane wave basis set Eq. (38) can be solved analytically by following the approach of Payne et al. [123]: with a time step Δt, the equation of motion for the coefficients $A_n(\boldsymbol{k}+\boldsymbol{G})$ becomes

$$A_n^{(t+\Delta t)}(\boldsymbol{k}+\boldsymbol{G}) = 2\cos\{\omega(t+\Delta t)\}\,A_n^{(t)}(\boldsymbol{k}+\boldsymbol{G}) - A_n^{(t-\Delta t)}(\boldsymbol{k}+\boldsymbol{G}) - \frac{2[1-\cos\{\omega(t+\Delta t)\}]}{\mu\omega^2}\sum_{\boldsymbol{G}\neq\boldsymbol{G}} V(\boldsymbol{k}+\boldsymbol{G},\boldsymbol{k}+\boldsymbol{G}')\,A_n^{(t)}(\boldsymbol{k}+\boldsymbol{G}') \tag{40}$$

with

$$\mu\omega^2 = \frac{\hbar^2}{2m}(\boldsymbol{k}+\boldsymbol{G})^2 + V(\boldsymbol{G}=0) - \varepsilon_{n,k}. \tag{41}$$

In Eqs. (40) and (41) $\varepsilon_{n,k}$ represents the eigenvalue in band n of an electron with wave vector $\boldsymbol{k}$, and $V(\boldsymbol{k}+\boldsymbol{G},\boldsymbol{k}+\boldsymbol{G}')$ is the Fourier transform of the effective Kohn–Sham potential as explained earlier.

In order to solve the ionic equations of motion in Eq. (39), Stumpf and Scheffler [125] used a damped steepest descent algorithm. Accordingly, a starting configuration can be assumed and after m iterations for ionic moves new ionic positions can be obtained as

$$\boldsymbol{R}_b^{(m+1)} = \boldsymbol{R}_b^{(m)} + \beta\boldsymbol{F}_b^{(m)} + \gamma(\dot{\boldsymbol{R}}_b^{(m)} - \dot{\boldsymbol{R}}_b^{(m-1)}) \tag{42}$$

with $\boldsymbol{F}_b$ as the Hellmann–Feynman force on ion b, β as a measure of inverse force constant, γ as a damping coefficient, and $(\dot{\boldsymbol{R}}_b^{(m)} - \dot{\boldsymbol{R}}_b^{(m-1)})$ as atomic coordinate 'velocity'. Thus relaxation of the system to the nearest local minimum can be achieved in a confident manner. In the results presented in this work the atomic starting geometries were relaxed until the forces acting on the atoms were smaller than 0.025 eV/Å. In addition to determining atomic geometry, the Hellmann–Feynman forces can also be used for calculations of phonon frequencies and eigenvectors. We describe this in Section 4.2 for the determination of interface vibrational properties.

2.2.4. Beyond density functional theory

The discussion so far has been focused on ground state properties and occupied (i.e., valence band) electronic states. Calculation of excited (i.e., conduction band) states requires a theory beyond the density functional theory, either in its local approximation or otherwise. Indeed it is found that LDA calculations lead to underestimation of band gaps in semiconductors. For example, the predicted band gap at experimental lattice constant of silicon is nearly half its experimental value. It was shown by Hedin [126] and Hedin and Lundqvist [127] that excited state energies are solutions of a Schrödinger-like equation in which the xc potential term is replaced by a non-local and energy-dependent 'self-energy' operator. The effect of including such an operator can be regarded as giving rise to a 'self-energy correction' to the eigenvalues obtained from DFT.

Full-scale calculations of self-energy corrections are computationally very demanding [128–130]. However, simple approaches seem to be resulting in respectable predictions of conduction-band energies in semiconductors and their surfaces [131–135]. We do not intend to discuss any of these schemes here, and the interested reader is referred to the original papers.

3. Submonolayer coverages

3.1. Chains, clusters and superstructures

The geometrical structures of the V/III–V (1 1 0) interface in the submonolayer regime are mainly determined by three characteristic features: (i) the adatoms move rather freely, though anisotropically, on the III–V (1 1 0) surface, (ii) the adatom–adatom interaction is attractive and comparable in strength with the adatom–substrate interaction and (iii) there is practically no tendency for penetration of the adatoms into the substrate or for an exchange reaction. The last two points hold at least for Sb and Bi adatoms. In the case of Sb and Bi adsorption the attractive adatom–adatom interaction together with the mobility of the overlayer atoms leads to two-dimensional clusters with local monolayer coverage. The p valence electrons of the group-V adatoms allow formation of directional bonds with each other and with the substrate. With two group-V adatoms per surface unit cell all the p electrons can occupy σ bonding states, producing a stable, energetically favourable configuration. The group-V adatoms are then threefold-coordinated and possess a lone pair of electrons in s-like states. This picture is consistently reproduced in the majority of experiments discussed below.

STM provides a poweful tool to gain insight into the initial stages of the adsorbate–semiconductor interface formation. In the case of As adsorption impressive micrographs schematically depicted in Fig. 3 have been published by Gwo et al. [136]. They show As adatoms mostly two lattice sites apart in the centre of the As sublattice surface unit cell. The adatoms are arranged in short chains along the [1 $\bar{1}$ 0] direction of the GaAs (1 1 0) surface. The As chains have some similarity with the

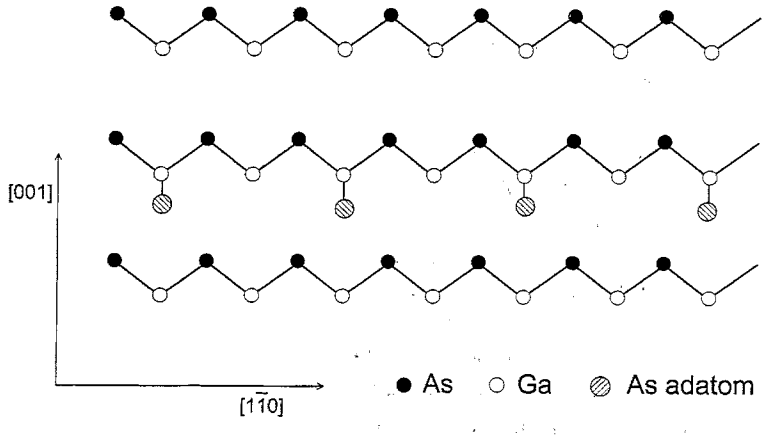

Fig. 3. A schematic model of the As adatom chain observed by STM [136].

zigzag chains of Cs adatoms on the GaAs (1 1 0) face [137]. The occupation of only every second sublattice position by Cs adatoms was explained by an effective repulsive interaction of the adatoms for low coverages [138]. Such a repulsive interaction in case of As could arise from the Coulomb interaction between slightly negatively-charged adatoms. Recent ab initio calculations [139] confirm these findings. Although in these calculations a pair-formation of As adatoms has been found to be favourable for a (2×2) surface unit cell, the atomic separation of the pair was found to be much larger than a covalent bond. Other geometrical details reported in [139] do not agree with the STM findings. However, we think that the disagreement can be explained by the computational difficulty to perform converged calculations for large reconstructions. Furthermore, a distinct anisotropy of the adatom motion on the GaAs surface has been concluded from the STM measurements [136]. As adatoms are highly mobile along $[1\,\bar{1}\,0]$, whereas no motion is observed in [001] direction. This agrees with the outcome of the ab initio calculations [139], according to which the energy barrier which hinders the diffusion along the $[1\,\bar{1}\,0]$ direction is 1.0 eV compared to 1.8 eV for the [001] direction. Both values are considerably higher than the ones found for Sb diffusion on GaAs (1 1 0) [110] (cf. next section). However, this is probably an artifact of the different calculation methods. In Ref. [110] the full total-energy surface has been calculated whereas the calculations of Ref. [139] are restricted to two trajectories.

In the case of antimony adsorption on GaAs (1 1 0), even at low coverages of some hundredths of a monolayer, Sb grows laterally in clusters which are relatively large ($\gtrsim 10$ Å according to STM observations by Mårtensson and Feenstra [10, 11]. A weak tendency towards an orientation of the islands along the $[1\,\bar{1}\,0]$ direction seems to exist. At about 0.2 ML the Sb clusters start to grow together, forming flat terraces (cf. Fig. 2). The apparent height of the terraces above the GaAs substrate is 2.5–2.8 Å, depending on the applied bias voltage. As the coverage is increased to 0.7 ML the Sb terraces coalesce, forming a continuous network extending over the entire GaAs surface. These terraces are well ordered, although some protrusions formed by excess Sb on top of the terraces as well as some small holes are found. Whereas the ordered terraces consist of two Sb atoms per GaAs (1 1 0) surface unit cell, regions of intermediate height near some terrace edges as well as in the middle of the terraces are interpreted to arise from a half-monolayer coverage. The STM finding of Sb growing in 1 ML high ordered patches has already been deduced by Carelli and Kahn [7] in their early LEED and AES study and is in accordance with EELS [140] and RHEED measurements [141].

The strong tendency towards formation of two-dimensional clusters with monolayer character even for very low coverages makes it difficult to identify a preferential bonding site for single Sb atoms on GaAs (1 1 0): EELS measurements by Strümpler and Lüth [12] are interpreted at variance to the STM findings discussed above. They found a rapid suppression of a Ga-characteristic excitonic transition which they explain in terms of a preferential bonding of Sb atoms to Ga sites. According to cluster formation such a transition should show a nearly linear decrease in intensity as a function of coverage, as was indeed observed in an earlier study by Li and Kahn [142]. On the other hand, Schäffler and co-workers [14,35] interpret the intensity of their observed Sb 4d spectra in terms of energetically favoured As sites. Since the ordered Sb layer gets much of its binding energy from the Sb–Sb bonds along the chains, they conclude that the preference of the As site is most likely limited to the end positions of chains with random length distribution. This conjecture is based on the assumption that the Sb atom bonded to Ga has less tightly bound core electrons than the Sb atom bound to As. This has recently been supported by a comparison of measured and calculated

PED intensities [71]. However, we mention that the intensity and the corresponding ratio of the two components seen in the Sb 4d spectra critically depend on the experimental conditions. It is quite likely that the intensity ratio is influenced by diffraction effects. Thus it is rather difficult to determine unequivocally the preferred bonding site of Sb for low coverages. Also for Sb/InP there is no unique opinion whether or not there occurs a preferential bonding of the adatoms to one of the substrate constituents. On the basis of Schottky barrier measurements by means of Raman [143] and PES [144,145] it was suggested that Sb–P bonding does not occur or that the Sb–In bond should be highly preferential. A preferential Sb–In bonding for coverages below half a monolayer has also been concluded from a cation surface-exciton study [146]. We tend to believe that the strong similiarities between the monolayer phase of Sb on GaAs and InP (1 1 0) surfaces which will be discussed in Section 4, should also apply to the submonolayer regime. Therefore we expect an epitaxial island growth involving both In and P sites as indeed concluded from their LEED experiments by Ford et al. [43]. More direct observations, possibly by means of STM, are needed to clarify this point.

STM has also been applied to study the onset of the interface formation for Bi/GaAs (1 1 0) [16,17,50,51]. Terraces are observed for a nominal half-monolayer Bi coverage, which appear to nucleate randomly on the surface and grow laterally in size as the coverage increases. The terraces are about 2.6 Å in height corresponding to local monolayer coverage and show (1 × 1) symmetry. However, there is a conspicuous difference compared with the case of antimony adsorption as the terraces grow laterally. Along the [1 $\bar{1}$ 0] direction there are approximately every six unit cells surface regions, where one or more Bi atoms are missing. These dislocations are associated with a misfit in lateral size between the Bi overlayer and the underlying GaAs substrate. A plausible explanation for the presence of these dislocations, which are not observed for antimony overlayers, is the size difference between Bi and Sb atoms. The covalent radius of Bi is more than 4% larger than that of Sb (cf. Fig. 1). The Bi overlayer nucleates randomly and grows non-preferentially until the chain length reaches the strain-limited critical length. This can also be concluded from measurements of the Bi 5d core levels which indicate the existence of two differently bound Bi atoms in the submonolayer regime [16,18]. Further cluster growth then occurs only in the [0 0 1] direction, which results in elongated islands. As clusters near critical size meet they do not coalesce, but rather maintain their common boundary in the form of the dislocation consisting of missing Bi atoms. LEED analyses [77,78] arrived at the same results for the interface structure in the submonolayer regime. The picture of the formation of two-dimensional patches in the submonolayer region which grow together with increasing coverage is corroborated by an analysis of the Bi 5d, Ga 3d, and As 3d core-level shifts during the interface formation. Joyce et al. [18] found for Bi coverages less than 1 ML two components in the Bi 5d core level. These two components have been assigned to Bi–Ga and Bi–As bonding configurations and are of equal intensity. The equal intensity of these two components even at very low coverages indicates that Bi has no preferential bonding site between the two available sites on the GaAs (1 1 0) surface but rather forms chains and two-dimensional patches on the substrate.

A two-dimensional island growth in the low coverage regime has also been deduced for Bi adsorption on InP (1 1 0) from LEED experiments [22,43]. However, in contrast to the GaAs substrate essentially no constraint of the chain length in [1 $\bar{1}$ 0] direction was observed. This can be understood as consequence of the about 4% larger lattice constant of InP compared with GaAs. Thus, the unit cell of InP accomodates the large Bi atoms more readily than GaAs. Essentially the

same picture arises from the evaluation of the core-level spectra during the interface formation between Bi and InP (1 1 0) [147]. Miyano and co-workers observed for Bi coverages below 1 ML a 5d core-level emission which is best fitted with two nearly equal intensity components (cf. Fig. 4), representing the two inequivalent sites on the Bi zigzag chain. However, core-level studies from another group [148,149] arrive at different conclusions: A strong asymmetry in the intensity of two observed 5d core-level components was interpreted as indication of a preferential bonding of Bi to one of the substrate species. On the basis of chemical arguments it has been said that the In atom is the more likely choice for a single adsorption site. The results of photoemission extended X-ray absorption fine-structure (PEXAFS) experiments [150] could also be interpreted as indication for a preferential Bi–In bonding in the submonolayer regime. Further experiments, in particular STM, would be helpful to clarify if the growth morphology of Bi/InP (1 1 0) is indeed different compared to other V/III–V (1 1 0) systems, at least for $\Theta < 1$ ML. On the basis of the experimental date available to date and on grounds of the similar monolayer properties between Bi/InP and most other V/III–V (1 1 0) interfaces we believe, however, that submonolayer Bi on InP (1 1 0) grows in flat, two-dimensional clusters with local monolayer structure. A laminar growth mode up to the first monolayer seems also to occur for Bi overlayers on InAs (1 1 0) as has been concluded from the linear development of the In core-level intensity vs. coverage [57]. The already mentioned misfit between

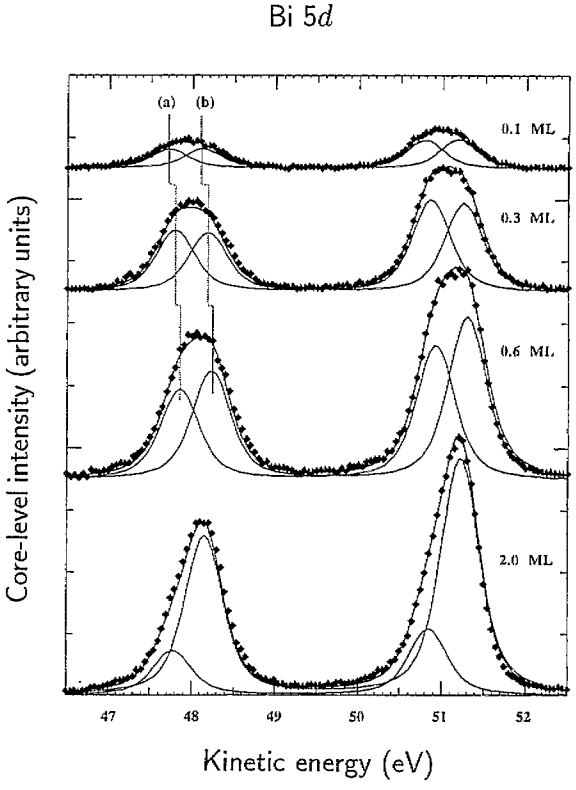

Fig. 4. Bi 5d core levels for selected Bi coverages on p-type InP. Between the two components of nearly equal intensity needed to fit the core level a splitting of about 0.4 eV is derived. From [147].

Bi overlayers and GaAs substrate is even more accentuated when Bi is deposited on GaP (1 1 0) substrates. The lattice constant of GaP is nearly 4% smaller than that of GaAs. Therefore we would expect the formation of ordered lattice matched overlayers structures to be even more hindered than observed for Bi/GaAs. Indeed, STM images show that at nominal monolayer coverage a significant fraction of the Bi atoms are in three-dimensional clusters rather than forming chains in the first monolayer [46].

The submonolayer structures discussed above show only local ordering. For antimony overlayers on III–V (1 1 0) substrates we are aware of only one report concerning unit cells larger than (1 × 1) for submonolayer coverage. In a RHEED study [141] of Sb adsorption on GaAs (1 1 0) a p(3 × 2) phase has been found with a coverage of 0.9 ± 0.1 ML. Such a phase could be prepared upon annealing of 20 ML Sb crystallized on GaAs (1 1 0). It was said to be thermodynamically more stable than the (1 × 1) (1 ML) structure and interpreted as a defect phase. In contrast to that a variety of superstructures are observed for annealed Bi adlayers. When Bi overlayers of one or more monolayers on InAs, GaSb or InSb (1 1 0) surfaces are annealed a (1 × 2) superstructure forms [52]. Further annealing of the Bi/InSb interface leads to a (1 × 3) ordering accompanied with a Bi loss from 0.6 ML to about 0.4 ML as measured with AES [52]. It has been speculated that the (1 × 2) and (1 × 3) symmetries arise due to regularly spaced missing [1 $\bar{1}$ 0] rows [151]. Thin bismuth films on GaSb (1 1 0) have been studied recently with a variety of techniques [58–60,152,153]. After annealing the ordered (1 × 1) monolayer structure at about 200°C a distinct (1 × 2) LEED pattern appears. The reconstructed phase is stable in a rather wide temperature range (~ 200–280°C) [60]. However, there is no consensus about the amount of bismuth involved in the formation of this superstructure. Ford et al. [52] observed in their combined LEED and Auger study that the (1 × 2) structure appears in a wide range of coverages, from 0.4 to 1.5 ML. From the photoemission intensity of the core levels McIlroy and co-workers conclude that the (1 × 2) phase corresponds to a coverage of one monolayer of Bi. However, more recent AES [59] and PES studies [58,60] indicate a smaller coverage between 0.6 and 0.7 ML. Owing to uncertainty in the determination of the coverage there are several structural models discussed which could possibly explain the experimental findings. The monolayer model by McIlroy et al. consists of two inequivalent Bi chains which are bound both to the substrate and to each other (cf. Section 4.1.1 and Fig. 5). On the other hand, the sudden reappearance of the Ga-related surface exciton in the (1 × 2) phase observed with EELS [59,60] demonstrates the presence of free Ga dangling bonds at the surface. Together with the estimation of a Bi coverage of ~ 0.6–0.7 ML this suggests that the reconstruction of the surface is accompanied by a partial uncovering of the topmost Ga atoms. In calculations for submonolayer Sb coverage on GaAs (1 1 0) we find that a missing chain structure (MCS) is rather favourable, where every second adatom zigzag chain is removed (cf. Section 3.2 and Fig. 7(c)). Possibly, such a structure could also explain the experimental findings for Bi/GaSb as has been proposed by van Gemmeren and Johnson on the basis of their photoemission experiments [58]. However, the investigation of larger reconstructions induced by submonolayer group-V adsorption on III–V (1 1 0) surfaces is still in the initial stages and more data are needed to develop a comprehensive picture of these complex structures.

3.2. *Born–Oppenheimer surface and the atomic structure*

Theoretical support for understanding the experimental results discussed above from a phenomenological point of view comes from ab initio studies of submonolayer antimony-covered

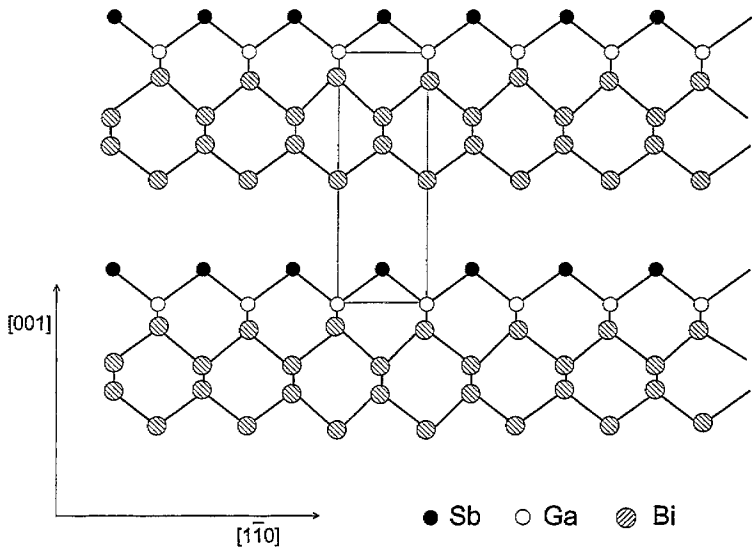

Fig. 5. Top view of the (1 × 2) phase of Bi/GaSb (1 1 0) according to the geometrical model proposed by McIlroy et al. [152]. The (1 × 2) surface unit cell is indicated.

GaAs (1 1 0) surfaces [110,154,155]. In particular the total-energy (or Born–Oppenheimer) surface mapped out by single adatoms on the substrate is useful to explain adsorption sites and diffusion phenomena for very low coverages. The total-energy surface was calculated by determining the adsorption energy of Sb for 32 adatom positions in the irreducible part of the 1 × 1 surface unit cell for $\Theta = 1/2$, i.e., one Sb atom per surface unit cell [110]. Thereby the adsorbate coordinates are fixed parallel to the GaAs (1 1 0) surface whereas both the adsorbate–surface distance and the substrate atomic positions are fully relaxed. The resulting Born–Oppenheimer energy surface of a Sb adatom is shown in Fig. 6. The most striking feature is the deep channel which is quite rectilinear and parallel to the [1 $\bar{1}$ 0] direction, i.e., the direction of the GaAs zigzag chains. There are no minima in front of the Ga or As dangling bonds. This is quite in contrast to the adsorption of group-I, group-III, or group-VI elements, where minima in front of the surface anion and/or cation have been found [138,156–158]. In the total-energy surface of Fig. 6 we find instead two equivalent flat minima per surface unit cell which correspond to a long-bridge-bond position of the Sb adatom between Ga and As atoms of different surface chains. These minima are separated in the [1 $\bar{1}$ 0] direction by barriers of 0.18 eV in front of the As atoms and 0.35 eV in front of the Ga atoms. Perpendicular to the channel, i.e., in the [0 0 1] direction, the energy barrier is calculated to be about 1.2 eV. Although the numerical accuracy of these results may be questionable, due to direct and substrate-related interaction between neighbouring Sb atoms (cf. Fig. 9 in [110]), qualitative conclusions can be drawn: The mobility of adatoms along [1 $\bar{1}$ 0] direction can be understood as they can run along the trench between the GaAs zigzag chains while the motion along the [0 0 1] direction requires that adatoms climb over the zigzag chains. Due to the isovalence of the considered systems we expect the Sb results to characterize well the general trends of the early stages of group-V adsorption on III–V (1 1 0) surfaces. In particular the large difference of the energy barriers in [1 $\bar{1}$ 0] and [0 0 1]

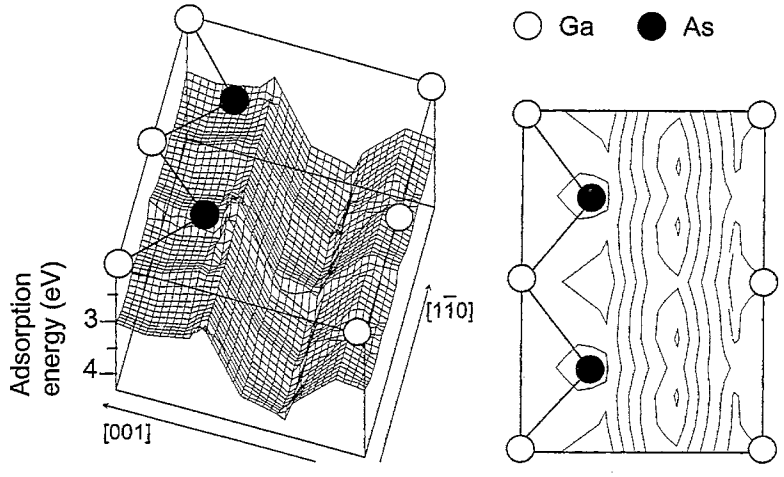

Fig. 6. The total-energy surface of the Sb/GaAs (1 1 0) ($\Theta = 1/2$) system is plotted over an area of two GaAs surface unit cells as three-dimensional perspective view and as a contour plot. From [110].

directions, $E_{\parallel}$ and $E_{\perp}$, should lead to a strong anisotropy of the diffusion of single adatoms on the substrate, since they would lead to a distinct difference between the diffusion coefficients $D_{\parallel,\perp} \sim \exp(E_{\parallel,\perp}/k_B T)$. These theoretical findings are qualitatively in agreement with experimental investigations of the motion of As on GaAs (1 1 0) [136]. Due to the strong tendency of all group-V elements to form two-dimensional patches on III–V (1 1 0) no experimental verification of the proposed long-bridge-bond position [154] for single Sb atoms on GaAs (1 1 0) has been given yet. Such a coordination of single antimony adatoms has also been proposed by Flores et al. [159], whereas a later study by the same group came to a different conclusion [160]. After slight modifications of their tight-binding (TB) approach they found a position in front of the As dangling bond to be more favourable for single Sb adatoms. The same position was also found to be favourable for single As adatoms [139,160,161].

Further information about the onset of the interface formation comes from ab initio studies of different surface reconstructions for the half-monolayer coverage [110,155]. The three structures considered consist of Sb chains of different form and orientation (Fig. 7) on GaAs (1 1 0). One geometry corresponds to the zigzag chain parallel to the [0 0 1] direction with Sb adatoms bonded to the Ga and As dangling bonds as shown in Fig. 7(a). Linear chains of Sb atoms along [0 0 1] on top of each second row of Ga atoms are considered in Fig. 7(b). Finally an MCS, consisting of Sb zigzag chains which are orientated along [1 $\bar{1}$ 0] and bonded to every second surface cation and anion (Fig. 7(c)) is investigated. All structures give rise to local minima in the total energy. However, the MCS is energetically much favoured over the two other structures. The adsorption energy per adatom is about 0.4 eV higher compared to the structure of Fig. 7(a). Even less favoured are linear chains of Sb adatoms. Also single Sb atoms on the GaAs surface bonded in long-bridge-bond position are energetically less favoured (by about 0.4 eV) than Sb atoms arranged in the MCS. There is a considerable amount of energy gain due to the condensation of single adatoms to zigzag chains along [1 $\bar{1}$ 0]. Comparing the energetical results for the MCS with those of Sb atoms adsorbed in the

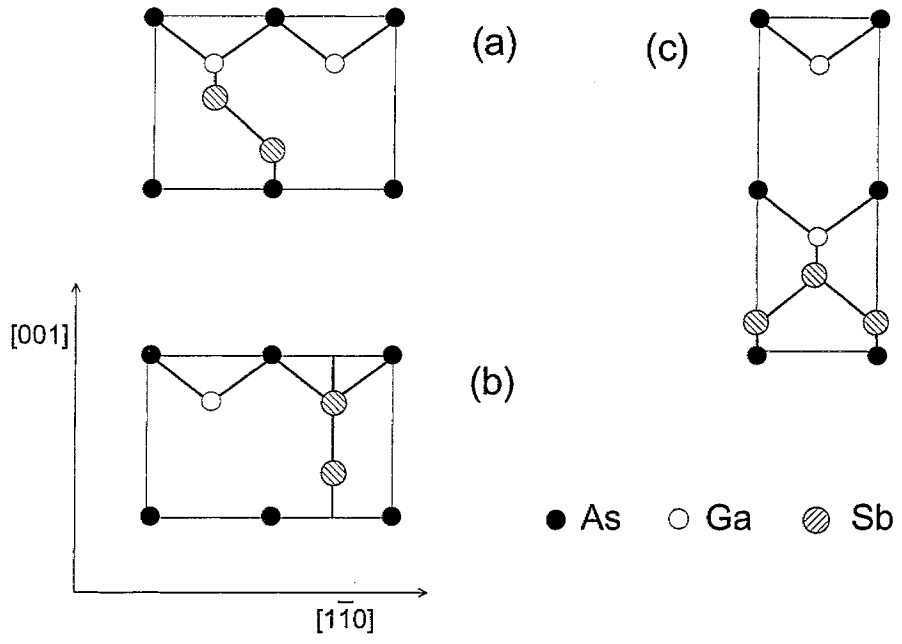

Fig. 7. Reconstructed geometries considered for Sb/GaAs (1 1 0) with $\Theta = 1/2$. Top views of 2 × 1 [(a) and (b)], and 1 × 2 (c) symmetries.

minimum energy configuration for the 1 ML (cf. Section 4.1.2) we find a further increase in the adsorption energy per atom by about 0.2 eV.

In conclusion, we find an energetical favouring of an inhomogeneous coverage over the homogeneous distribution of adatoms in the submonolayer case. There is an attractive force between the adatoms until the first monolayer is completed. This is in agreement with the experimental findings described above. The tendency underlying these results is the realization of completely filled bands and saturated bonds which becomes possible through the formation of overlayer zigzag chains, but cannot be achieved with adsorbed single atoms. Additionally, in contrast to group-I [156] or group-VI adsorption [158] there is little charge transfer between group-V adatoms and the substrate (see Section 6.1). Therefore there are no significant repulsive Coulomb forces to hinder the condensation of adatoms and the formation of islands with local monolayer coverage. This holds at least for Sb and Bi atoms whose electronegativities lie between the values of substrate anions and cations. In the case of As adsorption on GaAs (1 1 0) a slight charge accumulation around the adatoms may prevent the condensation for low coverages. The MCS is energetically most favourable of all submonolayer structures considered in the calculations. The bonding within the MCS resembles closely to the one for the ordered monolayer discussed in Section 4. This supports the interpretation of experimental results for ordered submonolayer Bi structures on InAs, GaSb or InSb (1 1 0) surfaces in terms of the MCS [58,151].

Because of their possible importance we will briefly discuss the atomic structure of the MCS as determined in ab initio calculations for Sb on GaAs [110,155]. The buckling of the free GaAs (1 1 0)

surface has been reduced to 0.42 and 0.18 Å for the As and Ga atoms bonded to the Sb overlayer chain. The substrate buckling induces a small tilt angle for the Sb zigzag chain. The Sb atom bonded to As is displaced outwards by 0.14 Å with respect to the one bonded to Ga. We calculate bond lengths $d_{Sb-Sb} = 2.78$ Å, $d_{Ga-Sb} = 2.61$ Å, and $d_{Sb-As} = 2.73$ Å which are close to the sum of the covalent radii 2.80, 2.66, and 2.60 Å (cf. Fig. 1), indicating the chemical stability of the MCS.

Sb zigzag chains on GaAs truncated in the $[1\,\bar{1}\,0]$ direction have been recently investigated for $\Theta = 5/8$ [162]. By means of ab initio total-energy calculations Magri finds an energetical tendency to terminate the Sb chains at substrate As atoms. This is in agreement with the early assumption of Schäffler and co-workers [14,35] based on their PES measurements. The chain-terminating Sb atoms tend to move towards a threefold coordinated position where they are bonded to both substrate species. This is achieved by considerable reduction in the adatom height with respect to the substrate plane.

3.3. Electronic structure

The electronic properties of the interfaces formed by group-V adsorption on III–V (1 1 0) surfaces for submonolayer coverages are direct consequences of their atomic structure discussed in Sections 3.1 and 3.2. In particular the strong tendency of the adatoms to coalesce into islands with local monolayer coverage determines properties like the local density of states. Within the area of these islands the interface electronic properties are like those of ordered monolayers (see Section 4.3), i.e., characterized by completely filled and empty bands mainly outside the bulk band gap region. Only at the edges of these islands and in regions where the ideal monolayer order is disturbed, broken bonds give rise to a finite density of electronic states within the bulk band gap region. The number of edge states depends on size and order of the two-dimensional clusters, which are influenced by the experimental conditions. Such a picture is in agreement with the available experimental data.

While detailed experimental studies on the surface atomic structure in the submonolayer regime are still missing, there exists a wide body of information pertaining to the change of the surface electronic properties during the early stages of the adsorption. Mattern-Klosson and Lüth [163] have studied the band bending changes due to the deposition of Sb on GaAs (1 1 0) surfaces by UPS. They found the dipole contribution to the work function change (for definitions see Section 6.1) to depend nearly linearly on the Sb coverage in the submonolayer region. However, the saturation band bendings of 0.65 and -0.5 eV for n- and p-type material were seemingly reached for Sb coverages around 0.1 ML. The results were explained using the defect model [164,165]. Similar results obtained by Cao et al. [13,166], applying soft XPS, are shown in Fig. 8. The Fermi level moves monotonically towards the mid-band gap and is stabilized around 0.75 and 0.5 eV above the VBM for n- and p-type GaAs, respectively. The pinning position for low temperature deposition is the same as for RT. The somewhat deviant data obtained at 150 K result probably from a sample with inferior quality. The drastic change of the Fermi level position already for relatively low coverages (~ 0.1 ML) was suggested to be due to native defects of GaAs created during the course of Sb deposition. Disorder was considered responsible for the 0.4 eV band bending caused by 0.5 ML Sb on n-type InP [40]. These findings for Sb/GaAs and Sb/InP are consistent with more recent studies by Geurts [90] and Esser et al. [69]. The assumption of an overlayer disorder-induced Fermi level pinning in the submonolayer regime is corroborated by investigations of annealing effects on the position of the Fermi level [14,35,69]. At all coverages a reduction in barrier height of up to

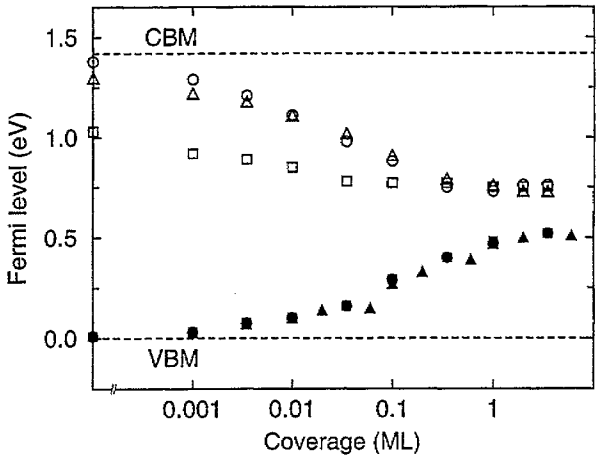

Fig. 8. Surface Fermi-level position at the Sb/GaAs (1 1 0) interface as a function of Sb coverage at three different temperatures (RT (circles), 150 K (squares) and 80 K (triangles)) as determined by PES [13,166]. Filled and empty symbols refer to measurements of p- and n-type substrates, respectively.

a factor of two upon annealing at 330°C has been observed for Sb adsorbed on p- and n-type GaAs cleaves. Also for Bi adsorption on InP the Fermi level seems to be governed by imperfections in the overlayer for $\Theta < 1$ ML [148, 149]. In particular the systematic turn-around in the barrier-height development on both n- and p-type InP for coverages between 0.3 and 1.0 ML supports the view that the submonolayer stages of band bending are due to states created at the edges of the two-dimensional patches [147].

Unfortunately, the measurements of the Fermi level give only integrated information about the pinning electronic states. However, a hypothesis about their nature can be checked by means of STM which by definition allows a spatially resolved measurement of the DOS. Feenstra and Mårtensson [9,167] have studied the Fermi level pinning at the Sb/GaAs (1 1 0) surface. They show spectra acquired on top of an Sb terrace and near the edge of a terrace. On top of the terrace the spectrum exhibits no DOS in the surface band gap which is equal in size to the GaAs bulk gap, indicating that the surface states do not extend significantly into the bulk gap. In contrast to that near the edges of ordered Sb islands on GaAs (1 1 0) additional states appear within the band gap region (cf. Fig. 9). The state P_2 is reproducibly observed in most edge spectra, whereas P_1 is only visible in some of the edge spectra. These band gap states comprise two separate bands of filled and empty states, with the surface Fermi level pinned between the two bands. These observations rule out proposed models for Fermi level pinning, at least for Sb/GaAs. In terms of defects, it is hard to imagine that antisites or other such defects are concentrated only at the edges of the Sb terraces. The states observed in [9,167] arise from dangling bonds localized near the edges of Sb terraces. This can also be reconciled with the observed tendency for reduced band bending upon annealing. The thermal energy allows to overcome the diffusion barriers and larger clusters form, thereby reducing the density of dangling bonds. A rather similar behaviour has been observed for Bi/GaAs (1 1 0). Gap states were associated with Bi terrace edges for coverages below one monolayer in an STM study by Ludeke et al. [16] and Feenstra et al. [51]. The energy location of the observed terrace feature is

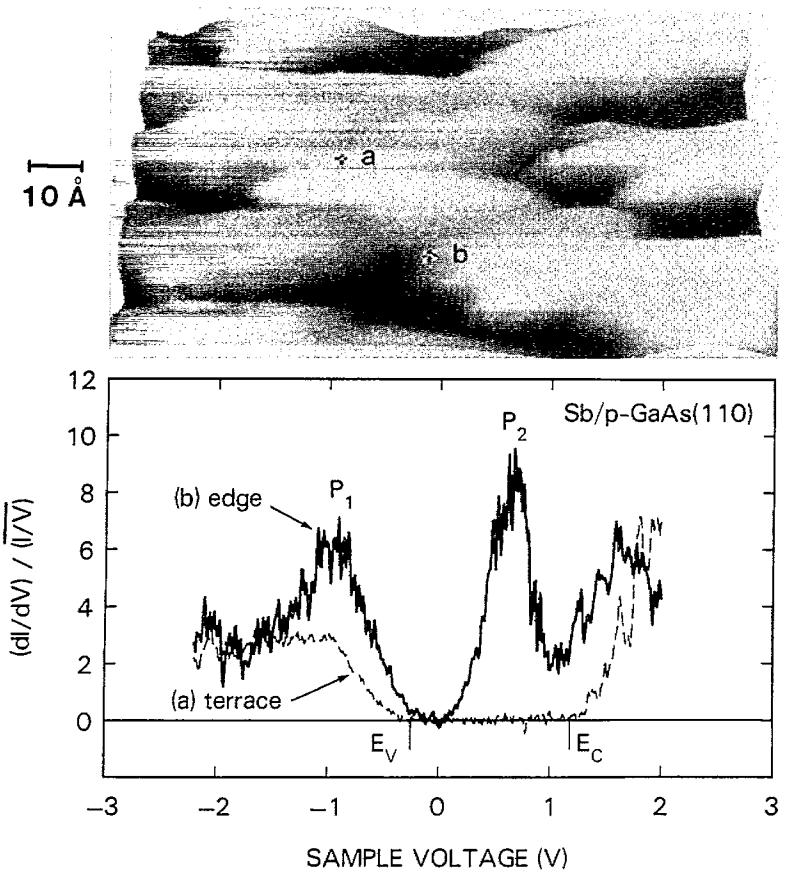

Fig. 9. Normalized conductivity vs. voltage, measured on top and on the edge of an Sb island. The associated STM image is shown in the top part of the figure, with the locations indicated at which the spectra were acquired. Pinning states observed in the edge spectrum are denoted by P_1 and P_2. From [9].

about 0.5 eV higher than the band gap states seen for Sb clusters on GaAs (1 1 0), but aside from this shift the nature of the spectrum is quite similar to that seen in Fig. 9. However, the precise character and atomic origin of these states is not fully understood yet. One can speculate that close to the terrace edges the buckling of the clean surface is lifted [138], so that the Ga and As dangling bond-related surface bands move into the fundamental gap. These states may pin the Fermi level in the n- or p-case if they are not completely empty or filled. They can be understood as metal-induced [168,169] or edge-induced defect [165] gap states.

Theoretical calculations by Menon and Allen [170] provide some explanation for the above observation. They find that disordered Sb or Bi clusters give rise to a spectrum of gap states similar to that which is observed. The states arise mainly from the dangling p-states of the Sb or Bi atoms in the cluster. A series of submonolayer Sb-induced reconstructions of the GaAs (1 1 0) surface have been investigated by Manghi and Calandra [171]. In their TB study they find that missing Sb chains

induce extra states in the GaAs band gap near the edges of valence and conduction bands. Truncated Sb chains give rise to very flat bands of p character in the optical gap. p-states have also been found responsible for the Fermi level pinning in more recent studies [162,172] for Sb/GaAs (1 1 0) for $\Theta = 5/8$. The corresponding 4×1 unit cell of Ref. [172] is indicated in Fig. 10. The resulting overlayer structure forms infinite terraces of width $\sqrt{2}a$ separated by stripes of the clean surface of the same width. Two Sb dangling bonds appear per unit cell. These states are strongly localized on the terrace edges in agreement with the STM results [9,167]. However, the inclusion of a Hubbard correlation between the Sb p-states was necessary to reproduce qualitatively the non-metallic spectrum experimentally observed. A transition into a Mott–Hubbard insulating state is proposed to be due to a Hubbard interaction $U = 1.2$ eV, similar to the case of alkali adsorption on GaAs (1 1 0) [138,173]. However, the considered geometrical models are certainly very simplified, and may be responsible for the deviation between theory and experiment. The computational necessity to limit the dimensions of the surface unit cell does not allow study of realistic reconstructions around the steps or complicated geometries of the terrace edges.

Little has been done so far to explore the electronic properties of large reconstructions in the submonolayer regime observed for some V/III–V (1 1 0) interfaces. An exception in that direction is the Bi/GaSb (1 1 0)(1 × 2) system (one hypothetical structure is shown in Fig. 5), on which some experimental studies have been performed in recent years. The occupied surface bands have been measured with ARPES [152], distinguishing four surface states. All of them were found to lie below the bulk valence-band edge. However, the results are in contrast to those obtained by means of HREELS [60,153]. In these measurements a semimetallic character of the interface due to a crossing of Bi-induced electronic states with the Fermi level has been deduced. More studies are needed to relate coverage, geometry and electronic structure in a correct manner.

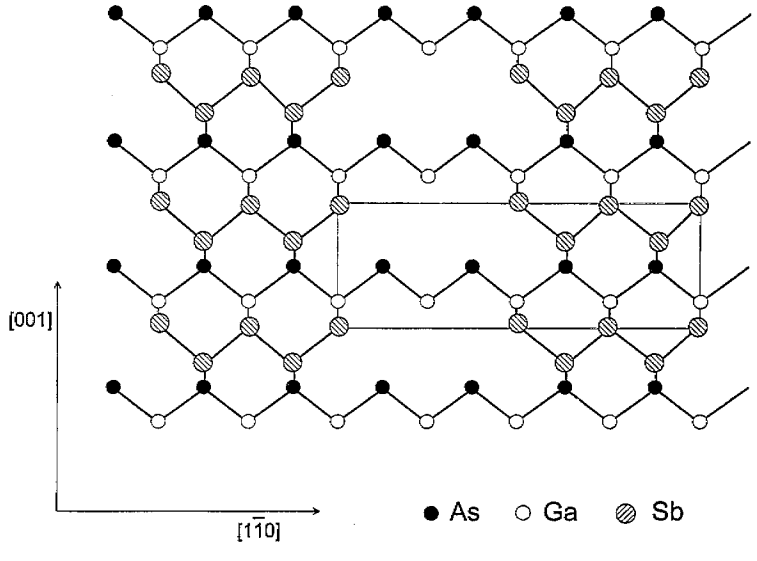

Fig. 10. Schematic diagram of the Sb/GaAs (1 1 0) surface for $\Theta = 5/8$ with 4×1 truncated symmetry. After [172].

4. Monolayer coverage

4.1. Atomic structure and bonding properties

4.1.1. Structural models

The determination of the atomic structure of surfaces and interfaces is, in spite of the availability of sophisticated experimental and theoretical tools, still dependent on some empirical input which comprises knowledge of general physical and chemical principles. The actual interface geometry is determined by a trade-off between the drive to saturate the dangling bonds and create an insulating surface, and the amount of strain which can be accommodated by the surface and subsurface layers of the material. It is the balance between the energy gain due to the reduction of dangling bonds and the energy cost due to induced strain that determines the nature of the adsorbate structure. The development of the understanding of the interface geometry for group-V atoms adsorbed on III–V (1 1 0) surfaces during the last 15 years shows how joint efforts of experiment and theory together with intuitive guesses are able to cast light on the interface structure.

From early PES and LEED studies by Skeath et al. [4] it has been concluded that Sb at the monolayer coverage binds to two different sites in the GaAs (1 1 0) surface unit cell. The authors recognized that for RT adsorption the Sb atoms form an ordered overlayer structure with the same translational symmetry as the clean GaAs (1 1 0) surface, i.e., a p(1 × 1) structure. The bonds between Sb and the substrate atoms were assumed to be highly directional and covalent. On grounds of chemical arguments they proposed two models [5,6,75] for the atomic arrangement of the Sb/GaAs (1 1 0) interface. A zigzag chain of antimony atoms has been chosen as a basis unit for the structural models. So each Sb atom is bonded to two other Sb atoms. The Sb zigzag chain is similar to the zigzag chains of alternating Ga and As atoms on the (1 1 0) surface and in Model I (in the following denoted as p^3-structure, cf. Fig. 11(b)) they are superimposed. In this configuration, all Sb p electrons are in tightly bound σ orbitals. One Sb atom is triply coordinated with two p electrons in the Ga–Sb bond orbital and one p electron is left for the Sb–Sb bonds, whereas the other Sb atom can accomodate all three 4p electrons in the Sb–Sb bonds. The 4s electrons are in tightly bound 'lone-pair' orbitals. Another possibility to accommodate the Sb zigzag chain has been proposed as Model II (in the following denoted as epitaxial continued layer structure (ECLS), cf. Fig. 11(a)). In such a geometry the relaxation of the GaAs surface lattice is lifted and the Sb chain may occupy the 'next lattice layer sites' defined nearly by GaAs bulk positions. The energetical requirement for the ECLS is that upon formation of the additional Sb–As bond there is an energy release which compensates for the energy required to remove the GaAs (1 1 0) relaxation (about 0.5 eV per surface atom according to Ref. [169]). In the ECLS the Sb valence electrons are more evenly distributed compared to the p^3-structure and both Sb atoms are three-fold coordinated, which may explain the thermodynamical stability of the ordered Sb monolayer. However, Skeath et al. [5,6,75] were not able to discriminate between the proposed structures on the basis of their experimental data.

Considering the strong tendency for column-V elements to form diatomic molecules and knowing that the ordered Sb monolayer has two atoms per unit cell, it is also natural to think in terms of an Sb_2 molecule (dimer) bonded inside each surface unit cell (Fig. 11 (e)). The empty p orbital on the Ga atom is a likely bonding site, but this takes care of at most two of the Sb_2 electrons. Such a Sb_2 molecule bonded to the surface Ga atom has been favoured in a preliminary LEED study by Carelli and Kahn [7]. A thorough examination of five qualitatively distinct classes of geometrical models

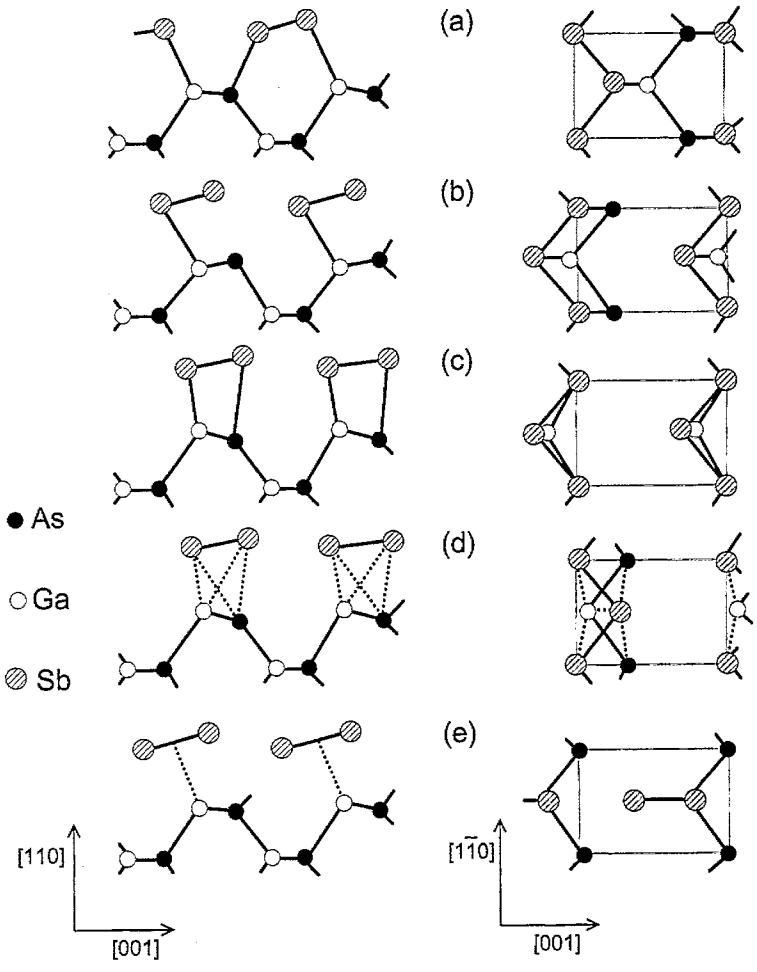

Fig. 11. Schematic representations of side and top views for five classes of surface geometries for the V/III-V (1 1 0)-p(1 × 1)(1 ML) system: (a) epitaxial continued layer structure (ECLS), (b) p^3-structure, (c) epitaxial on top structure (EOTS), (d) epitaxial overlapping chain structure (EOCS), and (e) dimer model.

for the Sb adsorption on GaAs (1 1 0) has been performed by means of a dynamical LEED analysis by Duke and co-workers [8]. Apart from the three models discussed above, the ECLS, the p^3-structure, and the Sb_2 dimer and epitaxial overlapping chain structure (EOCS) (Fig. 11(d)) and a defect model corresponding to $\Theta = 1/2$ have been considered. The EOCS corresponds to a diffuse π bonding between the Sb chains in the overlayer and the GaAs chains in the (1 1 0) substrate and is characterized by a high coordination of the Sb atoms. Only one of these models, viz. the ECLS, provided a reasonable description of the measured LEED intensities [8].

Interest in chemisorbed Sb on InP (1 1 0) was stimulated by the studies of Williams et al. [37,174] who noted that for RT Sb deposition ordered, saturated p(1 × 1) one monolayer structures occur in analogy with the observation of such structures on GaAs. Duke and co-workers [39] performed

a dynamical LEED analysis to determine the atomic structure of this interface. Within the class of the ECLS they found two surface geometries with different overlayer buckling which yielded an acceptable description of their experimental data. The atomic parameters of the ECLS for Sb adsorbed on a series of III–V (1 1 0) substrates were optimized by means of the minimization of the total energy within a TB scheme [63,175,176]. The structural parameters determined theoretically were found to be in reasonable agreement with the ones obtained from the dynamical LEED analysis for Sb/GaAs (1 1 0) [8] and Sb/InP (1 1 0) [39]. The atomic geometries of the four monolayer models discussed above have also been compared with STM images obtained for Sb/GaAs (1 1 0) (1 ML) [10]. The best fit between experiment and model was found for the ECLS. The STM study suggested, however, that the p^3-structure was also compatible with the experimental data as indicated in Fig. 12.

This ambiguous result motivated a re-examination of the problem. Using essentially the same model as described in [63,175,176] LaFemina et al. [95,177] found that the p^3-structure did not represent a local minimum in the potential energy surface of their TB total-energy approach, but rather relaxed into the epitaxial on top structure (EOTS), cf. Fig. 11(c). The EOTS saturates all of the surface atom and adsorbate dangling bonds, and, like the ECLS, leads to a chemically saturated surface. This structure differs from the ECLS by virtue of the registry of the Sb zigzag chains on top

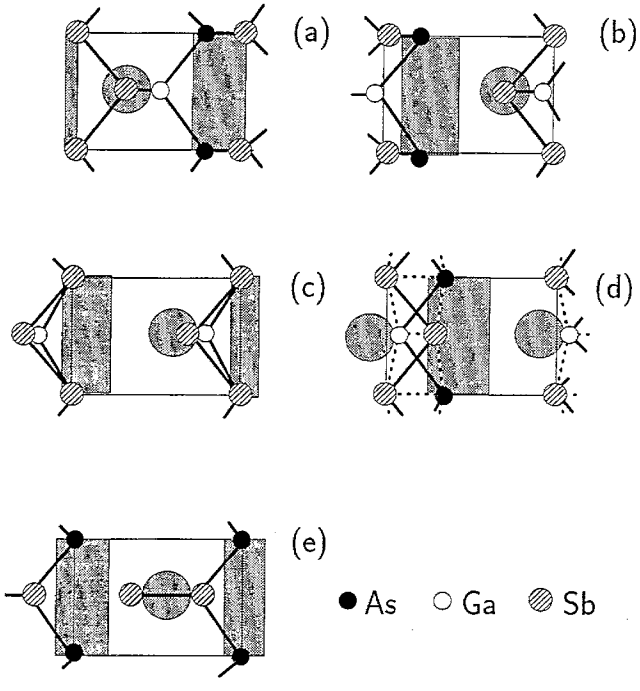

Fig. 12. Schematic diagrams of the surface geometry for the V/III–V (1 1 0)-p(1 × 1) (1 ML) system: (a) epitaxial continued layer structure (ECLS), (b) p^3-structure, (c) epitaxial on top structure (EOTS), (d) epitaxial overlapping chain structure (EOCS), and (e) dimer model. Shaded areas indicate the uncertainty in the position of Sb adatoms as determined by STM [10] for the Sb/GaAs (1 1 0) system.

rather than in between the substrate zigzag chains. The EOTS was found to be equally compatible with both photoemission and STM data [95,177]. Also experimental results such as a core-level study for Sb/InP [148] and resonant Raman scattering on Sb/GaAs and Sb/InP surfaces [83] have been interpreted to show an indication for the occurrence of the EOTS. Recent LEED analyses, however, which for the first time explicitly examined the EOTS, found that the EOTS did not describe the LEED intensities for Sb on GaAs (1 1 0) [178] or InP (1 1 0) [43] as well as the ECLS did. LaFemina et al. [95,97,177] also examined the possibility that the formation of the ECLS or EOTS is a function of the mismatch between the overlayer and the substrate. As the adatom–adatom bond length is increased (or the anion–cation bond length in the substrate is decreased), preservation of the p(1 × 1) symmetry of the surface requires the lateral expansion of the adatom zigzag chain. Such an expansion can take place in the [0 0 1] direction and/or perpendicular to the surface. However, the latter expansion would necessarily weaken the adatom–substrate bonding and should therefore be less important compared with the [0 0 1] expansion. Such an atomic shift diminishes the overlap between the dangling bond charge density of the substrate and the p-charge density of the overlayer chain in case of the ECLS, while in the EOTS this overlap is increased. However, up to now no experimental or theoretical evidence has been found for such a crossover between ECLS and EOTS for adsorption of column-V elements on the commonly available III–V (1 1 0) substrates. The reason for the failure of the EOTS as adsorption model may be traced back to the bond angles, which are distinctly different from the ideal sp^3 bond angles, whereas the ECLS allows the surface atoms to remain favourably sp^3-hybridized. Also more recent experimental techniques as XSW [64], GIXD [36] and PED [73] support the ECLS for Sb/GaAs. Even in case of Sb adsorption on the (1 1 0) surface of GaP, which has about 4% smaller lattice constant than GaAs, XSW [47] and surface extended X-ray-absorption fine-structure (SEXAFS) [179] studies by Miyano and co-workes strongly favour the ECLS over EOTS or p^3-structure.

Further support for the ECLS arises from theoretical studies. Srivastava [180–182] performed ab initio calculations on Sb/GaAs and Sb/InP comparing the ECLS and the p^3-structure in terms of their total energy. The ECLS was found to be remarkably favourable. Also the calculated band structures for the ECLS compare better with ARPES [183,184], ARIPS [40], HREELS [23,185] and reflectance difference [186] measurements than the calculated electronic properties of the p^3-structure. In 1993 Schmidt et al. [187] probed the energetics of all five structural models for Sb monolayer adsorption on GaAs (1 1 0) shown in Fig. 11 by means of ab initio calculations. The ECLS was found to be the ground state of the surface, followed by the EOTS which gave rise to a 0.25 eV lower adsorption energy. Later in a more detailed study [1 1 0] the calculated electronic states and ionization energies of the five models were compared with experimental findings. From these studies it was concluded that the ECLS is indeed the adsorption geometry for Sb/GaAs (1 1 0) (1 ML). To establish this structure further, calculated surface phonon frequencies [188] for the ECLS and EOTS of Sb/GaAs (1 1 0) and Sb/InP (1 1 0) were compared with the outcome of Raman scattering experiments. The results clearly favour the ECLS. A very similar picture arises for Sb/GaP (1 1 0) and Sb/InAs (1 1 0) [189,190]. In all considered cases ab initio total-energy minimization and the comparison between the calculated and measured electronic properties favour the ECLS over other adsorption geometries.

The discovery that Bi forms epitaxial overlayers on III–V (1 1 0) surfaces is more recent [17–19,50,53]. From core-level spectra the EOTS or p^3-structure has been proposed as the bonding geometry [148,149]. In contrast to that LEED analyses [43,52,191] for Bi/GaAs (1 1 0) and Bi/InP

(1 1 0) indicate that the best-fit p(1 × 1) structure is the ECLS. Also XSW [65] and GIXD [66] studies favour the ECLS as adsorption geometry for Bi/GaAs, although there are considerable variations in the determined structural parameters. The similarity between Sb and Bi monolayers on GaAs (1 1 0) has also been underlined by McLean and co-workers [17,50] as a result of their STM study. They point out, however, that in the case of bismuth adsorption the perfect overlayer is interrupted by misfit dislocations due to the larger size of the Bi atoms (cf. Section 3.1). Ab initio calculations by Umerski and Srivastava [120,192,193] for Bi adsorption on the (1 1 0) surface of GaAs, InP, and InAs find the ECLS to be the minimum energy configuration. They also noted fairly good agreement between their calculated surface bands and the corresponding ARPES values.

As already discussed in Section 3.1 there are experimental hints that the (1 × 2) phase of Bi/GaSb corresponds to one deposited monolayer of bismuth [152]. Mainly based on measured surface band structures [152] and polarization studies [194] for the (1 × 1) and the (1 × 2) phases, McIlroy and co-workers assume the Bi chains to remain intact after the phase transition. This assumption stems from their findings of relatively small changes in the polarization dependence and energy of the surface states. Accordingly, their geometry model (shown in Fig. 5) consists of a combination of both the ECLS and the EOTS. The inequivalent Bi zigzag chains are bonded both to the substrate and to each other. As discussed above, both the ECLS and the EOTS saturate all dangling bonds at the surface. Therefore the driving force for the bonding between the two Bi chains remains somewhat unclear. We would rather support other authors who assign the (1 × 2) phase to submonolayer coverage [58–60]. Currently efforts using resonant photoemission, GIXD and surface X-ray diffraction are undertaken in order to cast some light on the atomic structure of that reconstruction [195]. However, no definite answer has been given yet.

Comparatively little is known about As monolayers on III–V (1 1 0) surfaces. Kübler et al. [25] reported an arsenic-rich GaAs (1 1 0) surface with a (1 × 1) LEED pattern. They also found that the surface relaxation is lifted upon As deposition. Chiang and Spicer [27] found the saturation coverage to be about one monolayer. An ab initio study [28] has shown that the ECLS is thermodynamically stable for As/GaAs (1 1 0) in the extreme As-rich limit. In TB studies [160,161] the ECLS was also found to be the ground state of As/GaAs (1 1 0) (1 ML). However, recent polarization studies on As/GaAs (1 1 0) [33] indicate a bonding mechanism different from the ECLS in contrast to the theoretical studies above. A possible explanation for that apparent contradiction may be found in low interface order. The formation of a saturated monolayer structure characterized by two different adsorption sites for As and rather flat surface electronic bands has also been reported for As/InP (1 1 0) [62,196].

4.1.2. Epitaxial continued layer structure

In Section 4.1.1 we have established that the ECLS is now the widely accepted adsorption geometry for the V/III–V (1 1 0) (1 ML) systems. Consequently, the question of structural details and accompanying vibrational and electronic properties arises. We start with the geometries.

Details of side and top views of the ECLS are given in Fig. 13. The corresponding geometrical data predicted by ab initio pseudopotential and empirical TB calculations as well as determined in experiments are summarized in Table 3. When comparing values obtained within one method with those resulting from another, one has to take the accuracy and the actual measured quantities into account. One example concerns the XSW analysis. The XSW parameter $d_{12,\perp}$ for Sb/GaAs and Sb/GaP has a slightly different meaning than indicated in Fig. 13. XSW does not measure the

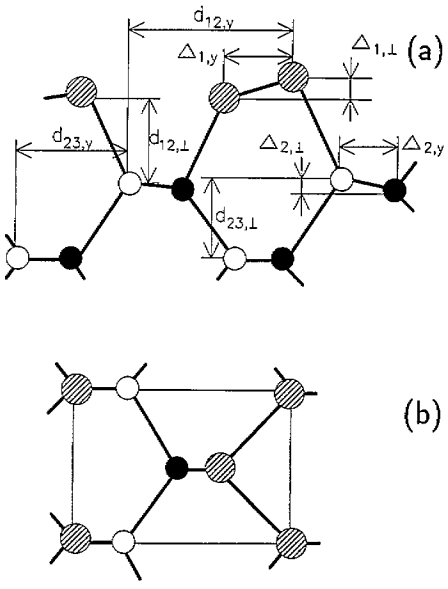

Fig. 13. Schematic side (a) and top (b) views of the V/III–V (1 1 0) overlayer system in the ECLS. Open (black) circles indicate substrate cation (anion) atoms, whereas the group-V overlayer atoms are indicated by hatched circles.

vertical distance between the uppermost overlayer atom and the cation from the first substrate layer, but rather the average perpendicular displacement of the overlayer chains from the extrapolated bulk (220) plane [47]. However, from the ab initio calculations we find a small contraction of the uppermost substrate plane with respect to its ideal, bulk-like position for Sb/GaAs and Sb/GaP. We observe values of about 0.1 Å which have to be added to the XSW data for $d_{12,\perp}$. In general there is excellent agreement between the measured data and the predictions from ab initio calculations. With respect to the lateral extension of the Sb zigzag chain on GaAs (1 1 0), $\Delta_{1,y}$, PED finds a value which is about 10% smaller than determined by LEED or in ab initio calculations. However, in the PED study [73] no relaxation of the substrate was taken into account and the search for minimum R-factor was done for a rather coarse mesh of different structures. Another crucial point seems to be the characterization of the lateral position of the Bi overlayer with respect to the substrate. For Bi/GaAs the distance in (0 0 1) direction between the uppermost Bi atom and the Ga atom of the first substrate layer, $d_{12,y}$, varies between 3.2 Å [191] and 4.51 Å [120]. An extreme lateral distortion of the first substrate layer has been found in a GIXD study [66], but is not reported by other authors. The reason for these deviations could be the formation of strain-induced dislocations on the Bi/GaAs (1 1 0) interface. Because of these dislocations we expect local changes in the bonding geometry. However, due to the limited spatial resolution of the experimental techniques such as LEED for example a geometry with averaged structural parameters will be derived. On the other hand, the existing calculations are based on (1 × 1) symmetry in contrast to the real overlayer systems, i.e., assume the artificial construction of a perfect monolayer without dislocations. The early TB study by Mailhiot et al. [175] gives in general results which deviate somewhat more from experiment or ab initio calculations. The limited accuracy of the TB calculations is also stated in a recent comparison between measured and calculated PED intensities for Sb/InAs (1 1 0) [45]. It

Table 3
Structural parameters (in Å) for V/III–V (1 1 0) (1 ML) in the ECLS (cf. Fig. 13)

		$\Delta_{1,\perp}$	$\Delta_{1,y}$	$d_{12,\perp}$	$d_{12,y}$	$\Delta_{2,\perp}$	$\Delta_{2,y}$	$d_{23,\perp}$	$d_{23,y}$
As/GaAs	ab initio [28]	0.01	1.58	2.05	4.36	0.02	1.46	2.01	2.81
Sb/GaP	ab initio [190]	0.10	2.03	2.38	4.34	0.07	1.35	1.91	2.61
	TB [175]	0.34	1.89	2.12	3.91	0.00	1.36		
	PED [72]	0.07	1.91	2.32	4.56				
	XSW [47]	0.04		2.31					
Sb/GaAs	ab initio [190]	0.05	2.00	2.37	4.52	0.09	1.41	2.01	2.73
	TB [175]	0.09	1.87	2.29	4.39	0.08	1.42		
	LEED [178]	0.08	1.99	2.34		0.11	1.40		
	PED [73]	0.06	1.80	2.36					
	XSW [64]			2.27					
	GIXD [36]		1.96		4.55		1.42		2.81
Sb/InP	ab initio [190]	0.16	1.98	2.44	4.44	0.07	1.46	2.04	2.77
	TB [175]	0.57	2.02	2.23	4.00	0.09	1.47		
	LEED [43]	0.13	1.91	2.32					
	PED [72]	0.13	1.87	2.41	4.59				
Sb/InAs	ab initio [190]	0.12	1.94	2.31	4.63	0.08	1.51	2.14	2.88
	TB [175]	0.22	1.76	2.23	4.34	0.20	1.54		
	PED [74]	0.10	1.93	2.39					
Bi/GaAs	ab initio [120]	0.16	2.09	2.38	4.51	0.17	1.36		2.76
	LEED [178]	0.09	1.98	2.52		0.11	1.46		
	LEED [191]	0.10	2.13	2.48	3.20	0.08	1.41		
	XSW [65]	0.14	2.00	2.50	3.85				
	GIXD [66]		2.04		3.76		1.76		2.62
Bi/InP	ab initio [120]	0.20	2.08	2.41	4.47	0.10	1.37		2.99
	LEED [43]	0.20	2.14	2.48					
Bi/InAs	ab initio [120]	0.15	2.06	2.43	4.59	0.13	1.43		3.06

has been concluded that the structural data determined in the TB study have to be modified in order to explain the experimental findings. In particular we notice that the buckling of the Sb overlayer atoms seems to be systematically overestimated in the TB calculations by a factor two to three both in comparison to experiment and ab initio theory.

In spite of the slight variations between the different approaches used, we find that there are some characteristic features common to all V/III–V (1 1 0) systems which have been found by means of all experimental techniques and also ab initio calculations applied to determine the surface geometry. There is an agreement about a small counter relaxation of the uppermost substrate layer, i.e., the surface cations move outwards and the anions inwards. This leads to a noticeable vertical distance $\Delta_{2,\perp}$ between the atoms in the first substrate layer. The amount of the counter relaxation seems to be mainly governed by the species of the overlayer atoms rather than by the substrate itself. We find a very small value of $\Delta_{2,\perp}$ of 0.02 Å for As/GaAs, a moderate value of 0.07–0.11 Å for Sb/III–V (1 1 0) and a somewhat larger buckling of 0.08–0.17 Å for Bi/III–V (1 1 0). As a consequence of the counter relaxation and the difference between the bonds from the overlayer atoms to substrate anion and cation there is also a buckling between the overlayer atoms. The adatom bonded to the substrate cation moves out of the surface compared to the adatom at the anion site. In Fig. 14(a) we have

plotted the magnitude of the buckling of Sb and Bi overlayers as determined experimentally or by means of ab initio calculations vs. the relative difference of the tetrahedral radii of the substrate atoms given in [197]. Even though there is a certain scatter between the values for $\Delta_{1,\perp}$ determined by the different methods we can clearly observe three trends: (i) As in case of the substrate buckling $\Delta_{2,\perp}$, we find a correlation between the size of the overlayer atoms and the vertical shear $\Delta_{1,\perp}$. We find that the vertical shear between the overlayer atoms increases as we go to larger overlayer atoms. For As/GaAs the buckling is negligible, somewhat larger are the corresponding values for Sb/III–V (1 1 0) (between 0.04 and 0.16 Å) and even larger (0.09–0.20 Å) is the shear for Bi/III–V (1 1 0). This can be understood as an expression of the increasing stress induced by the substrate on the zigzag chain, which has to be accommodated. (ii) There is also a significant influence of the substrate properties on the overlayer buckling. For a given overlayer species the buckling increases with growing geometrical inequivalence of the substrate constituents (cf. Fig. 14(a)). (iii) Less obvious, but recognizable from data obtained with the same method for a series of substrates, e.g., the ab initio results for Sb/III–V (1 1 0) and Bi/III–V (1 1 0) (empty and filled squares in Fig. 14(a)) is the trend with the substrate lattice constant. The lattice constant increases as follows: $a(\mathrm{GaP}) < a(\mathrm{GaAs}) < a(\mathrm{InP}) < a(\mathrm{InAs})$. The larger lattice constant of InAs compared to the other III–V substrates induces less strain on the overlayer chain, resulting in a reduced buckling. Thus we find that the buckling of the overlayer atoms for V/InAs (1 1 0) is smaller than that expected from the trends determined by (i) and (ii). We also find a dependence on the ionicity of the substrate chemical bond. Fig. 14(b) exhibits the vertical shear vs. the charge asymmetry of the III–V compounds calculated according to a new definition [198]. Essentially the same picture arises as in Fig. 14(a).

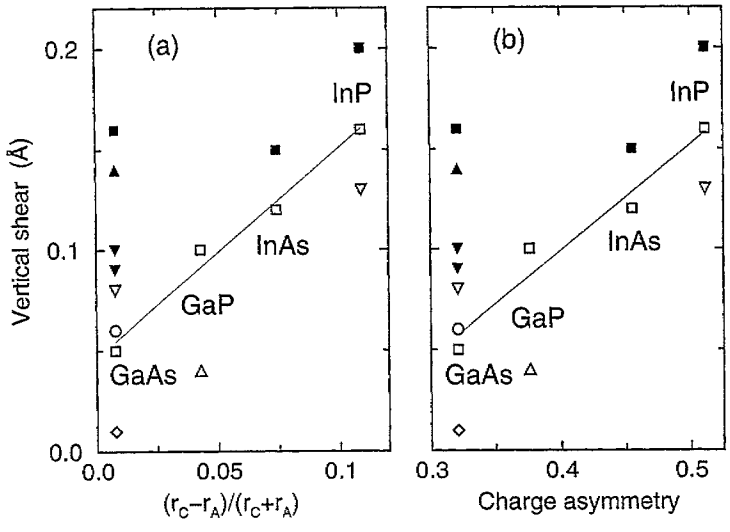

Fig. 14. The vertical shear between the group-V overlayer atoms plotted as a function of (a) the relative difference of the tetrahedral radii [197] of the substrate atoms, and (b) as a function of the charge asymmetry defined in [198]. Filled and empty symbols denote the buckling for bismuth and antimony overlayers, respectively. Squares, triangles down, triangles up, and circles indicate values from ab initio calculations [190,120], LEED [43,191,178], XSW [47,65] and PED experiments [73], respectively. The empty diamond represents the ab initio result for As/GaAs (1 1 0) from [28]. The solid line is a least squares fit of the ab initio results for antimony overlayers.

Further quantities which can be used to characterize the surface chemistry are bond lengths and angles. In Table 4 we compare calculated and measured bond lengths at the V/III–V (1 1 0) surface and the angle α between the V–V bonds in the zigzag chains. For comparison we also give the corresponding sum of the covalent radii [199]. In general we find a reasonable agreement between the bond lengths obtained by the different approaches. The deviations are typically less than 5%. The bond lengths within the overlayer zigzag chain are very close to the sum of the covalent radii. The slight deviations can be easily correlated to the different lattice constants of the substrates as discussed above. The chain bonds are somewhat stretched in case of larger substrate lattice constants. A slightly different picture arises for As/GaAs. The As–As bond within the chain is more than 6% longer than the sum of two covalent As radii. However, the surface bond lengths exhibit the same tendency as the bond lengths in the rhombohedral bulk A7 structures. The calculated bulk values 2.52 Å (As), 2.90 Å (Sb), and 3.06 Å (Bi) [200] are nearly reproduced. In the As/GaAs case the value is somewhat increased since the substrate Ga atoms are larger than the adsorbate As atoms. In the case of Bi overlayers the opposite effect occurs due to the smallness of the substrate atoms compared to the adatoms (cf. also covalent radii in Fig. 1).

The sum of the covalent radii turns out to be a more or less reliable guideline also for the distance between the overlayer atoms and the substrate anions and cations. However, there are slight differences between As and Sb on the one hand and Bi overlayers on the other. For As and Sb we find

Table 4
Bond lengths (in Å) and bond angle between the overlayer atoms for V/III–V(1 1 0) (1 ML) in the ECLS

		O–O		*O–A*		*O–C*		α
			$\sum r_{cov}$		$\sum r_{cov}$		$\sum r_{cov}$	
As/GaAs	ab initio [28]	2.55	2.40	2.46	2.40	2.42	2.46	103°
Sb/GaP	ab initio [190]	2.78	2.80	2.55	2.46	2.59	2.66	86°
	SEXAFS [179]	2.88		2.60		2.79		
Sb/GaAs	ab initio [190]	2.81	2.80	2.66	2.60	2.59	2.66	89°
	LEED [178]	2.77		2.66		2.64		90°
	PED [73]	2.70		2.70		2.57		96°
	GIXD [36]	2.80						91°
Sb/InP	ab initio [190]	2.82	2.80	2.55	2.46	2.72	2.84	91°
	LEED [43]	2.82		2.52		2.80		95°
Sb/InAs	ab initio [190]	2.84	2.80	2.66	2.60	2.72	2.84	94°
Bi/GaAs	ab initio [120]	2.89	2.92	2.61	2.66	2.64	2.72	87°
	LEED [178]	2.87		2.77		2.73		88°
	LEED [191]	2.92		2.69		2.70		86°
	XSW [65]	2.85						89°
	GIXD [66]	2.85						
Bi/InP	ab initio [120]	2.94	2.92	2.58	2.52	2.83	2.90	89°
	LEED [43]	2.98		2.58		2.88		88°
	PEXAFS 150]		2.42					
Bi/InAs	ab initio [120]	2.98	2.92	2.67	2.66	2.85	2.90	92°

For comparison we give also the sum of the covalent radii [199]. *O* denotes the overlayer atoms, whereas *A* and *C* are used for substrate anions and cations.

that the bonds to the surface anions are approximately 4% longer than the sum of the covalent radii, whereas the bonds to the cations are slightly shorter than predicted by this rule. This finding can be understood from simple chemical arguments. The ECLS continues the ideal zinc-blende structure of the substrate. Thus, the overlayer group-V elements substitute both lattice anions and cations. It is therefore natural to assume the III–V bonds to be stronger than the V–V bonds, which take part of the bonding to a 'substitutional atom'. Obviously the same argument does not hold for Bi. The Bi bonds to substrate anions and cations follow more clearly the trend set by the covalent radii. One reason could be that Bi does not form III–V compounds as known for lighter column-V elements.

Considering the angle α between the overlayer bonds in the zigzag chain we find a strong tendency towards the formation of right angles. In all cases apart from As/GaAs we find the deviation from 90° to be less than about 5%. This seems to confirm the early prediction of Skeath et al. [5,6,75] that the bonding within the chain is at least partly characterized by in-plane ppσ bonds. If the group-V atoms can only be accomodated on the III–V (1 1 0) surface with large deformations of the right angles or correspondingly stretched or compressed bond lengths, the monolayer tends to be less stable or ordered as evident in case of As/GaAs [25] or As/InP [62], but also observed for Bi/GaAs [16,17,50,51] and Sb/GaP [46,47].

If we examine the situation of lighter column-V elements on commonly available III–V (1 1 0) substrates, we notice that under the constraint of the substrate lattice a strong bond stretching accompanied by a rapidly increasing bond angle α makes the ECLS an unfavourable bonding configuration. Skeath and co-workers [5] pointed out that lighter group-V elements may adsorb rather as molecules. Also exchange reactions may occur for smaller adatoms as observed for the As/InP (1 1 0) interface [34,61,62]. This means that already from simple geometrical considerations one can limit the number of possible stable V/III–V (1 1 0) (1 ML) systems, at least within the ECLS bonding configuration. However, apart from these geometrical considerations there are also chemical trends to be observed. The role of the chemical bonding for the formation of ordered V/III–V (1 1 0) systems has been underlined by Ford et al. [52]: Using the ratio of the adatom covalent radius to the substrate lattice constant as a measure of relative size one would expect that if atomic size were the only important factor, the Bi/GaSb (1 1 0) system, with a ratio of 0.24, should order in a similar fashion to Sb/InAs (1 1 0), with a ratio of 0.23. This is not the case. Instead Bi forms a stable (1 × 2) overlayer on GaSb, whereas Sb forms only a (1 × 1) structure on InAs, although GaSb is only slightly larger than InAs. However, attempts to deposit Sb on GaSb (1 1 0) failed to yield any epitaxial structure in contrast to the case of InAs [52].

To conclude, we find distinct chemical trends of the overlayer geometry vs. substrate properties which determine the geometrical details of the V/III–V (1 1 0) adsorption configurations in the ECLS. Simple geometrical considerations and empirical concepts such as covalent radii allow reasonable predictions about the stability and geometry of the specific system. Of course, not all experimental findings can be explained in such a (naturally) simplified picture.

4.2. Interface phonons

While there is a long standing interest in the atomic and electronic properties of ordered group-V monolayers on III–V (1 1 0), the exploration of their dynamical properties has started comparatively recently. By analysing the results of Raman scattering measurements carried out for various coverages Hünermann et al. [41] detected interface phonons characteristic for the ordered antimony

monolayer on III–V (1 1 0). Typical polarization-dependent spectra are shown in Fig. 15 for the Sb/InP (1 1 0) system. The intensity of the phonon lines depends remarkably on the incident photon energy. The corresponding resonance energies, i.e., photon energies yielding maximum Raman scattering intensities, could not be attributed to bulk transitions and thus have been related to the electronic surface band transitions [83,84,201]. The detected phonon modes correspond to vibrations involving the epitaxial layer of Sb and the upper substrate layer. The Raman spectra of the various overlayer systems are different despite the similarities of the atomic structure and the bonding behaviour. For Sb/InP (1 1 0) eight pronounced peaks have been reported. On the other hand, the scattering intensities for Sb/GaAs were found to be less impressive: only four peaks could be assigned to the monolayer system [83,202]. The experiments on Sb/GaP (1 1 0) were complicated by strong multiphonon signals of GaP, which may have masked interface peaks. Only one sharp monolayer-related peak has been found [41]. Another explanation for the difficulty to detect Sb/GaP interface phonons may lie in comparatively inferior ordering of these monolayer systems which has been reported by several authors [46,47]. More recently, Sb/InAs (1 1 0) has also been found to exhibit characteristic monolayer-related phonons [81].

The interface phonon frequencies found experimentally are compiled in Table 5. The interface phonons at the centre of the surface Brillouin zone, Γ, can be classified according to the irreducible representations of C_s (or m), the point group symmetry of the surface unit cell. Thereby A″ modes

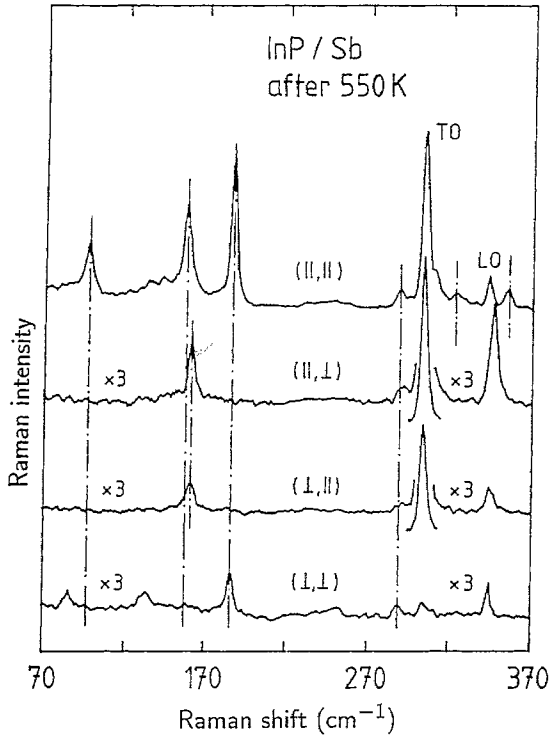

Fig. 15. Raman spectra for different backscattering configurations for annealed one Sb monolayer on InP (1 1 0). The notations ∥ and ⊥ indicate the polarization directions (1 $\bar{1}$ 0) and (0 0 1) with respect to the Sb chain direction. From [41].

Table 5
Comparison of measured and calculated interface frequencies for Sb/III–V(1 1 0) (1 ML) at Γ (frequencies $\hbar\omega$ in meV)

	GaP/Sb		InP/Sb		GaAs/Sb		InAs/Sb	
Mode	Raman Ref. [41]	ab initio Ref. [190]	Raman Ref. [41]	ab initio Ref. [190]	Raman Ref. [83, 202]	ab initio Ref. [190]	Raman Ref. [81]	ab initio Ref. [190]
1A′		11.1	11.9	11.0	9.2	9.8		7.5
2A′		13.1	19.5	17.7	11.0	11.1	11.9	10.3
3A′		21.9	22.9	20.9	22.3	23.2		20.2
4A′		26.6	35.8	24.0		24.1	21.6	22.5
5A′		39.7	39.8	37.5		27.2	24.5	25.1
6A′		51.3	43.9	47.6		34.6		31.3
1A″		8.4		8.4		7.8		6.9
2A″	20.7	20.8	20.0	19.6	20.6	19.9	19.1	19.0
3A″		44.0	36.0	40.3		30.5		27.4

describe lattice distortions along the [1 $\bar{1}$ 0] direction, i.e., along the Sb zigzag chain, and A′ modes correspond to atomic movements perpendicular to the chain direction. If one considers a four atom basis in the surface unit cell, i.e., the two overlayer antimony atoms and the uppermost substrate anion and cation, one would expect to find 12 branches, three acoustic and nine optical ones (of which there are 6 A′ and 3 A″ modes). The Raman tensors for first-order allowed scattering for the A′ and A″ modes can be found in [203]. For backscattering at (1 1 0) surfaces, scattering from the six A′ modes can only be obtained for diagonal polarization configurations, while the three A″ modes can only appear non-diagonal. The experimental results for Sb/InP are in good agreement with this: Eight out of nine possible optical modes are observed, six in diagonal and two in non-diagonal configurations as shown in Fig. 15. It is surprising that for the other systems only comparatively fewer modes were detected. This could be due to experimental difficulty in preparing the ordered Sb monolayer and/or due to the low Raman scattering efficiency for some modes.

The first theoretical attempt to determine the eigenvalues and eigenmodes for Sb/GaAs (1 1 0) (1 ML) was undertaken by Godin et al. [204]. They employed a TB total-energy scheme to calculate the force constants between the overlayer atoms and between overlayer and substrate atoms. In a later publication [205] the same group applied a TB molecular dynamics scheme to study interface phonons of Sb/GaAs and Sb/InP with a rather similar outcome. The results obtained by their restricted dynamical model describe qualitatively the available experimental findings. This holds at least for the eigenvalues. However, the eigenmodes cannot reliably be described without taking the atomic displacements of the substrate atoms (at least partly) into account. This has been shown by a comparison between solutions for the four and two atom eigenvalue problems with the experimental data for Sb/InP and Sb/GaAs [188]. More reliable are the results of a recent ab initio calculation by Schmidt and Srivastava [190]. The eigenvalues and eigenvectors were obtained by diagonalizing the matrix equation

$$\boldsymbol{M}\ddot{\boldsymbol{u}} = \boldsymbol{K}\boldsymbol{u}, \tag{43}$$

where $\boldsymbol{M}$ represents the diagonal matrix of the atomic masses. The matrix elements $k^{ij}_{\alpha\beta}$ of the harmonic force constant matrix $\boldsymbol{K}$ were obtained by displacing atom i from its equilibrium position

in the direction α and calculating the force acting on atom j in the direction β. Here $\alpha,\beta = (x, y, z)$ and $i,j = 1, N$, where N is the number of atoms in the uppermost three layers. This method gives excellent results for clean III–V(1 1 0) surfaces [206]. The resulting phonon frequencies and polarizations explain the experimental findings [207–209] quite well.

A comparison of theoretically obtained eigenvectors and eigenvalues for localized modes at the V/III–V (1 1 0) interfaces with the experimental results is made in Table 5. Some eigenmodes for Sb/GaAs (1 1 0), which will be discussed in more detail below, are depicted in Fig. 16. The eigenmodes are classified according to their representations and enumerated with increasing frequency. Obviously most of the calculated frequencies compare quite well with the experimental results. This is especially valid for the 2A″ modes, which are highly localized shear modes (cf. Fig. 16) and therefore appropriate for the restricted approach of Ref. [190]. A large deviation between experimental and theoretical data occurs for the 4A′ mode for Sb/InP. The difference of more than 30% is certainly too large to be only due to calculational or experimental uncertainties. Perhaps the origin of the feature experimentally observed is a mode which deeply penetrates into the bulk and which cannot be described by our restricted model.

The characters of the displacement patterns exhibited for Sb/GaAs (1 1 0) in Fig. 16 change only quantitatively if we consider other Sb/III–V (1 1 0) systems. In particular the ratio between the displacements of the substrate cations and anions changes if one looks at substrates with a larger mass difference between the respective constituents. Thus, a comparison between the frequencies associated with these modes for different substrates should be interesting. The overlayer atoms are little or not involved in the atomic displacements of the 6A′ and 3A″ modes as can be seen from Fig. 16. Since these surface modes are mainly localized in the substrate layers underneath the antimony atoms one expects their frequencies to be strongly related to substrate properties as the masses of the substrate constituents. This influence is indicated in Fig. 17(a) where we have plotted

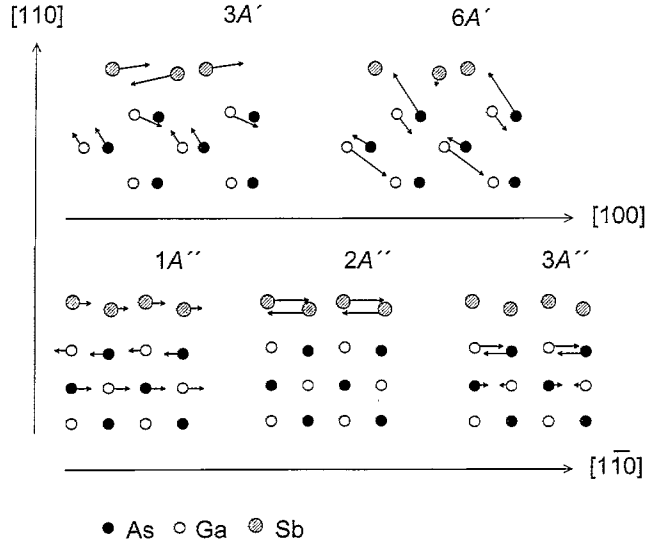

Fig. 16. Displacement patterns of surface Γ opticals phonons of Sb/GaAs (1 1 0) (1 ML). The notation of the eigenmodes corresponds to Table 5.

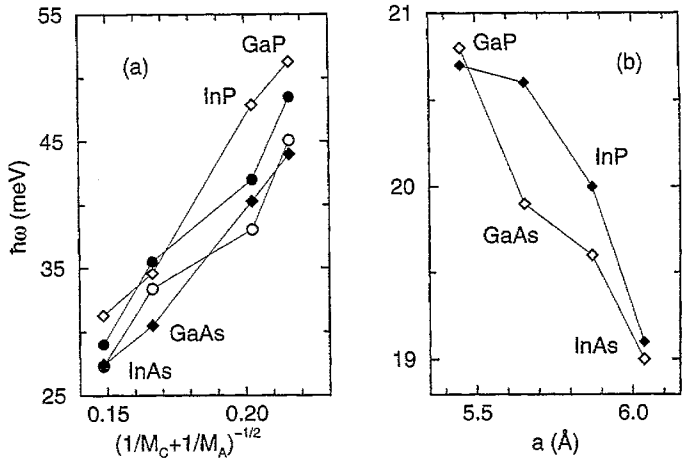

Fig. 17. (a) Calculated frequencies of the 3A″ and 6A′ modes (filled and empty diamonds, respectively) vs. the square root of the inverse reduced mass of the substrate atoms for the Sb/III–V (1 1 0) (1 ML) system. Filled and empty circles indicate the Fuchs–Kliewer and bulk TO(Γ) frequency of the respective III–V compound [55,206]. (b) Measured [41,81] and calculated frequencies of the 2A″ mode (represented by filled and empty diamonds, respectively) vs. the respective substrate lattice constant.

the 6A′ and 3A″ modes vs. the square root of the inverse reduced mass of the substrate atoms. We find a nearly linear relation. This indicates the validity of the mass approximation where the force constants are kept fixed independent of overlayer and substrate.

It is also interesting to note that the frequencies of both modes follow the trend set by the bulk TO(Γ) frequencies of the corresponding material. Thus in all cases the calculated 6A′ frequency is higher than the corresponding bulk TO(Γ) frequency [55]. In the case of Sb/InP this has been confirmed experimentally [41]. However, the calculated frequencies of all significantly substrate-related interface phonons for the indium compounds are overestimated with respect to the experimental results. The same effect of an overestimated bond strength has also been observed for the calculated bulk TO(Γ) frequencies [190] and is apparently due to the underestimation of the theoretical lattice constant of these compounds [109]. The displacement pattern of the 6A′ mode is dominated by a bond stretching between first substrate layer anion and second substrate layer cation. A rather similar displacement pattern has very recently been reported for the Fuchs–Kliewer mode of free III–V (1 1 0) surfaces [206]. The free III–V (1 1 0) surfaces were investigated with the same ab initio frozen-phonon method which has been applied to the Sb/III–V (1 1 0) systems. Therefore a comparison between the Fuchs–Kliewer phonon frequencies calculated for the free III–V (1 1 0) surfaces [206] and the calculated 6A′ modes for Sb/III–V (1 1 0) should be meaningful. The calculated values in meV for $\hbar\omega_{FK}$ ($\hbar\omega_{6A'}$) are for GaP: 49.8 (51.3), InP: 46.7 (47.6), GaAs: 35.8 (34.6), and InAs: 31.1 (31.3). Clearly the energies for the 6A′ interface phonons are very close to the Fuchs–Kliewer phonon frequencies for the corresponding clean substrate surface. Together with the similar distortion patterns this is a strong indication that the 6A′ modes can be interpreted as Fuchs–Kliewer phonons. Further support for this hypothesis comes from HREELS experiments on Sb/GaAs (1 1 0) [23,210,211] and Sb/InP (1 1 0) [210] which show that upon deposition of up to

a few monolayers of Sb the frequency of the Fuchs–Kliewer phonon remains roughly at the value for the clean III–V (1 1 0) surface, while its intensity decreases.

The phonon modes which are more strongly localized at the overlayer atoms than the 6A′ and 3A″ modes discussed so far, are less effected by the masses of the substrate constituents. This is especially obvious for the 2A″ modes which are entirely localized in the overlayer zigzag chain (cf. Fig. 16). Their frequencies are all very close to 20 meV. However, there is a small substrate effect. The frequency decreases slightly if one goes to substrates with larger lattice constants as can be seen in Fig. 17(b). This is due to the weaker Sb–Sb bonds at larger substrate lattices. Also the 3A′ modes which mainly describe a stretching of the overlayer chains in [1 0 0] direction (cf. Fig. 16) show only small variations in frequency as we consider different substrates. However, since there is some substrate contribution to that mode, no distinct trend with the chain bond length can be found as in the case of the 2A″ modes. Frequencies whose displacements are more equally divided between overlayer and substrate atoms, as for example in the case of the 1A″ modes, show less distinct trends.

Starting from the eigenvectors discussed above an attempt has recently been made to calculate the Raman scattering cross-section for surface vibrations on InP(1 1 0) and GaAs(1 1 0) surfaces terminated with an antimony monolayer [212]. The results describe qualitatively the resonance behaviour and the polarization dependence of the Raman cross-section determined experimentally.

To conclude we can state that the ordered Sb monolayer on III–V (1 1 0) gives rise to distinct interface phonons which have been detected experimentally. The frequencies, symmetries and scattering efficiencies of these interface phonons have been well described theoretically. We find distinct chemical trends which confirm the validity of the mass approximation for these systems. In principle, similar interface phonons should exist for the Bi/III–V (1 1 0) (1 ML) systems. However, no distinct peaks could be detected, perhaps due to a high number of defects in the first Bi monolayer and the limited overlayer chain length [65,90]. Only some weak structures appear which probably arise from Bi clusters.

4.3. Electronic states

4.3.1. Band structure and excitation energies

Most of the ordered V/III–V (1 1 0) monolayer systems investigated so far have proven to be semiconducting. For Sb monolayers on GaAs the semiconducting character of the interface has been shown by means of UPS and ellipsometric spectroscopy [15], HREELS [23,88], and STM [9,10,213] which indicate that the semimetal-induced states do not extend significantly in the bulk gap. This is also in agreement with the ARIPS data obtained by Drube and Himpsel [40], who found an overlayer-induced empty state 2.1 eV above the bulk valence-band maximum (VBM), and ARPES measurements by Mårtensson et al. [183] and Tulke et al. [44,214]. Flat band conditions or only small Schottky barriers for the first-ordered Sb layer on n- and p-type GaAs (1 1 0) have also been found by PES [14,35], EFIRS [48] and SXPS [69]. On the other hand, there are reports from an earlier PES study [166] of a considerable band bending of about 0.8 eV even after annealing the Sb overlayers on n-type GaAs. However, these findings have not been confirmed by other groups and may be related to inferior sample quality.

The existence of Sb derived interface states in the bulk band gap of InP is more controversial. The lowest empty state for Sb/InP occurs well above the conduction-band minimum (CBM) according

to ARIPS [40] while HREELS [185] detects an empty Sb-induced state below the CBM of the projected bulk band structure. The existence of a donor-type gap state has been concluded by Esser et al. from EFIRS [48] and SXPS studies [69]. This state at about 0.5 eV above VBM, has been associated with the bonding of the regular Sb monolayer on InP [145] but could also be due to phosphorus defects at the interface [69]. Somewhat in contrast to that ARPES studies [37,42,174] place the two highest occupied bands near to the bulk VBM, and from PES experiments [215,216] nearly flat band conditions are reported for one Sb monolayer on n- and p-type InP.

ARPES data are also available for one monolayer antimony on GaP(1 1 0) [44,217] and InAs (1 1 0) [218]. Accordingly the highest occupied state lies slightly above and below the bulk valence-band edge in GaP and InAs, respectively.

A variety of band structure calculations with a different degree of sophistication have been published for Sb/III–V (1 1 0) (1 ML). Based on local pseudopotentials and the X_α scheme to describe exchange–correlation effects Bertoni and co-workers [219] performed self-consistent calculations for Sb/GaAs (1 1 0) taking the atomic geometry from LEED data [8]. Manghi et al. [220] utilized a similar approach to calculate the electronic states for Sb/GaP (1 1 0). Srivastava and Martin [221] gave a detailed analysis of the surface bands of the Sb/InP (1 1 0) interface based on their pseudopotential calculation for the atomic structure determined by LEED [39]. Applying a TB total-energy minimization scheme Mailhiot et al. [63] optimized the atomic geometry for Sb on the (1 1 0) surfaces of GaP, GaAs, GaSb, InP, InAs, and InSb. For these optimized geometries the TB band structures have been derived. Also more recently TB attempts were undertaken to determine the band structure of Sb/GaAs (1 1 0) [95,222] and Sb/GaP [223]. All the calculations mentioned above suffer from uncertainty with respect to the exact interface geometry. Either they rely on information available from experiment, or in some cases on a TB total-energy minimization scheme with intrinsic inaccuracy (see discussion in Section 2.1). Since details of the band structure are rather sensitive to structural parameters such as bond lengths or overlayer buckling it is not astonishing that the calculated electronic structures agree only in their main features. Northrup [28] for the first time applied the ab initio pseudopotential approach to determine the atomic structure of As/GaAs and Sb/GaAs. He also calculated the surface band structure for one monolayer As adsorbed on GaAs (1 1 0) in the ECLS. In the last few years the present authors have published results of ab initio calculations for the atomic and electronic structure of Sb/III–V(1 1 0). In particular band structures for Sb/GaAs [181,110], Sb/InP [181], and Sb/GaP [189] were calculated. The calculated band structures compare reasonably well with the available experimental data. Moreover, a comparison of band structures calculated for different structural models has in all cases shown that the ECLS derived bands are the most suitable to describe the experimental findings. Unfortunately ARIPS data are available only for a relatively small part of the SBZ for Sb/GaAs and Sb/InP [40]. Therefore no meaningful comparison with calculated bands can be made.

In order to allow a precise comparison between the band structures with respect to the identification of chemical trends we have calculated the band structures for Sb adsorbed on GaAs, GaP, InP and InAs with the same set of numerically technical parameters. The calculations are based on the ECLS geometries from Table 3 which are derived from ab initio total energy and force calculations [190]. The corresponding band structures are shown in Fig. 18. The computational details are given in [190] and explained in Section 2.2. The structural optimizations have been done with the theoretically determined equilibrium lattice constants, which are somewhat smaller than the actual ones (GaAs: − 1.5%, GaP: − 1.6%, InAs: − 2.9%, and InP: − 3.5%). As a consequence of

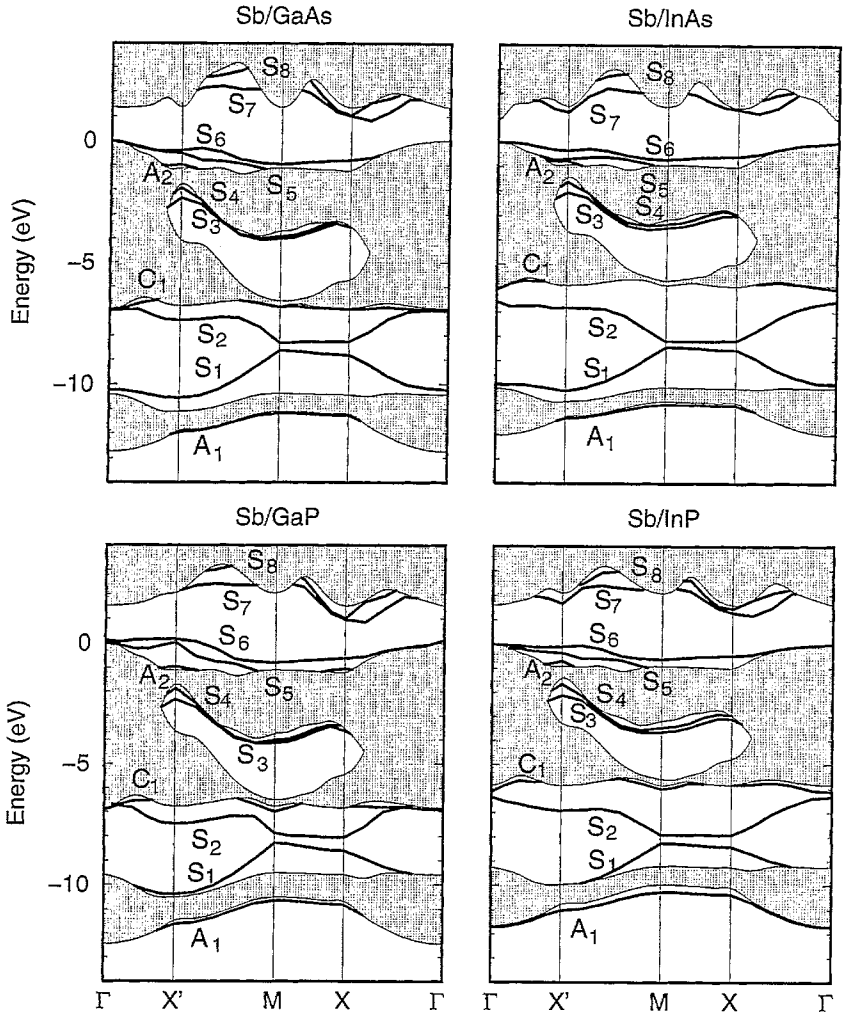

Fig. 18. Surface band structure (bound states) for Sb/III–V (1 1 0) (1 ML) plotted over the projected bulk band structure (dotted regions) of the respective III–V substrates. C_i and A_i denote states localized on cations and anions of the substrate. S_i denote either chemisorbed states or states localized on the overlayer. This notation is taken from Bertoni et al. [219]. All energies are referred to the bulk VBM at 0 eV at Γ.

the underestimation of the lattice constants one finds an overestimation of the excitation energies. A competing factor determining the gap width is the well known DFT gap problem, which tends to reduce the gap sizes below the experimental values (see Section 2.2.4). As a result the calculations underestimate the excitation energies for the Ga compounds, whereas the In compounds, for which the theory gives rise to a significant underestimation of the lattice constants, have larger band gaps than observed experimentally. Also the neglect of relativistic effects in our calculation has to be mentioned. We calculated the following fundamental band gaps for the bulk materials (the value in brackets is the experimental extrapolation [55] for zero temperature): GaAs: 1.35 eV (1.52 eV), GaP: 1.50 eV (2.35 eV), InAs: 0.86 eV (0.42 eV), and InP: 1.57 eV (1.42 eV).

For GaAs there seems to be a near compensation of the different effects mentioned. As a consequence we obtain a nearly correct gap for the bulk crystal. Assuming that the energetical positions and dispersion of the unoccupied surface states are roughly correctly described in our DFT–LDA calculation for Sb/GaAs one can try to assign experimentally observed electronic transitions to the calculated bands. Table 6(a) presents a collection of experimental results for transition energies for Sb/GaAs. The experimental findings are energetically ordered and arranged in groups of similar values. The transition energies of about 2.3, 2.6, 3.2, and 3.7 eV are reproducibly observed within the different excitation spectroscopies. They should therefore be attributed to maxima in the combined density of states of the monolayer system. Considering the Sb/GaAs band structure in Fig. 18 the listed energies can be assigned to transitions between the filled (S_5 and S_6) and empty (S_7 and S_8) surface bands. If one considers only the bound surface states we find an appreciable density of states at or close to X′ (S_5, S_6, S_7, and S_8) and near or at X (S_6, S_7, and S_8). In Table 6 we have given some excitation energies for these high-symmetry points or points on the high-symmetry lines $\overline{X\Gamma}$ and $\overline{X'M}$ and assigned to measured data. While comparing these theoretical transition energies with the experimental data a word of caution is in order. Apart from theoretical problems to determine reliable gap values which have been discussed above there are also other difficulties, since the symmetry of the initial and final states involved in the experiments is in general

Table 6
Transition energies (in eV) derived from STM spectroscopy, spectroscopic ellipsometry, reflectance difference spectrsocopy, EELS, HREELS and resonance Raman scattering for V/III–V (1 1 0) (1 ML)

Method	Transition energy					
(a) Sb/GaAs (1 1 0)						
STM [68]			2.2	2.7	3.1	3.7
Ellipsometry [15]				2.65	3.2	3.75
Reflectance [186]			2.25	2.65		
Reflectance [228]	1.5	1.7	2.2	2.6		
EELS [210]		2.0	2.3			3.4
HREELS [23]	1.55	1.9	2.3	2.6	3.2	3.6
Raman [201]			2.2–2.4			
Band structure (Fig. 18)	S_6–S_7 ($0.2\,\overline{X\Gamma}$) 1.5	S_6–S_8 (X) 1.8	S_6–S_7 ($0.2\,\overline{X'M}$) 2.5		S_5–S_7 ($0.2\,\overline{X'M}$) 3.0	S_5–S_8 ($0.2\,\overline{X'M}$) 3.4
(b) Sb/InP (1 1 0)						
EELS [250]			2.4	2.65		
HREELS [185]	1.4	2.0	2.3			
Raman [201]		1.9	2.3–2.6			> 3.0
(c) Bi/GaAs (1 1 0)						
HREELS [250]				0.85	1.2	1.9
HREELS [224]	0.35	0.55	0.65	0.85		

In case of Sb/GaAs they are compared with transitions between the calculated surface bands for Sb/GaAs shown in Fig. 18.

unknown and the oscillator strengths of the considered excitations have not been calculated. Therefore such an assignment as given in Table 6 has to be considered to be somewhat speculative. In Table 6(b) measured energies of transitions between surface states at the Sb/InP (1 1 0) interface are listed. The onset of the transitions seems to lie at slightly lower energies compared to the Sb/GaAs system. However, also the bulk band gap of InP is slightly smaller compared to GaAs (1.34 eV instead of 1.42 eV at RT [55]). Therefore, smaller transition energies do not necessarily indicate the extension of interface states in the bulk band gap.

The four Sb/III–V (1 1 0) interfaces considered in Fig. 18 show common features in their surface band structures. In the ionic gap between valence bands one observes two bound states S_1 and S_2. These bands show dispersion mainly along X′M and $\overline{\text{X}}\overline{\Gamma}$, i.e., along the chain direction in real space. They are comparatively flat along the direction perpendicular to the chain, i.e., along $\overline{\Gamma}\overline{\text{X}}'$ and $\overline{\text{MX}}$. The quasi-one-dimensional dispersion of S_1 and S_2 indicates that these states are most likely derived from the overlayer chains in [1 $\bar{1}$ 0] direction. This is indeed the case as will be shown in the next section. There are differences in the appearance of these bands between GaAs and GaP on the one hand and InAs and InP on the other. In particular, the S_2 state lies at a somewhat lower binding energy in case of the In compounds and follows the wider ionic gap for the more ionic compounds. Within the stomach gap in the upper valence-band region there appear two nearly degenerate states S_3 and S_4 only a few tenths of one eV below the projected bulk band structure. They have distinctly different energies only at the X′ point. In case of the indium compounds we observe also some splitting along MX. For all substrates considered we find rather a strong dispersion of these states, in particular along ΓX′M. The largest dispersion of more than two eV is observed for Sb/GaP. The energy difference between the VBM and S_3, S_4 is larger in case of the Ga compounds compared to the two other interfaces.

Slight variations with respect to different substrates are also observed between the two highest occupied surface bands S_5 and S_6 in the fundamental gap. They exhibit a relatively small dispersion along the high symmetry lines. In particular in case of the In compounds the surface bands S_5 and S_6 are rather flat. For example, the band S_6 varies between -0.63 and 0 eV for Sb/InP and between -0.7 and 0 eV for Sb/InAs, where the energy zero is identified with the bulk VBM at Γ. In case of Sb/GaAs and Sb/GaP the dispersions of 0.96 and 0.93 eV, respectively, are somewhat larger. A likely reason for the different bandwidths may be the different substrate lattice constants. The smaller lattice constants of the Ga compounds induce a stronger interaction between the overlayer atoms giving rise to stronger dispersion. For Sb/GaP the states S_5 and S_6 extend slightly into the bulk band gap. The band S_6 has its maximum 0.16 eV above bulk VBM at X′. There S_5 also reaches its maximum with 0.04 eV. In case of Sb/GaAs, Sb/InP, and Sb/InAs the bands S_5 and S_6 are below the bulk VBM in agreement with the experimental findings discussed below.

The two lowest unoccupied bands in the fundamental gap, S_7 and S_8, show similarities in their general shape for the four systems under consideration. However, their energetical positions with respect to the bulk CBM are different. In case of Sb/InAs (1 1 0) we find the lowest empty surface state well above the bulk CBM, whereas in the other cases with wider substrate bulk band gaps S_7 extends into the bulk band gap. In particular, we observe a minimum close to the X point, which is 0.5 (Sb/GaAs), 0.7 (Sb/GaP), and 0.4 eV (Sb/InP) below the bulk CBM. The existence of an empty state below the bulk CBM is seemingly in agreement with some of the experimental findings discussed above. However, the determination of exact excitation energies is rather complicated within the DFT–LDA and requires quasi-particle calculations (cf. Section 2.2.4), which have not yet been

performed for the considered interfaces. The calculations show further differences between the four monolayer systems. For example, the band S_7 for the Sb monolayers on the In compounds shows a pronounced minimum at X′ which is not observed for Sb/GaAs or Sb/GaP, where S_7 is resonant with bulk states in that part of the SBZ. Together with the high density of states for S_5 and S_6 at X′ the critical point of the state S_7 at X′ for Sb/InP and Sb/InAs might give rise to transitions which are not observed for the other systems.

The occupied states are reliably described within the applied theory and therefore allow a meaningful comparison with experimental data as shown in Fig. 19. Obviously there is rough agreement for the energetical positions of the interface states. Given the uncertainty in the energies of the surface states with respect to the bulk in both the experimental works and the calculations the observed shifts are not unreasonable. The data by Mårtensson et al. [183] for Sb/GaAs agree well with the calculated dispersion of the bands S_3 and S_4, which is indeed much stronger than predicted earlier by TB studies [63,175,176]. Mårtensson et al. could not resolve the two states probably due to the near degeneracy of S_3 and S_4. However, as will be shown in the next section, the surface localization of these states is rather weak, especially of S_4, which could also be a source of difficulty

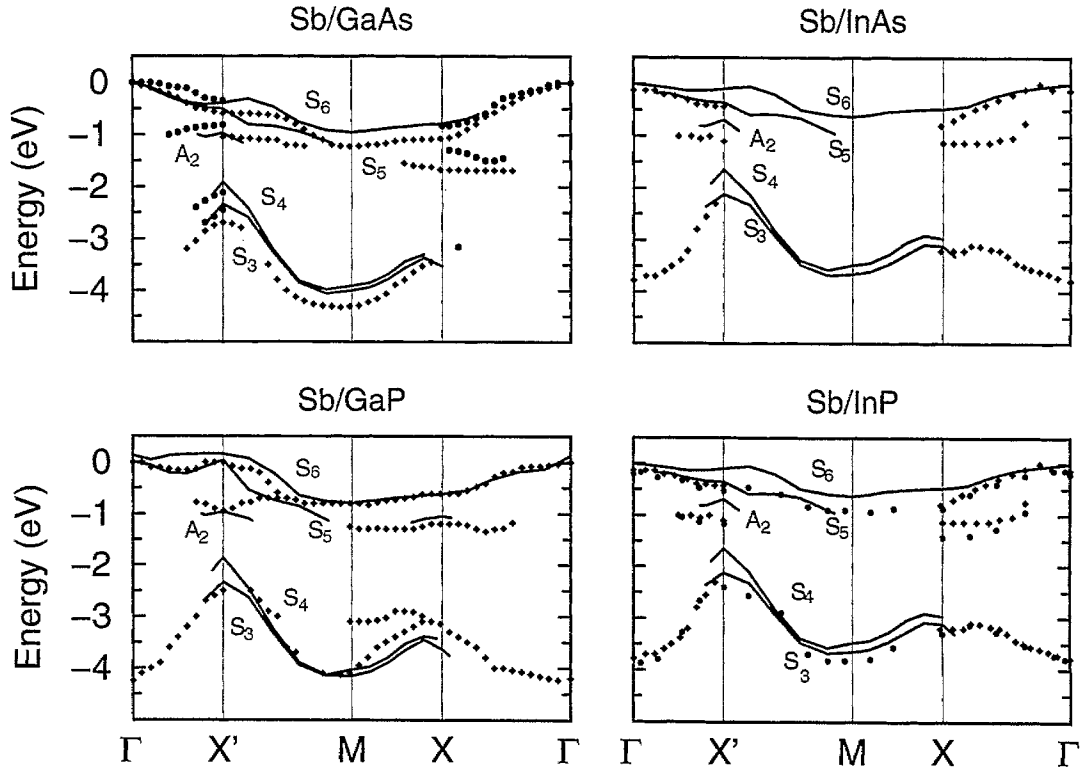

Fig. 19. Comparison of the dispersion of calculated surface bands (bound states shown by solid lines) for Sb/III–V (1 1 0) (1 ML) with ARPES results. Diamonds and circles represent the experimental findings for Sb/GaAs [44,183], Sb/InAs [218], Sb/GaP [217], and Sb/InP [42,184].

for detecting S_4. On the other hand, Tulke and Lüth [44], found an energy splitting at X′ which is quite close to our calculations. Less perfect is the agreement between measured and calculated bands in case of the uppermost occupied states of Sb/GaAs. However, in the energy region in question there are, apart from the resonant states, at least three bound surface states which complicate a unique assignment between theory and experiment. In contrast to that, the agreement between theoretical values and measured bands for Sb/GaP is nearly perfect. Only the band splitting between S_3 and S_4 and between S_5 and S_6 around the X′ point is not observed in the experiment by Whittle et al. [217]. In agreement with our calculations the ARPES data [217] show that the highest occupied surface state forms a distinct maximum at X′. Srivastava [189] has shown earlier that ARPES data [44] along $\overline{\Gamma M}$ also agree well with the calculated bands in this direction. Rather satisfactory is also the comparison between theory and experiment for Sb/InAs and Sb/InP. Looking at the experimental results in Fig. 19 one can also detect similarities between the different Sb/III–V interfaces with respect to the resonant states which are less well accessible in our slab calculations than the bound surface states. For all monolayer systems a resonant surface states less than 1.0 eV below S_6 has been detected at X. The band S_3 seems to be nearest to the VBM at X′. Around the Γ point the band energy is comparable to that at M. The state A_2 is a bound state only in very small part of the SBZ around X′ and has been detected in all experimental studies.

Because of the isovalency of Bi and Sb, and similar bonding geometries for monolayer coverage, the band structures of Bi/III–V (1 1 0) have a number of features in common with the bands of Sb/III–V (1 1 0) discussed above. However, different orbital energies and differences in bond lengths and angles induce some quantitative changes in the surface bands between these two overlayer systems. For instance the p(s) orbital energy of Bi lies about 0.4 (0.8) eV above that of Sb (cf. Fig. 1). This has consequences for the energetical positions of the Bi related states, e.g., the highest occupied band. In case of Bi/III–V (1 1 0) there is almost consensus about semimetal-induced surface states within the bulk gap in contrast to the Sb/III–V systems. In PES [18] and ARPES [16,21] a Bi derived occupied surface state has been found about 0.5 eV above the VBM of the projected bulk band structure for Bi/GaAs (1 1 0). From ARIPS [77,78] and ARPES studies [17] it was concluded that the surface band gap narrows to 0.7 eV for one monolayer Bi on GaAs. This is in agreement with STM data [16,51], which place the surface band gap rather in the middle of the GaAs bulk band gap. Structural features as the peculiarity of the Bi/GaAs interface to form strain induced dislocations also influence the electronic properties. With STM it has been found that these dislocations on Bi/GaAs (1 1 0) generate deep-lying acceptor levels in the GaAs band gap [16]. The ordering of the dislocations seems to produce actual extended one-dimensional electronic bands [224]. These bound states pin the Fermi level for n-doped GaAs substrate at ~ 0.6 eV above the GaAs VBM. Also for Bi/InP (1 1 0) [56] there is experimental evidence of occupied states within the bulk band gap. ARPES measurements by McIlroy and co-workers [57] for ordered Bi overlayers on InAs (1 1 0) show no significant extension of occupied interface valence bands into the bulk band gap region in contrast to GaAs and InP substrates as discussed above. For Bi/GaSb (1 1 0) (1 × 1) (1 ML) ARPES [152] found four occupied surface states below the bulk valence-band edge which could be resolved across the entire SBZ. However, HREELS and photoemission experiments [60,153] state that the Bi/GaSb interface is semimetallic, i.e., there occurs a crossing of Bi-induced electronic bands with the Fermi level.

On the basis of the geometry obtained by LEED [191] a band structure calculation for Bi/GaAs (1 1 0) based on the FLAPW method has been performed which explains essential experimental

features discussed above [225]. In 1994 the first ab initio band structure for a structurally optimized geometry for Bi/GaAs (1 1 0) was published by Umerski and Srivastava [193]. For the occupied bands a good agreement with the ARPES data of Ref. [21] was found. In Fig. 20 we present results of ab initio calculations [120] of the surface band structures of Bi monolayers on GaAs, InP, and InAs (1 1 0) surfaces in comparison with ARPES data. The bands appear qualitatively very similar to the Sb/III–V (1 1 0) systems shown in Fig. 18. There are, however, differences in particular with respect to the energetical positions of the bands. The lowest-energy valence state A_1 is observed in each of the three systems entirely below the bottom of the lowest s-like band and therefore lower in energy than the corresponding state for antimony overlayers. Within the ionic gap we find two bound states S_1 and S_2 (for Bi/InP only S_2 is found) which show a quasi-one-dimensional dispersion as already observed for Sb/III–V (1 1 0). S_3 and S_4 are two bands which skirt across the top of the stomach gap for each of the three considered systems. For the InP substrate their maximum separation is fractionally greater than that of InAs and GaAs, which may explain why both bands have been experimentally observed only in this case, and single bands in the other cases. In their dispersion and energetical positions they are quite similar to the S_3 and S_4 bands for Sb/III–V (1 1 0). The second highest occupied state is S_5. It lies above the bulk valence-band edge everywhere except for part

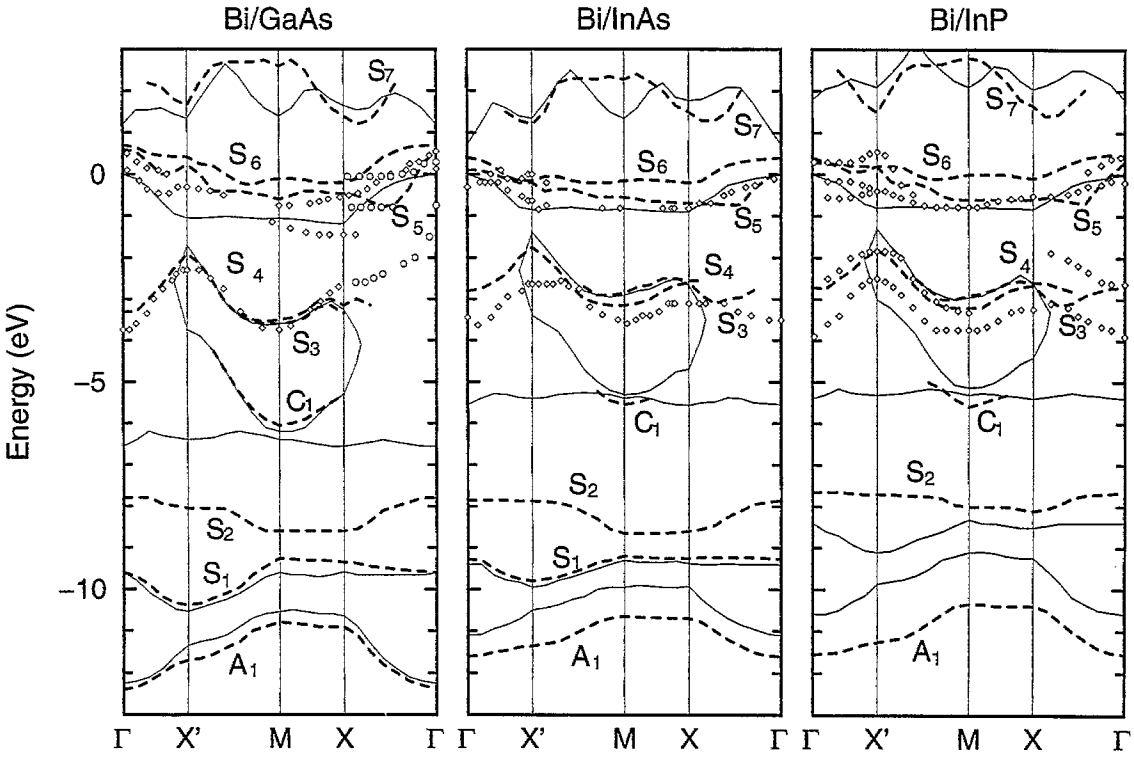

Fig. 20. Surface bands from ab initio pseudopotential calculations [120] (dashed lines) for Bi/III–V (1 1 0) (1 ML) are plotted over the projected bulk band structure (solid lines) of the respective III–V substrate. Experimental data are taken from [17] (open circles) and [21,56,57] (open diamonds).

$\overline{\Gamma X}$. The highest occupied state S_6 lies entirely above the valence-band edge, with relatively flat dispersion along $\overline{XMX'}$. These two highest filled bands correspond to S_5 and S_6 in the case of Sb/III–V. Although the energetical position of the bands is different, we find rather close agreement between their dispersion in case of antimony and bismuth adsorption. The lowest unoccupied band S_7 disappears into the bulk band regions around Γ and M, with a minimum at 0.8 $\overline{\Gamma X}$ and a slightly higher lying minimum at X'. The state S_7 lies below the conduction-band edge in InP, but is above that for GaAs and InAs. It resembles strongly the lowest unoccupied state for antimony overlayers. However, when comparing the calculated band structures of Figs. 18 and 20 one has to observe that they are obtained with different sets of technical parameters. Apart from other details the basic set for describing the atomic orbitals used in [120] for the calculations of the bismuth overlayers is smaller than the one used by the present authors for the antimony overlayers. This has some effect on the energetical position and dispersion of bands as shown for free III–V (1 1 0) surfaces by Alves et al. [109]. Additionally, the neglect of spin–orbit interaction in the calculations is a stronger impairment of the accuracy in the case of bismuth overlayers compared to the lighter antimony atoms.

Photoemission measurements [16,17,21,56,57] have only been able to detect surface or overlayer states with low binding energies, typically up to 4 eV below the bulk VBM. As seen from Fig. 20, these can be identified with the states S_3–S_6 obtained in the ab initio calculation. In the binding-energy range 2–3.5 eV, these measurements have produced two surface bands for Bi/InP, and only one surface band for Bi/GaAs and Bi/InAs. These can be compared with the nearly degenerate bands S_3 and S_4. In the energy range $+0.5$ to -1.0 eV around the bulk VBM, photoemission measurements have mapped out two surface states. These show reasonable agreement with the bands S_5 and S_6. A clear feature of the highest occupied state, from both experiment and theory, is that it possesses very little dispersion along $\overline{XMX'}$. In addition, both experiment and theory identify two bands along $\overline{\Gamma X'}$, which cross and anticross. The leading edge of S_6 has been calculated to lie at about 0.7 eV above the VBM in GaAs, and about 0.5 eV above the VBM in InP or InAs in approximate agreement with experiment. This energy edge can be regarded as the Fermi level pinning position for p-doped substrates. According to the calculations the band S_7 lies below the bulk conduction-band edge for the substrates GaAs and InP, but above it for InAs. The unoccupied state S_7 could pin the Fermi level for n-type substrates in case of GaAs and InP. The transition $S_6 \rightarrow S_7$ is indirect with approximate energies of 0.5, 0.8, and 0.7 eV for GaAs, InP, and InAs substrates, respectively.

In conclusion one can say that the seven systems considered in detail, namely ordered Sb and Bi monolayers on GaAs, InP, InAs as well as Sb/GaP show qualitatively rather similar features in their interface band structure. They are all semiconducting with the highest occupied interface states close to the bulk valence-band edge for Sb/III–V or about 0.5 eV above it for bismuth overlayers. For all substrates apart from InAs we find that overlayer-induced empty states extend into bulk gap. The bound surface states show very similar dispersion for all systems considered. However, there are differences in the energetical positions between the different overlayer systems. For the highest occupied state these differences may come from different orbital energies for the p valence electrons of Bi and Sb. In contrast to the systems discussed above, however, the Bi/GaSb (1 1 0) (1 × 1) system has been indicated to be a semimetallic interface according to HREELS studies by Gaviola et al. [60,153].

4.3.2. Orbital character of states and bonding

In contrast to extensive reports about excitation energies and band structures there are fewer and more contradictory investigations of the orbital characters of the interface states. Mårtensson et al. [183] performed ARPES measurements for Sb/GaAs (1 1 0) and observed three occupied antimony derived states. Two of them (S_5 and S_6 in Fig. 19) lie partially above the GaAs bulk valence-band edge and are reported to have predominantly p_z character (with z parallel to the surface normal [110]). A state at lower energy in the stomach gap of the projected GaAs bulk band structure (S_3 and/or S_4 in Fig. 19) was found to be more p_{xy}-like (with x along the zigzag chain direction (1 $\bar{1}$ 0) and y along (0 0 1). This agrees with the findings of Ref. [226]. For Bi/GaAs a detailed experimental study of the orbital character for the three highest occupied interface states S_4–S_6 in Fig. 20 has been given by McLean and co-workers [21]. From the intensity dependence of the emission from the states on the polarization of the synchrotron radiation they conclude on a predominantly p_z character of all the three states. The p_{xy} contribution to these states was found to be about 15% for the two states in the fundamental gap, whereas the state at the upper edge of the stomach gap (S_3 and/or S_4 in Fig. 20) has with 25% a slightly higher p_{xy} percentage. For Bi/InAs (1 1 0) a completely different picture arises from the porlarization studies of McIlroy and co-workers [57]. They observed the energetically lower state (S_3 and/or S_4 in Fig. 20) to be almost exclusively p_z-like, whereas the higher states S_5 and in particular S_6 are found to be dominated by in-plane p_{xy} orbitals. Although we cannot give an explanation for the different results with respect to the polarization properties of Sb/GaAs and Bi/GaAs on the one hand and Bi/InAs on the other, we do not share the opinion of the authors of Ref. [57] that the surface bonding and overlayer structure of Bi/InAs deviates significantly from that of other V/III–V systems. Polarization studies have also been performed for As/GaAs (1 1 0) [33]. They indicate an in-plane rather than p_z character of the highest occupied state.

Detailed theoretical studies of the orbital character of states on the basis of energy-minimized surface geometries have been published for Sb/GaAs [110], Sb/InP [182], Sb/GaP [189], Bi/GaAs [193,120], and Bi/InAs [120]. All adsorbate systems exhibit similar geometrical features. This also holds for the orbital character of band states. As an example we present and discuss in the following the orbital character of the interface states for Sb/GaAs (1 1 0) according to the band structure in Fig. 18. The results of our wave function analysis are plotted in Fig. 21.

Below the bottom of the valence band we find A_1, which is an s-like state localized at the first substrate layer anion. This state has already been described by Bertoni et al. [219]. For the free GaAs (1 1 0) surface a corresponding state slightly less tightly bound has been observed around the second layer anion [227]. S_1 and S_2, the two states giving rise to nearly one-dimensional bands in the heteropolar gap are strongly localized s-orbitals at the overlayer Sb atoms. A similar character of these states has already been described by Bertoni et al. [219] and Mailhiot et al. [63]. Both S_1 and S_2 are involved in the overlayer–substrate bonding as well as in the adatom–adatom bonding: a small charge accumulation along the Sb–substrate and Sb–Sb bonds is found. Less pronounced is the surface character of C_1 which shows, however, some localization around the Sb bonded to substrate As atom and between first and second substrate layer cation and anion, respectively. The states S_3 and S_4 appear in the stomach gap of the projected GaAs bulk band structure and show weak localization at the surface. S_3 forms a bonding combination of Sb states with an As sp^3 dangling bond as already stated by Bertoni et al. [219]. Additionally there are remarkable contributions to back-bonding bulk states and little charge accumulation between the adatoms (cf.

also [110, Fig. 5]). Our results deviate from earlier TB studies [63,228], which state that S_3 and S_4 are associated predominately with the p^2 bonding states (p_x and p_y) in the plane of the Sb chain. However, since the two states in the stomach gap are nearly degenerate with bulk states a clear classification of these states by means of slab calculations is rather difficult. A_2 is a bound surface state only in a small region of the SBZ around X′ and is mainly a p_y state localized at the uppermost substrate anion, but contributes also to the bonding between antimony and the substrate cation. The two highest occupied surface states S_5 and S_6 are easier to characterize. They exhibit a strong p_z character as already discussed by Mailhiot and co-workers [63]. These p orbitals are not only localized at the Sb atoms. Rather, there are also contributions from substrate As and Ga atoms. These states realize a strong σ bonding between the adatoms and the underlying substrate atoms, and also give rise to some bonding within the antimony zigzag chain. We find the character of S_5 to

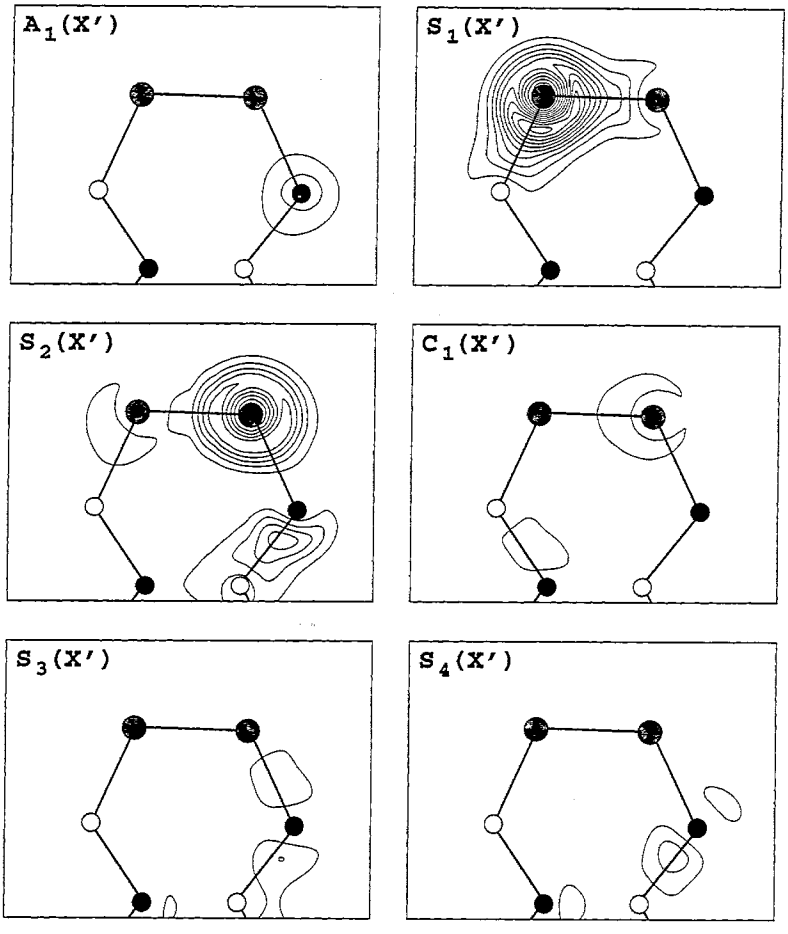

Fig. 21. Contour plots of the squared wave functions for Sb/GaAs(1 1 0)(1 ML) for the bound surface states A_1, A_2, C_1 and S_1–S_8 (cf. Fig. 18). The plots are drawn in three vertical planes containing the As–Sb, Sb–Sb, and Sb–Ga bonds. The contour spacing is 0.0075 e × bohr^{-3}. Grey (black, open) circles indicate Sb (As, Ga) atoms.

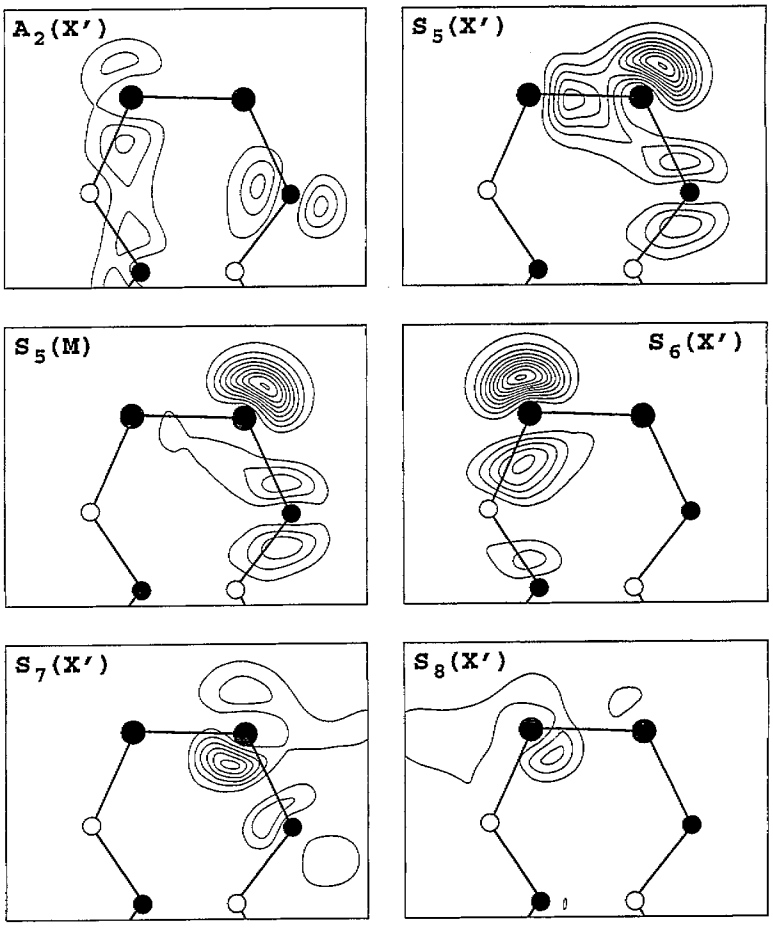

Fig. 21 (continued).

be rather ***k***-dependent. The slight accumulation of bonding charge between the Sb atoms visible at X′ disappears around the M point. Our interpretation of S_5 and S_6 differs from the early paper by Bertoni et al. [219] and a more recent work of the Del Sole group [228]. They described S_5 and S_6 as lone pairs, accomodating two p electrons not taking part in bonding. S_7 and S_8 arise from the corresponding antibonding p combinations to S_5 and S_6. With this orbital analysis we reproduce essential results of the earlier works by Bertoni et al. [219] and Mailhiot et al. [63]. However, our results are at variance with these earlier interpretations, in particular for the states S_3 and S_4. We do not find a clearcut p_{xy}-like state which is responsible for the bonding within the chain according to Ref. [63]. One probable reason for this discrepancy is the fully relaxed structure used in our calculation. Such a hypothesis is corroborated by an earlier orbital analysis by Srivastava and Martin [221], who found for the LEED determined monolayer structure of Sb/InP [39] a p_{xy}-like bonding state between the overlayer atoms. The energy of this state, within the fundamental gap in [221], is expected to change if a more realistic description of the geometry, in particular a much smaller buckling, is used for the calculations. Our search was constrained to bound surface states.

Therefore we cannot exclude the existence of such a state, localized possibly just below the bulk valence-band edge of GaAs. Such a ppσ bonding gave a natural explanation for the nearly right angles within the overlayer chain observed for all stable monolayer configurations.

In case of Bi adsorption there are slight differences to the Sb/III–V (1 1 0) interfaces, in particular with respect to the low-energy states. An extensive wave function analysis has been given in [120]. For example A_1 is derived from an ssσ-type bonding between the s-type wave functions located on the substrate anion and the neighbouring Bi adatom in the surface. The corresponding state for Sb/III–V (1 1 0) interfaces is less localized at the surface and virtually does not contribute to the bonding (cf. Fig. 21). The different localization properties also carry their signature in the band structures. While A_1 for Bi/III–V (110) is well separated from the projected bulk band structure (cf. Fig. 20) the corresponding antimony derived state is resonant along large parts of the SBZ as shown in Fig. 18. Slight differences can also be found in the orbital character of S_2. This state is localized both at the overlayer Bi atoms and around the first substrate layer anion. For Sb overlayers this orbital is mainly localized at the overlayer atoms. The bands which skirt across the top of the stomach gap (S_3 and S_4 in Fig. 20) are related to p orbitals located at the first substrate layer anion as already found for Sb/GaAs. It seems, however, that in case of Bi/GaAs these states exhibit a stronger surface localization than observed for antimony overlayers. Inspite of these slight differences discussed above, the key features, i.e., the states within the fundamental band gap region are characterized by similar bonding and antibonding combinations of overlayer and substrate orbitals. The above theoretical results are in overall agreement with the experimental findings discussed at the beginning of this section. Some contradictions remain unresolved with respect to the character of the highest occupied state (S_6 in Fig. 20). While McIlroy et al. [57] observed a distinct in-plane character in their polarization study, theory predicts a p_z-like state.

Apart from these small discrepancies there is consensus about strong covalent bonds between substrate and overlayer atoms. The covalency of the interface bonding can be concluded from the orbital analysis above and also becomes obvious from Fig. 22 where we have plotted the total valence charge density for the Sb/GaAs interface. It is clear from this figure that the overlayer atoms are linked to the substrate by directional covalent bonds. Sb charge is accumulated along the direction of the neighbouring substrate atoms, as well as in the direction of the missing neighbour at the surface. Thus we find a rather sp^3-type bonding in the overlayer chain and between substrate and overlayer. This interpretation of the calculated orbital character of states and the total valence charge density is in agreement with voltage-dependent STM images [11]. From the relative density of empty and filled states Mårtensson and Feenstra conclude that a significant amount of sp^3 hybridization occurs in the Sb overlayer. While in case of the Sb–Sb bond the charge is essentially symmetrically distributed between the overlayer atoms, we find a small charge asymmetry along the Sb–As bond. The maximum of the charge density is somewhat closer to the As site. The asymmetry of the Sb–Ga bond appears to be slightly stronger and with opposite sign. The ionicity of the Sb–substrate bond reflects the electronegativities (cf. Fig. 1): Ga: 1.81 < Sb: 2.05 < As: 2.18. The same trend in the electronegativities for substrate anion and cation and the overlayer atom is also observed for the other epitaxial V/III–V monolayer systems. We speculate that this trend is responsible for the stability of the respective monolayer system. Attempts to grow interfaces where the above trend is violated, such as As/GaAs (1 1 0), Sb/GaSb or Sb/InSb, turned out to be unsuccessful [25,52].

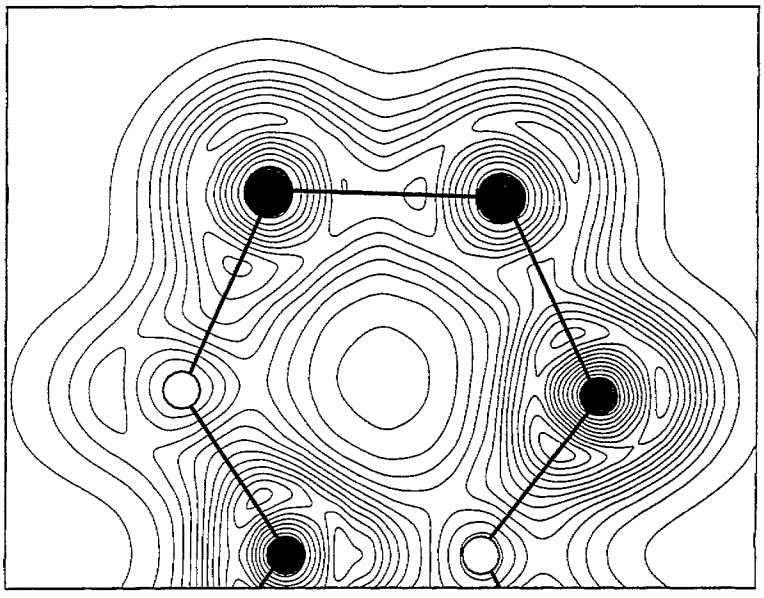

Fig. 22. Contour plot of the total valence pseudocharge density for Sb/GaAs (1 1 0) (1 ML). The plot is drawn in three vertical planes containing the As–Sb, Sb–Sb, and Sb–Ga bond. The contour spacing is 0.0075 e × bohr^{-3}. Grey (black, open) circles indicate Sb (As, Ga) atoms.

4.3.3. Local density of states and STM images

Mårtensson and Feenstra [11] performed voltage-dependent imaging of antimony on the GaAs (1 1 0) surface with STM. For negative sample voltages, the images reflect occupied surface states. Depending on the magnitude of the voltage, either one or both of the two Sb atoms in the surface unit cell are seen. In particular they find that for large negative voltages (between -2 and -3 V) there is only a single maximum per unit cell, thus indicating the location of one of the Sb atoms. Measurements of the registration of this Sb atom reveal a shift relative to the As atoms in the uncovered substrate of about half a unit cell in both crystallographic directions. Thus, they conclude that this particular Sb atom seen at large negative voltages is bonded to a Ga atom in the substrate. In STM images acquired at -1.5 V additional rows appear, located midway between the original rows. These additional rows have been associated with the second antimony atom in the unit cell, which is bonded to an As atom in the substrate. These Sb (As) atoms are only observed at small negative voltages. The fact that not all surface atoms are seen at one particular voltage is a common feature of STM for semiconductor surfaces. It arises from the fact that the images actually reveal the electronic states, and the various dangling bonds which compose these states have amplitudes which are energy dependent. Mårtensson and Feenstra [11] tried to explain their findings in a simple TB picture of a chain of nearest neighbour dangling bonds corresponding the Sb zigzag chain. However, the observation of only one of the Sb species for large negative voltages could not be explained and was attributed to the tip sharpness and tip–sample separation.

The self-consistent electronic-structure calculations of Sb/GaAs (1 1 0) should allow a description of the STM findings, provided that the assumed ECLS geometry is correct and the STM images are

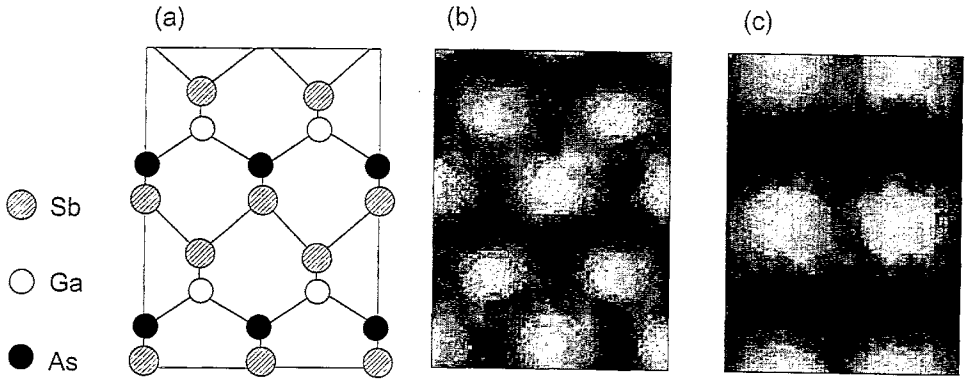

Fig. 23. Energy-resolved LDOS of Sb/GaAs (1 ML) at (b) 1.7 and (c) 2.5 eV below the VBM of bulk GaAs plotted over an area of a 2 × 2 unit cell. The spatial position of substrate and adatoms is indicated by the schematic drawing in (a).

really strongly correlated to the spatially resolved density of states. We have calculated the energy-resolved local density of states (LDOS) for energies 1.7 and 2.5 eV below the valence-band edge for bulk GaAs. Our result for the LDOS 3 Å above the Sb cores is shown in Fig. 23. Obviously our results are in relatively good agreement with the experimental findings. For 2.5 eV below VBM we find only one maximum of the LDOS per unit cell. However, the lateral position of this maximum does not fully coincide with the Sb atom bonded to Ga. While its position is perfectly matched in $(1\,\bar{1}\,0)$ direction, we observe an appreciable shift of about half a lattice constant in (0 0 1) direction. The local DOS at lower binding energy has two maxima per surface unit cell. The lateral positions of these maxima are very close to the positions of the two Sb cores. However, even at lower binding energy we observe some shift of the LDOS maximum with respect to the core position. Both maxima, corresponding to Sb bonded to As and Ga, respectively, are slightly shifted away from the Sb–Sb bond. The reason for that can be rather easily understood. In the low binding energy range the major contribution to the LDOS above the surface comes from the states S_5 and S_6 (cf. band structure in Fig. 18). On the basis of the orbital analysis these states are assigned to partially sp^3-like orbitals pointing in the directions of the missing neighbours at the surface (cf. Fig. 21). This orbital character is reflected in the LDOS which consequently points slightly away from the Sb–Sb bond.

5. Higher coverages

The initial stage of growth of thin films has historically been divided into three limiting-case modes: layer-by-layer growth (Frank–van der Merwe), three-dimensional cluster growth (Volmer–Weber), and monolayer, followed by three-dimensional cluster growth (Stranski–Krastanov) [229]. The resulting structures represent equilibrium situations and are established on the basis of a competition between adatom–adatom and adatom–substrate interactions. For both Sb and Bi overlayers it seems appropriate to say that Stranski–Krastanov or monolayer plus simultaneous multilayer (modified Stranski–Krastanov) growth mode occurs. However, for adatom coverages

beyond one monolayer a rich variety of growth phenomena can be studied. The appearance and modifications of different structures depend very much on the peculiarities of the surface preparation, such as the interplay between annealing temperature, amount of deposited material and the characteristics of the layers underneath the freshly deposited material. Thus one observes some differences in the growth behaviour of Sb and Bi overlayers. The different bulk properties of Sb and Bi play only a minor role for the adsorbed monolayers discussed in Section 4, but become more important as the amount of deposited material increases. For example the lower melting point of Bi results in the formation of large crystallites at RT, whereas an annealing procedure or a comparatively large amount of deposited material is required for the formation of large Sb crystallites.

5.1. *Antimony overlayers*

Shih et al. [68] have reported that Sb films grown at 300 K on GaAs (1 1 0) exhibt a definite layered structure with an average terrace height of ~ 6 Å. This layered growth mode is in accordance with the observations made by Patrin et al. [230,231] who attributed the appearance of a disordered multilayer structure to the formation of small clusters and stray atoms. The experimental findings have been explained with a model by Strümpler and Lüth [12] for simultaneous multilayer growth induced by the small lateral diffusion of Sb. The multilayer height corresponds to the stacking of three layers perpendicular to the pseudocubic (1 1 0) surface with the (1 1 1) direction inclined from the surface normal [231]. Fig. 24 schematically depicts a multilayer region on a 1×1 monolayer that is in contact with the substrate. Growth at 300 K produces these multilayers but also the small

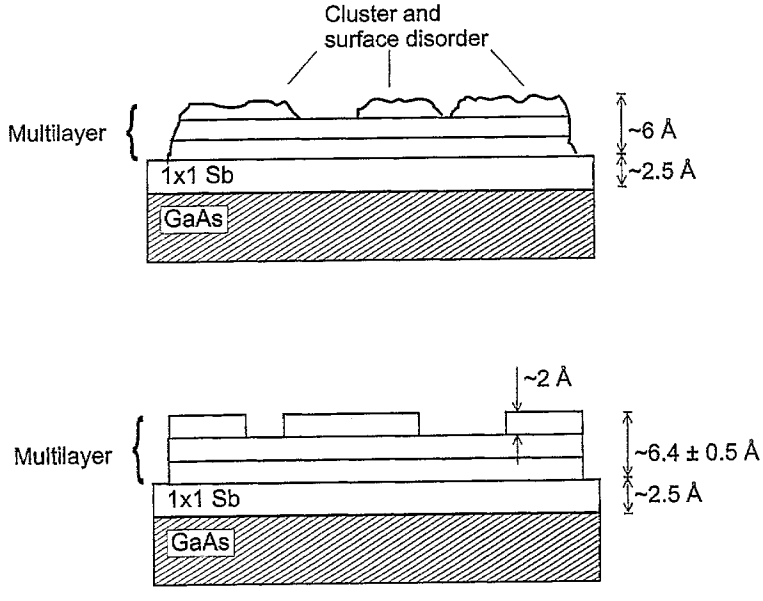

Fig. 24. Schematic cross-section depicting Sb multilayers on GaAs (1 1 0) substrate. The upper panel shows the disorder apparent in STM images. Annealing produces the better ordered structure shown in the lower panel with double and triple layers of Sb on the 1×1 monolayer. After [231].

clusters and depressions shown as irregularities in the upper panel of Fig. 24. Annealing enhances surface ordering, as depicted at the bottom of Fig. 24, and clear separation into two- and three-layer structures occurs driven by a reduction in the number of steps in order to minimize step energy costs. Further annealing at 525 K leads to ordered overlayers containing grains with two distinctly oriented 25 Å periodic superstructures. This superstructure was interpreted in terms of a moiré effect in which the Sb (1 1 0) pseudocubic plane is rotated by $\pm 7°$ with respect to the substrate [1 $\bar{1}$ 0] orientation [230,231]. Such structures have also been observed in LEED experiments on annealed samples [22]. Without thermal treatment a (1 × 1) symmetry can be detected until 10 ML, without indications of superstructures. But the (1 × 1) pattern disappears at about 15 ML [23,82,88, 91,143].

In the high-coverage range up to 20 ML a direct link between the overlayer structure and the evolution of the electronic states has been provided by scanning tunneling spectroscopy. Shih et al. [68] reported for Sb film thicknesses of 10 and 20 ML a region of low conductivity near the Fermi level. The width of this 'approximate band gap' was found to be about 0.5 eV. Patrin and co-workers [231] observed in their current–voltage (I–V) measurements that the 6.4 Å layer (cf. Fig. 24) has a band gap of 0.6 ± 0.2 eV and the 12.8 Å layer of 0.15 ± 0.1 eV. In HREELS spectra for antimony coverages above one monolayer a tail appears in the band gap region, corresponding to the existence of overlayer-induced states in the GaAs bulk band gap. At 7 ML the measured gap width is approximately 0.5 eV [23] and thus somewhat larger than determined by means of STM. The presence of the GaAs Fuchs–Kliewer phonon in the spectrum provides additional evidence for prevailing the semiconducting character of the overlayer that cannot completely screen the microscopic electric field accompanying that phonon mode. The analysis of the intensity and position of the Fuchs–Kliewer phonon indicates the presence of a critical coverage of about 15 ML. At this thickness, antimony undergoes a phase transition from a more or less amorphous to a polycrystalline structure which is accompanied by a semiconductor–semimetal transition as concluded from HREELS [88]. Eventually the metallic islands coalesce into a fully polycrystalline semimetallic bulk-like layer. These structural and morphological changes vs. the coverage have also been monitored in Raman scattering experiments [41,85,91,143,202,232]. Indirect evidence for a transition from a semiconductor-like to a metal-like stage at a somewhat higher deposition of about 20 ML Sb at GaAs (1 1 0) arises from UPS [15]. This is in agreement with RHEED measurements by Savage and Lagally [141] who observed that at an adlayer of 20 ± 3 ML the transformation from a random arrangement of atoms to a crystalline structure takes place. The crystallites are found to have the lattice constants of bulk Sb. Their orientation is such that the (0 0 0 1) basal plane is parallel to the GaAs (1 1 0) surface whereas the azimuthal orientation is random. The average size of these crystallites was estimated to be of the order of 30–40 Å. A detailed description of the crystallites formed at even higher coverages and upon annealing may be found in [231].

Raman scattering experiments [41,90,91,202] on Sb/InP show a rather similar development of the crystal structure with increasing coverage as observed for Sb/GaAs. In Fig. 25 the coverage-dependent evolution of the overlayer structure reflected on the Raman spectra is shown. For one adsorbed monolayer pronounced peaks appear at 96, 157, and 185 cm^{-1} corresponding to the interface phonons discussed in Section 4.2. For higher coverages the spectrum changes considerably and shows features of bulk Sb. The semimetallic crystals of As, Sb and Bi have a diatomic base which allows for optical phonons in contrast to most metals which possess a monoatomic base. These

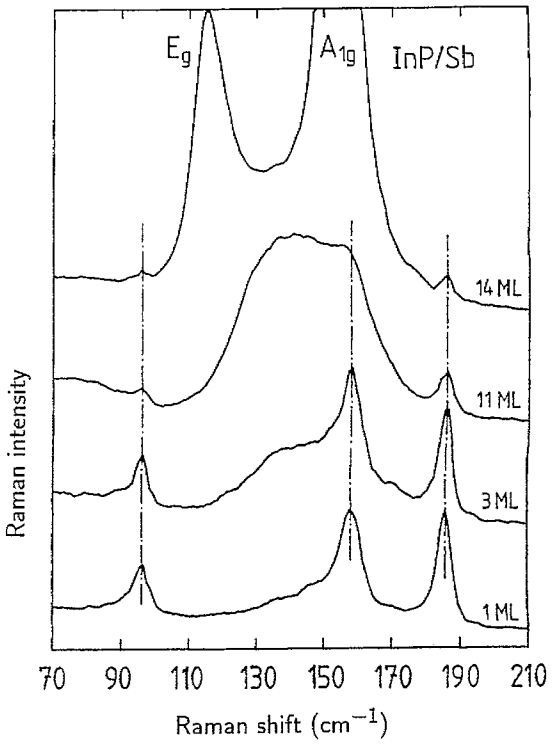

Fig. 25. In situ Raman spectra of Sb between 1 and 14 ML on InP (1 1 0). From [41].

group-V elements crystallize in the A7 structure (see, e.g., Ref. [200]). In the resulting uniaxial layered structure the optical phonon is split into an A_{1g} mode (deformation along the crystal axis) and a doubly degenerate E_g mode (deformation perpendicular to the axis). In the case of Sb their frequencies at the centre of the Brillouin zone are 151.5 and 113 cm^{-1}, thus yielding the Raman peak frequencies for crystalline Sb [233]. For amorphous Sb the Raman spectrum essentially reflects the phonon density of states throughout the Brillouin zone. A broad band appears, centred near 135 cm^{-1} with a half-width of about 30 cm^{-1} [234]. Bearing this in mind the spectra in Fig. 25 can be interpreted as evidence for the slow accumulation of amorphous Sb for coverages higher than one monolayer. Then at about 13 ML the overlayer abruptly crystallizes, leading to distinct peaks originating from A_{1g} and E_g phonons. However, even at 14 ML two of the interface vibrational peaks are still observable. This means that the epitaxial first monolayer is essentially preserved after the crystallization beyond this layer. The conclusions of these Raman studies are in contrast to HREELS measurements by Mariani et al. [210]. Based on their monitoring of the Fuchs–Kliewer phonon energy and intensity as well as on the development of the elastic peak intensity and width, they rule out the presence of crystalline Sb below a thickness of at least 20 ML. This contradiction is all the more astonishing as similar experiments of the same group on Sb/GaAs [88,211] show an overall agreement with other groups concerning the amorphous–polycrystalline transition at about 15 ML. Annealing of 4–5 ML Sb on InP at about 390 K results in a phase transition from amorphous Sb to islands of crystalline Sb [48]. The crystalline nature of the Sb is indicated by

a sharp peak in the Raman spectrum which does not coincide with the phonon modes of bulk Sb discussed above, thus indicating a surface-stabilized Sb modification distinct from bulk Sb.

5.2. Bismuth overlayers

The growth morphology of thick Bi overlayers on GaAs (1 1 0) is different from that of antimony. After completion of the semiconducting monolayer clear LEED images are preserved, indicating a crystalline growth. Some authors report a two-dimensional layer-by-layer growth for up to two monolayers [18,19,22,53,91]. Calculations of the atomic and electronic structure for two ordered Bi monolayers assuming the ECLS have been performed by Umerski and Srivastava [192,193]. However, while the first layer grows epitaxially the subsequent two-dimensional growth seems to be geometrically more disordered [19]. Other authors [231] employing STM found that on top of the first epitaxial monolayer ~ 7 Å high islands form which exhibit superstructures with 21 Å periodicity orientated $\pm 55°$ relative to the substrate [1 $\bar{1}$ 0] direction. Additional Bi deposition results in island coalescence so that large crystallites are formed. These anisotropic crystallites exhibit a superstructure that can be modelled as a moiré effect in which the (1 0 0) direction of the Bi pseudocubic (1 1 0) plane is rotated by $\pm 10°$ from the substrate (1 $\bar{1}$ 0) direction. The fact that Bi forms crystallites for all coverages at 300 K, whereas Sb crystallite formation requires annealing, is probably due to the considerably lower melting temperature of Bi (cf. Fig. 1).

Controversy exists as regards the presence of superstructures in the observed LEED patterns. Ludeke et al. [16], Joyce et al. [18], and Guo et al. [19] did not observe any significant change in the (1 × 1) LEED pattern at different Bi coverages, while a new superstructure, consisting of extra spots orientated along the (1 $\bar{1}$ 1) and ($\bar{1}$ 1 1) directions between 2 and 10 ML, was observed by other authors [22,23,54,77,78]. The presence of this intermediate crystalline phase up to 10 ML was also stressed by Raman spectroscopy [90,91,238]. Beyond one monolayer two distinct peaks at 74 and 90 cm^{-1} reveal a crystalline Bi growth. However, the frequencies are distinctly different from the bulk Bi phonons. It therefore appears that there exists a substrate stabilized, possibly strongly stressed modification. With increasing coverage, the peaks gradually disappear. Crystalline, bulk-like Bi appears beyond 7 ML with phonon peaks evolving at 72 and 98 cm^{-1} For the Bi/GaAs (1 1 0) interface the Fuchs–Kliewer phonon intensity decreases by one order of magnitude in the 1–10 ML coverage range [89] while for Sb this level of attenuation is present only above 10 ML[23,210]. After the completion of one monolayer the more ordered growth morphology for the Bi/GaAs interface, in comparison to Sb/GaAs, is indicated by the formation of semimetallic islands which screen the dipole charge more effectively. However, the Fuchs–Kliewer phonon is still detectable at 10 ML, indicating that the Bi metallic islands take up only a part of the first semiconducting layer. In the same coverage range the partially metallic character is confirmed by the huge enhancement of the elastic HREELS peak [23]. Beyond 10 ML two slightly rotated hexagonal-like LEED images distinctly appear superimposed on the (1 × 1) pattern [22,23,91]. These images were explained with trigonal symmetry caused by Bi facets having their C_3 axis perpendicular to the surface and tilted by 10° with respect to the (1 1 0) direction in the substrate (1 $\bar{1}$ 0) plane. Bi crystallites elongated preferentially in the substrate ($\bar{1}$ 1 0) direction have been observed by STM [231] for coverages higher than 50 ML. A strong clustering of bismuth after the completion of the first monolayer has also been concluded from core-level spectroscopy [147,149]. At about 20 ML the bismuth islands seem to begin to coalesce.

Also for bismuth films on GaSb (1 1 0) a growth mode with the formation of a continuous first layer followed by the clustering of additionally deposited Bi atoms has been concluded from PES [58] and Auger studies [59].

6. Surface dipole and Fermi level pinning

6.1. Changes in the work function

As described previously, adsorbed atoms generally have a significant influence on the electronic structure of a surface. A surface dipole layer is changed or created through formation of new chemical bonds and rearrangement of the electronic charge within the substrate chemical bonds. Consequently the work function of the system changes. The work function Φ describes the energy needed to transfer an electron from inside the crystal through the surface to the outside region. Φ is consequently given by the energy difference between Fermi level E_F and vacuum energy E_{vac} (cf. Fig. 26)

$$\Phi = E_{vac} - E_F. \tag{44}$$

The microscopic interpretation of Φ contains several contributions. Surface relaxation or adsorption of adatoms results in general in a surface dipole layer which the emitted electron must pass through. Also the band bending V_b at the semiconductor surface may be affected by adatoms leading to a change ΔV_b in the work function. It is convenient to describe the total work function by means of

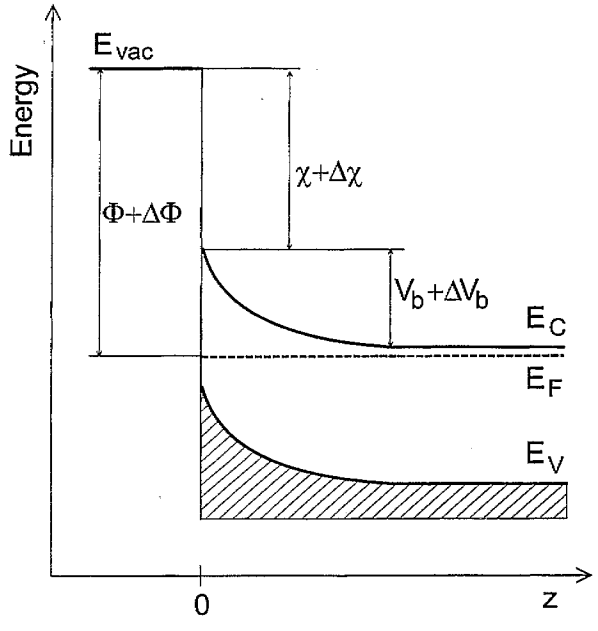

Fig. 26. Schematic energy-level diagram for Sb/GaAs (1 1 0) in the low-coverage limit.

three contributions (see, e.g., Ref. [235]):

$$\Phi = \chi + V_b + (E_C - E_F)_{bulk}, \tag{45}$$

where χ is the electron affinity and E_C denotes the position of the CBM. The variation of the surface dipole potential $\Delta\Phi_{dip}$ due to adsorbed atoms is assumed to change the electron affinity from χ to $\chi + \Delta\chi$. The total work function change $\Delta\Phi$ upon adsorption is therefore obtained as

$$\Delta\Phi = \Delta\chi + \Delta V_b = \Delta\Phi_{dip} + \Delta V_b. \tag{46}$$

Mattern-Klosson and Lüth [15, 163] investigated the work function changes due to deposition of Sb on GaAs (1 1 0) by UPS. On n-doped samples the saturation value of 0.4 eV for $\Delta\Phi$ is reached essentially after the completion of the first monolayer, whereas on p-type GaAs a further decrease occurs up to 7 ML of Sb. The work function has then changed by about -0.6 eV with respect to the value for the clean GaAs (1 1 0) surface.

In an experimental setup with a strong initial band bending which allows no further adsorbate-induced changes ΔV_b, the work function change equals $\Delta\Phi_{dip}$ and is independent of doping. Measurements [163] for the adsorbate-induced surface dipole changes are shown in Fig. 27. A dipole pointing out of the substrate which causes a decrease of the work function is observed. The dipole potential changes steadily with increasing coverage until the value is saturated at about -0.3 eV for one monolayer antimony adsorbed on GaAs (1 1 0). Further adsorption does not lead to a significant change of the dipole. On the other hand, a surface dipole pointing into the substrate is created upon relaxation of the free GaAs (1 1 0) surface. The dipole potential induced by the outward (inward) movement of the surface anion (cation) at the clean surface is estimated to lie between 0.2

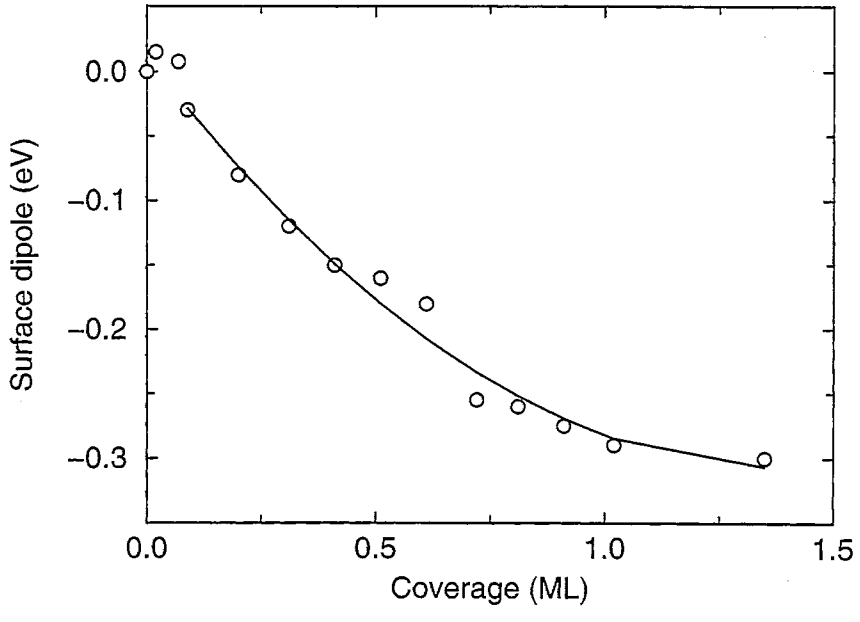

Fig. 27. Dipole contribution to the work function change $\Delta\Phi_{dip}$ plotted against Sb coverage on GaAs (1 1 0). After [163].

[236] and 0.4 eV [138]. So the dipole contribution to the change in the work function observed for Sb adsorption is basically due to the resulting de-relaxation of the GaAs surface. An additional contribution due to a significant charge transfer between adatoms and substrate atoms is unlikely. This can be explained by the small differences in the electronegativities between Ga, As, and Sb. The charge flow from Ga to Sb should be roughly compensated by the charge transferred from the adatom to As.

The macroscopic surface dipole and the accompanying electrostatic potentials which cause the changes of the work function upon group-V adsorption can be obtained from the microscopic electrostatic potential $V_C(r) = V_{ps}^{local}(r) + V_H(r)$ calculated within DFT–LDA. Here V_{ps}^{local} is the local part of the crystal pseudopotential and $V_H(r)$ is the Hartree potential (see Section 2.2). $V_C(r)$ is periodic in the planes perpendicular to the surface normal. As one is mainly interested in the macroscopic spatial dependence of the electrostatic potential in (1 1 0) direction it is convenient to perform a planar ((1 1 0) plane) average of $V_C(r)$. The planar averaged function can then be passed through a filter of the length L in order to extract the macroscopic changes of the elctrostatic potential [138]. The averaged and smoothed electrostatic potential in (1 1 0) (z-) direction is thus given by

$$\overline{V_C(z)} = \frac{1}{L}\int_{z-L/2}^{z+L/2} dz' \frac{1}{A}\int_A dx\, dy\, V_C(x, y, z'), \tag{47}$$

where A corresponds to the area of the surface unit cell in the (1 1 0) plane and L is chosen to be the distance between two substrate layers. In the bulk region as well as in the vacuum $\overline{V_C(z)}$ tends to certain values. In order to elaborate on the surface features and changes due to the antimony adsorption it is interesting to look at the difference of $\overline{V_C(z)}$ between the Sb covered and the clean relaxed GaAs (110) surface. The resulting difference function $\Delta\overline{V_C(z)}$ for one monolayer Sb on GaAs can be seen in Fig. 28. The variation of the potential difference from the vacuum region through the interface into the bulk corresponds to a surface dipole $\Delta\Phi_{dip}$ of about -0.4 eV. This is in rather good agreement with the experimental value [163] of -0.3 eV. The change in the surface dipole equals the change in the ionization energy. Schmidt et al. [110] calculated the difference of the ionization energy with respect to the clean GaAs (1 1 0) surface for the five structural models discussed in Section 4.1.1. Only for the ECLS the change of the ionization energy is in reasonable agreement with experiment.

6.2. *Band bending and Schottky barrier formation*

6.2.1. *Antimony overlayers*

In first photoemission studies of the Sb/GaAs (1 1 0) interface Skeath et al. [4,6] found that the surface Fermi level was shifted to about 0.55 eV above the VBM after depositing between one and two monolayers of Sb on p-type GaAs. Similar results were also reported by Mattern-Klosson and Lüth [163] using the same technique. They reported saturation values for the Sb-induced band bendings of 0.5 and 0.65 eV for p- and n-type GaAs, respectively. Since the pinning positions are essentially the same as for other metals and non-metals on the GaAs surface, the pinning mechanism at these interfaces was suggested to be the same, that is, the native defects of GaAs are responsible for the Fermi level pinning. This interpretation has been challenged since then: In their work performed

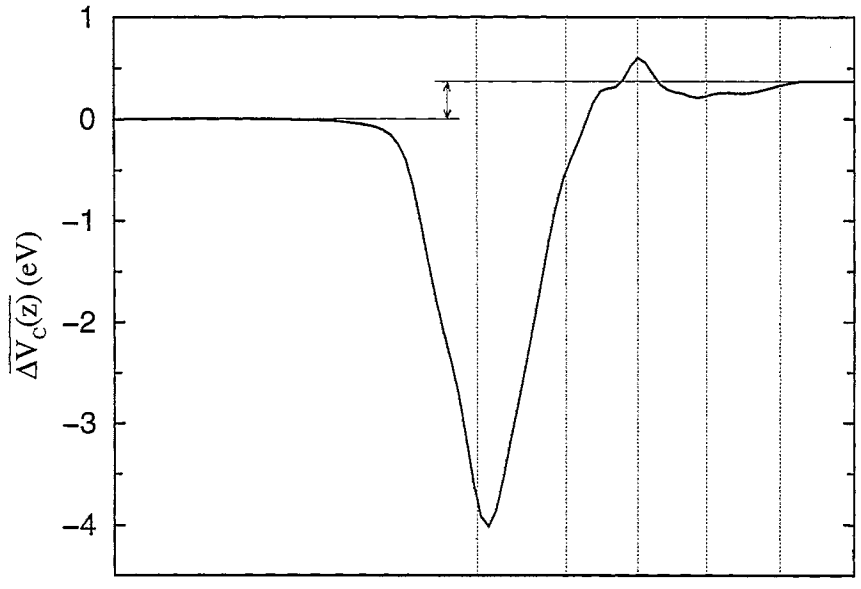

Fig. 28. Plot of the difference of the averaged electrostatic potential $\overline{\Delta V_C(z)}$ between Sb/GaAs (1 1 0) (1 ML) and the clean relaxed GaAs (1 1 0) surface against distance z parallel to the surface normal. Dashed lines mark the averaged positions of the Sb and GaAs (1 1 0) layers, respectively. The macroscopic surface dipole is indicated. From [1 1 0].

on the Sb/n-GaAs (1 1 0) interface, using surface photovoltage measurements, Li and Kahn [142] reported a maximum band bending when the GaAs (1 1 0) surface was covered by half a monolayer of Sb and the recovery of the flat band conditions when full monolayer coverage was reached. It was suggested that the Fermi level pinning in the submonolayer region was related to the unsaturated bonds near the edge of the Sb covered islands. When these islands grow together upon further deposition the density of these states is reduced and flat band conditions are recovered. Such an interpretation is in agreement with a study of the Schottky barrier formation at the Sb/p-GaAs interface by Schäffler et al. [14,35]. It has already been described in Section 3.3.

Annealing 3 ML Sb on p-type GaAs at 300°C leads to a large reduction of the band bending from 0.5 to 0.2 eV above VBM towards flat band conditions [13,166]. This is in qualitative agreement with Refs. [14,35]. The effect of reduced band bending upon annealing can be explained by the formation of a stable ordered Sb monolayer. The annealing temperatures studied lie above the desorption threshold for Sb atoms above the first monolayer (cf. Section 1.2). According to the Sb/GaAs surface band structure (Fig. 18) there are no intrinsic interface states which could explain the Fermi level pinning on p-type GaAs above VBM for the ordered monolayer. Defects remaining in the overlayer or native defects of the GaAs surface could provide a possible explanation for the persistent Fermi level pinning near VBM.

For n-type GaAs quite a different behaviour was noted in [13,166]. The Fermi level position remained pinned at about 0.75 eV above VBM over a large annealing temperature range from RT to 400°C. Whereas the findings for p-type GaAs agree with the general trend observed in other experiments and can be explained using the band structure results for an ordered monolayer, the results for n-type GaAs are hard to reconcile with a corresponding picture for unoccupied states. The

Fermi level position at the Sb/GaAs interface has also been derived from EFIRS spectra [48,85]. In accordance with the results discussed above a strong increase of the Schottky barrier is observed on n- and p-type substrates with Sb deposition. On annealing to 450 K the barrier is reduced which has been attributed to the transition from amorphous to crystalline Sb [48]. Upon further annealing, the barrier height gradually decreases until the barrier has finally vanished on n-type or is small on p-type GaAs. The latter is in agreement with the discussion above, whereas the vanishing barrier on n-type substrate contradicts the findings in [13,166], but has also been confirmed by later SXPS measurements [69,91].

A compilation of experimental results for the interface Fermi level position in the band gap for GaAs (1 1 0) for RT deposition of Sb at different coverages is shown in the left panel of Fig. 29. The values are obtained for overlayers without subsequent annealing. Although there is some scatter in the data obtained by different groups and aquired by different techniques, a trend for the coverage dependence of the Fermi level position can be recognized. Major shifts of the Fermi level occur for coverages below half a monolayer. On both p- and n-type substrates the Fermi level moves towards midgap. For higher coverages there is a slight upward shift of the Fermi level for both substrate types: the Schottky barrier gets slightly larger on p-type substrates and slightly smaller on n-type substrates. However, the Fermi levels on p- and n-type GaAs remain separated by about 0.25 eV. Conceivable origins of the pinning states are edge states, surface and interface defects, and certain disorder in the overlayer. However, contributions from overlayer-induced gap states cannot be excluded. When Sb overlayers of more than one monolayer are annealed, so that one ordered monolayer remains on the surface, the Fermi level position changes remarkably as shown in the right

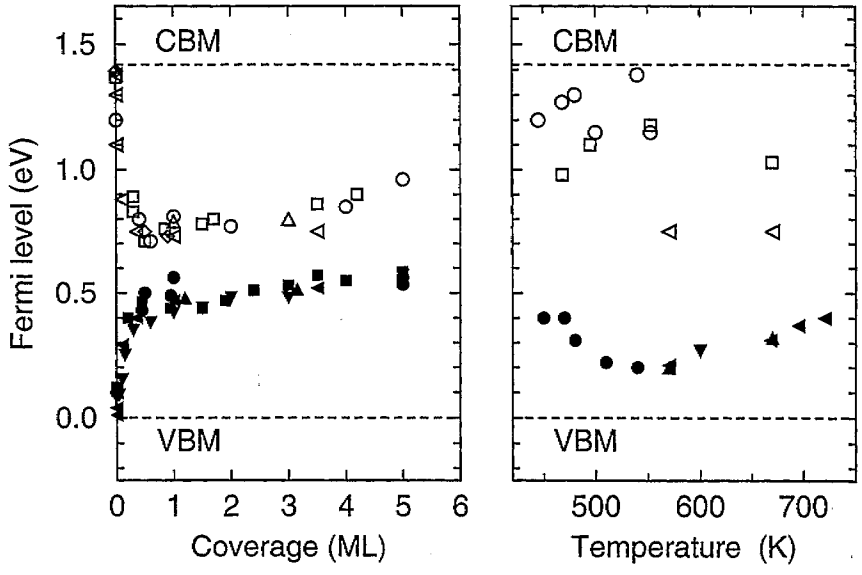

Fig. 29. Experimental results for the interface Fermi level for Sb deposited onto GaAs (1 1 0) at or below RT (left panel) and after subsequent annealing of several monolayers (right panel). Filled (empty) symbols refer to p- (n-) type substrates. Circles, squares, triangles up, triangles down, diamonds, and triangles left correspond to EFIRS data from [91,48] and PES measurements of [91], [248], [35,14], [163] and [166,13], respectively.

panel of Fig. 29. There is fair agreement between the experimental data concerning the reduction of the barrier towards flat band conditions upon annealing the overlayer until only the first Sb monolayer is left on p-type GaAs. On the other hand, we observe quite a scatter of the Fermi level position determined after annealing of Sb on n-type GaAs. With spatially resolved EFIRS measurements Esser [91] observed in some parts of the sample a nearly vanishing barrier, whereas the Spicer group [13,166] found no shift in the Fermi level position at all. The reason for this discrepancy is not understood. Perhaps, different preparation conditions and sample quality are responsible. According to the calculated band structure for Sb/GaAs (1 1 0) (Fig. 18) the lowest unoccupied Sb-induced surface state occurs about 0.8 eV above VBM, which agrees rather well with the Fermi level position for one monolayer Sb on n-type GaAs as determined in [13,166]. However, this agreement may be fortuitous, as indicated further. On the other hand, the vast majority of experimental results indicate no significant extension of interface states in the bulk band gap for ordered Sb monolayers as discussed in Section 4.3.1. Therefore we think that the barrier height reduction upon annealing for Sb deposited on n-type GaAs is plausible. The annealing procedure gets rid of most defects and helps generate the ordered monolayer structure. The states related to the ordered overlayer are pushed towards the substrate bulk band edges. The seeming contradiction to the band structure in Fig. 18 can most probably be explained by the DFT–LDA gap problem discussed in Section 2.2.4. The quasi-particle corrections shift empty surface states much more than empty bulk states towards higher energies [132,133,135]. As a result of the many-body effects the band ordering could therefore be changed.

The dynamics of the Fermi level pinning for coverages which are larger than a few monolayers can hardly be observed with PES, but have been studied with EFIRS and I–V measurements. Fig. 30 shows the Fermi level position for such high coverages without additional heat treatment. As already discussed one observes a considerable Fermi level shift below one monolayer with a quasi-saturation at 1 ML. Beyond 1 ML, however, for n-GaAs strong further changes occur: towards 10 ML the band bending decreases and then increases again. This increase coincides with the transition to crystalline Sb, which is semimetallic. For deposition at 80 K, where no crystallization occurs, no increase of the band bending is observed [85]. The final value for the Fermi level position on p- and n-type GaAs is reached for coverages of about 100 ML and is in agreement with I–V measurements at about 0.7 eV above VBM[91]. The midgap position independent on the substrate doping comes close to the 'canonical' Fermi level position defined as the local charge neutrality level for the non-polar (1 1 0) face [237].

The coverage- and temperature-dependent development of the Fermi level position for the Sb/InP interface observed experimentally seems to be qualitatively different compared to GaAs. Sb deposition on p-type InP at or below RT without an additional heat treatment leads to a large increase in Schottky barrier height [48,69,91,215,216,247,249] as shown in the left panel of Fig. 31. The Fermi level position for several disordered Sb monolayers lies at about 0.7–0.9 eV above the bulk valence-band edge. However, there is an appreciable scatter in the experimental results. With desorption of Sb at higher annealing temperatures, the barrier is reduced as on GaAs (right panel of Fig. 31). The barrier takes its minimum value for an annealing temperature of about 500 K. This has been correlated with the formation of a single ordered antimony monolayer [48]. On further annealing, the barrier increases again due presumably to the destruction of this monolayer and the correspondingly induced surface disorder. However, there is also quite a scatter in the data for the remaining Schottky barrier height after annealing. In Refs. [48,69,91,247] rather large values of

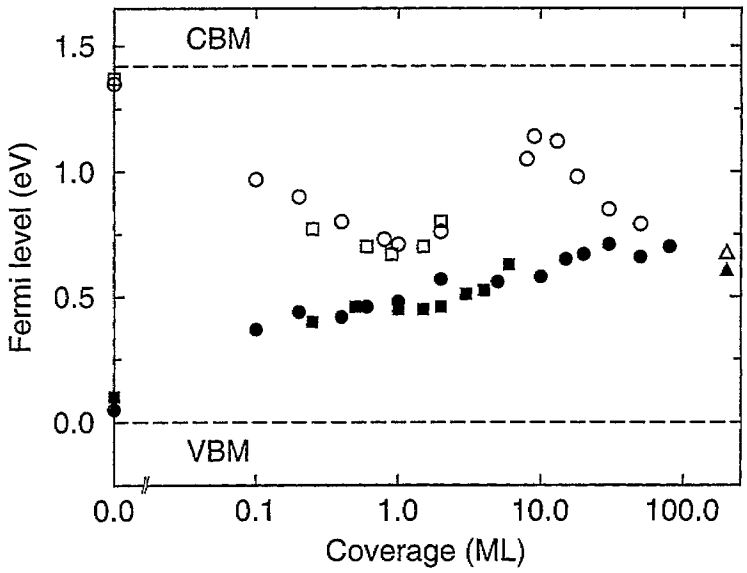

Fig. 30. Surface Fermi level at GaAs (1 1 0) for high Sb coverages deposited at RT. Filled and empty symbols refer to measurements on p- (Ref. [91]) and n-type substrates (Ref. [85]). Squares and circles denote SXPS and EFIRS data, respectively.

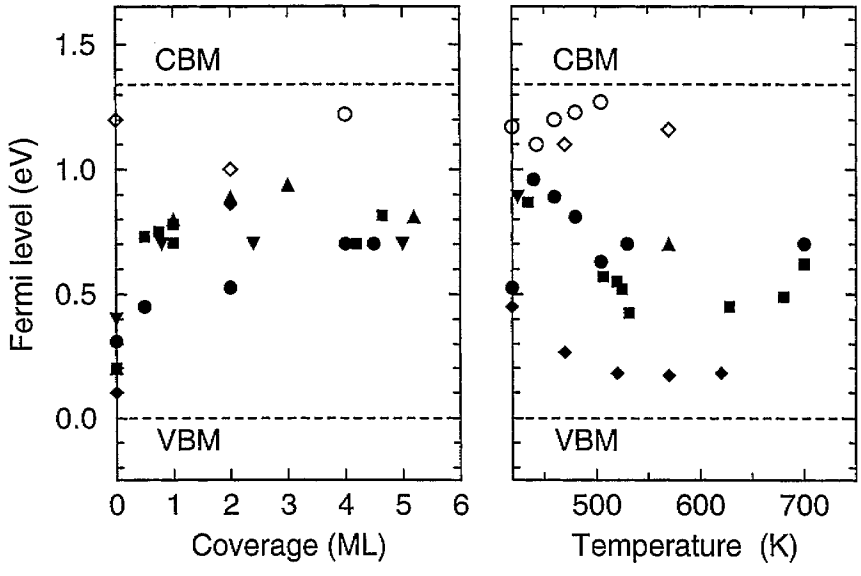

Fig. 31. Experimental results for the interface Fermi level for Sb deposited onto InP (1 1 0) at or below RT (left panel) and after subsequent annealing of several monolayers (right panel). Filled (empty) symbols refer to p- (n-) type substrates. Circles, squares, triangles up, triangles down and diamonds correspond to EFIRS data from [91,48] and PES measurements of [91,247,249] and [215,216] respectively.

around 0.5 eV are reported. Such a barrier for a well ordered monolayer Sb on p-type InP cannot be explained with the surface band structure of Sb/InP (Fig. 18). The absence of any occupied states higher than a few tenths of one eV above the VBM in the calculated band structure for the ECLS has led to speculations about alternative bonding mechanisms [48,69,145]. For reasons discussed in Section 4 we do not doubt the ECLS to be the actual bonding configuration. Several other explanations have been put forward. One such is due to Esser et al. [69] who attributed the Fermi level position to phosphorus defects in the interface. At this stage the precise origin of the relatively large Schottky barriers for annealed Sb overlayers on p-type InP observed in [48,69,91,247] remains somehow an open question. More recent PES measurements of Yamada et al. [215,216] showed for annealing temperatures between 200°C and 350°C a movement of the Fermi level to nearly flat band condition with a residual band bending of less than 0.2 eV for Sb on p-type InP. This is in reasonable agreement with the calculated band structure (cf. Fig. 18). Therefore we think that the large Schottky barriers observed by some groups for Sb/InP monolayers are related to interface imperfections and remaining disorder. In Section 1.2 we have pointed out that the Sb monolayers on InP are thermally and chemically less stable than Sb/GaAs interfaces. Therefore we believe that the reason for the differences observed for the Fermi level pinning on p-type substrates of GaAs and InP lies at least partially in experimental difficulty to obtain reproducible data for the perfect Sb/InP interface.

Antimony adsorption on n-type InP leads to the formation of a much smaller Schottky barrier compared to p-type substrates [48,91,215,216] as shown in the left panel of Fig. 31. The reported values lie between about one and three tenths of one eV. Upon annealing a small decrease of the Schottky barrier is observed unanimously in all measurements [48,215,216]. The reproducibility of the results by different groups suggests that the monolayer adsorption after annealing on n-InP is either essentially disorder free or the disorder-induced states lie close to the conduction-band edge. Besides the relation of the observed Fermi level position to overlayer disorder also native surface defects come into question. It is known that defects such as phosphorus vacancies could be responsible for the experimentally observed pinning positions [239]. However, this remains a matter of speculation, since there are only comparatively few data available on the Fermi level pinning on n-InP.

For higher coverages differences between Sb/GaAs and Sb/InP interfaces are also observed. For InP substrates Fermi level movement occurs up to 100 ML. The most striking feature is a minimum of the barrier height for Sb on p-InP at about 12 ML, followed by a steep re-increase [91]. By means of annealing experiments it could be shown that the increase of the Schottky barrier for coverages higher than 12 ML is due to the formation of relatively large crystallites. The Fermi level is finally pinned at about 1.1–1.35 eV (0.1 eV) above VBM (below CBM) for coverages of more than 100 ML for p-(n-) type substrate [91,240]. The different Fermi level positions for n- and p-substrates could indicate pinning mechanisms due to electronic states in the gap.

The deposition of Sb onto n-InAs (1 1 0) has been found to lead to a movement of the Fermi level position from the gap region into the bulk conduction band [45]. This Fermi level movement can be explained by the formation of an accumulation layer in the semiconductor and has already been observed for a series of adsorbates on InAs (1 1 0). It is due to the relatively small density of states at the CBM. However, annealing the sample reduces the band bending, i.e., the surface Fermi level shifts back to the CBM. As a result flat band conditions are nearly restored as found for Sb/GaAs and Sb/InP.

6.2.2. Bismuth overlayers

The peculiarity of Bi to form zigzag chains on GaAs (1 1 0) which are periodically interrupted by an ordered array of dislocations seems to be the key element for the electric barrier formation for the near monolayer deposition. As already discussed earlier, the dislocations give rise to acceptor-like states which lead to a Fermi level pinning near midgap on n-type samples as observed with core-level spectroscopy [16,18,53,91] and EFIRS [91]. Contrary to the rather continuous shift of E_F towards 0.6 eV above VBM reached for one monolayer on the n-type substrates, p-type samples initially exhibit a slow rate, followed by a rapid rise and an overshoot, until the Fermi level position is nearly fixed for one monolayer at roughly 0.4 eV above VBM. The Fermi level position 0.4 eV above the bulk valence-band edge for the first completed monolayer of Bi on p-type GaAs (1 1 0) agrees very well with the calculated position of the highest occupied surface band (cf. Fig. 20). Annealing does not have an essential influence on the band bending. This is much in contrast to antimony overlayers, but can be readily explained: (i) The superior quality of Bi monolayers already at RT due to the lower melting point compared to Sb and (ii) the existence of donor- and acceptor-like interface states in the bulk band gap as intrinsic properties of these interfaces strongly reduce the effect of annealing procedures on the Fermi level position.

Higher coverages of up to 1000 ML of Bi on GaAs (1 1 0) have been studied with EFIRS and I–V measurements [238]. Beyond one monolayer the n-doped sample shows a significant difference in Schottky barrier formation compared to the p-doped sample. At RT the Schottky barrier for n-GaAs is diminished between monolayer coverage and coverages near 50 ML. The re-increase of the band bending for coverages higher than 50 ML coincides with the formation of large crystallites as discussed in Section 5.2. This behaviour is quite similar to the case of thick antimony overlayers on GaAs (1 1 0). At coverages beyond 100 ML one common Fermi level at 0.61 eV above the VBM is obtained for both n- and p-type GaAs [238].

EFIRS [241] and PES [147–149] measurements have been employed to monitor the Fermi level shift on InP (1 1 0) upon bismuth deposition. The final position of the Fermi level (about 0.8 eV above VBM for p-InP) is only approached for coverages beyond the onset of metallicity at as much as 60 ML. The variation of the band bending for thinner overlayers is likely to be induced by imperfections in the overlayer for submonolayer coverages and partial healing of those for higher coverages. In particular the systematic turn-around in the barrier-height development on both n- and p-type InP for coverages between 0.3 and 1.0 ML supports the view that the submonolayer stages of band bending are due to states created at the edges of two-dimensional islands. Electrical measurements [241] of the Schottky barrier height for thick Bi contacts to InP (1 1 0) yielded 0.83 eV (I–V) and 0.85 (C–V) (p-type) and 0.48 eV (I–V) (n-type). Surprisingly high Schottky barriers were measured at low temperature deposition of Bi on p-InP [148]. These barriers of more than 1 eV are conserved even after warming up the sample to RT.

Only a weak dependence of the band bending on the coverage was found for Bi/GaSb (110). For coverages beyond one monolayer a final Fermi level position of 0.06 eV above VBM has been measured on the p-doped sample [58]. This is of particular interest since it indicates that no extension of occupied interface bands into the bulk band gap occurs as observed for Bi interfaces with GaAs, InP, and InAs (cf. Fig. 20). This is in agreement with ARPES measurements [152], which place the occupied surface states at or below the bulk valence-band edge. The band bending on n-type GaSb seems to be more pronounced as estimated through an analysis of the substrate-related

phonon and dopant-induced free-carrier plasmon by Gavioli et al. [60]. For a coverage of 0.6 ML a barrier height of 0.27 eV is reported. The ordered (1 × 1) and (1 × 2) phases give rise to a band bending of 0.20 and 0.14 eV, respectively. The different Fermi level positions on n- and p-type substrates are, however, hard to reconcile with the apparent metallicity of the interface already for low coverages [60,153].

From the experimental results discussed above, it becomes evident that the method of interface preparation plays a crucial role in determining the final barrier height. To our mind different preparation methods may also explain a number of the contradicting results obtained experimentally. Summarizing the results for the Fermi level pinning of Sb and Bi on III–V (1 1 0) we have to differentiate between several coverage regimes. For adsorbed submonolayers the Fermi level pinning is mainly governed by edge states at two-dimensional islands. The small Schottky barriers for perfect monolayers can partially be explained by the existence of the interface states [242,243] S_6 and S_7 (cf. Figs. 18 and 20), which may be interpreted either as virtual [244] or metal-induced gap states (MIGS) [168,169]. A realistic description of the Fermi level pinning in the picture of the Bardeen model [245] may additionally account for the role played by defects in the overlayers, native defects in the substrate and dislocation-derived states (in particular for Bi/GaAs (110)). In the coverage regime between one and several dozen monolayers further strong dynamics of the Fermi level position occurs, which can be related to structural changes in the overlayer. Saturation values of the Fermi level are only reached after metallization of the overlayer, which is distinctly delayed for Sb or Bi overlayers on III–V(1 1 0) compared to other metal–semiconductor interfaces and occurs only beyond 100 monolayers. The reason for the relatively high amount of deposited material needed for the metallization of the overlayer may be found in quantum size effects, which lift the overlap between valence and conduction bands in the Sb and Bi crystallites [251]. The final positions of the Fermi level for Sb and Bi on GaAs and Bi on InP are in fair agreement with the canonical Schottky barrier heights [237] of 0.7 and 0.76 eV, respectively. The large deviation for Sb on InP substrate can possibly be explained by using a model which takes into account the correct geometry at the interface.

7. Summary

The interfaces formed between group-V elements – in particular the semimetals antimony and bismuth – and III–V (1 1 0) surfaces show a number of properties which make them model systems from the points of view of both experimental and theoretical surface and interface physics. The onset of adsorption occurs in two-dimensional clusters with local (1 × 1) symmetry which grow together forming ordered first monolayers. The formed interfaces are abrupt and atomically smooth. In most cases the structural, electronic and vibrational properties of these ordered first monolayers are very similar and can be related to chemical trends with the covalent radii, electronegativities, orbital energies and masses of the constituents. Further deposition leads to a variety of structural phases which are additionally influenced by the actual growth conditions and show a complex coverage dependence of the band bending. Only for high coverages beyond several dozen monolayers the Fermi level is finally pinned indicating the completion of the metal–semiconductor interface.

Although most V/III–V (1 1 0) interfaces studied are fairly well understood by now, there are still some open questions. Firstly, little information is available regarding the adsorption geometry and

related properties for overlayers of other group-V atoms than Sb and Bi on III–V (1 1 0) surfaces. Some activities concerning the adsorption of As on GaAs and InP have recently started. Secondly, only little is known about the precise geometry and origin of reconstructions larger than (1 × 1) as observed for example for Bi adsorption on InAs, GaSb and InSb. Thirdly, even systems which have been extensively studied are not fully understood. In particular, there exist discrepancies in the various studies on the band bending at Sb/GaAs and Sb/InP interfaces and the relationships between interface geometry, intrinsic electronic states, and Fermi level pinning. These aspects remain subjects of current investigations.

Glossary of symbols

a	lattice constant
AES	Auger-electron spectroscopy
ARIPS	angle-resolved inverse photoemission electron spectroscopy
ARPES	angle-resolved photoemission electron spectroscopy
ARUPS	angle-resolved ultraviolet photoemission electron spectroscopy
CBM	conduction-band minimum
DFT	density functional theory
DOS	density of states
E_C	energy of conduction-band minimum
E_F	Fermi energy
E_V	energy of valence-band maximum
E_{vac}	energy of vacuum level
ECLS	epitaxial continued layer structure
EELS	electron-energy-loss spectroscopy
EFIRS	electric field-induced Raman scattering
EOCS	epitaxial overlapping chain structure
EOTS	epitaxial on top structure
FLAPW	full potential linearized augmented plane wave
GIXD	grazing-incidence X-ray diffraction
HREELS	high-resolution electron-energy-loss spectroscopy
LEED	low-energy electron diffraction
LDOS	local density of states
LDA	local density approximation
M_A	anion atomic mass
M_C	cation atomic mass
MCS	missing chain structure
MIGS	metal-induced gap states
ML	monolayer
PED	photoelectron diffraction
PES	photoemission spectroscopy
PEXAFS	photoemission extended X-ray absorption fine-structure
r_A	anion covalent radius
r_C	cation covalent radius

RAS	reflectance-anisotropy spectroscopy
RHEED	reflection high-energy electron diffraction
RRS	resonance Raman spectroscopy
RT	room temperature
SBZ	surface Brillouin zone
STM	scanning tunneling microscopy
SXPS	soft X-ray photoemission spectroscopy
TB	tight binding
V_b	band bending
UPS	UV photoemission spectroscopy
VBM	valence-band maximum
XSW	X-ray standing wave
Θ	coverage
Φ	work function
Φ_{dip}	surface dipole potential
χ	electron affinity

Acknowledgements

We have benefited from discussions with many colleagues on the subject matter. In particular we acknowledge detailed discussions with M. Scheffler, F. Flores, W. Mönch, and R. Whittle. We are grateful to N. Esser for a critical reading of the manuscript. This work was supported in part by the Deutsche Forschungsgemeinschaft (DFG project No. Be 1345/6–1) and the DAAD/BC (ARC project No. 637).

References

[1] J.F. McGilp and A.B. McLean, J. Phys. C 21 (1988) 807.
[2] A. Kahn, Surf. Sci. Rep. 3 (1983) 193.
[3] C.B. Duke and A. Patton, Surf. Sci. 164 (1985) L797.
[4] P. Skeath, C.Y. Su, I. Lindau and W.E. Spicer, J. Vac. Sci. Technol. 17 (1980) 874.
[5] P. Skeath, I. Lindau, C.Y. Su and W.E. Spicer, J. Vac. Sci. Technol. 19 (1981) 556.
[6] P. Skeath, C.Y. Su, W.A. Harrison, I. Lindau and W.E. Spicer, Phys. Rev. B 27 (1983) 6246.
[7] J. Carelli and A. Kahn, Surf. Sci. 116 (1982) 380.
[8] C.B. Duke, A. Paton, W.K. Ford, A. Kahn and J. Carelli, Phys. Rev. B 26 (1982) 803.
[9] R.M. Feenstra and P. Mårtensson, Phys. Rev. Lett. 61 (1988) 447.
[10] P. Mårtensson and R.M. Feenstra, Phys. Rev. B 39 (1989) 7744.
[11] P. Mårtensson and R.M. Feenstra, J. Microsc. 152 (1988) 761.
[12] R. Strümpler and H. Lüth, Surf. Sci. 182 (1987) 545.
[13] R. Cao, K. Miyano, T. Kendelewicz, I. Lindau and W.E. Spicer, Surf. Sci. 206 (1988) 413.
[14] F. Schäffler, R. Ludeke, A. Taleb-Ibrahimi, G. Hughes and D. Rieger, J. Vac. Sci. Technol. B 5 (1987) 1048.
[15] M. Mattern-Klosson, R. Strümpler and H. Lüth, Phys. Rev. B 33 (1986) 2559.
[16] R. Ludeke, A. Taleb-Ibrahimi, R.M. Feenstra and A.B. McLean, J. Vac. Sci. Technol. B 7 (1989) 936.
[17] A.B. McLean, R.M. Feenstra, A. Taleb-Ibrahimi and R. Ludeke, Phys. Rev. B 39 (1989) 12925.

[18] J.J. Joyce, J. Anderson, M.M. Nelson and G.J. Lapeyre, Phys. Rev. B 40 (1989) 10412.
[19] T. Guo, R.E. Atkinson and W.K. Ford, Phys. Rev. B 41 (1990) 5138.
[20] G.B. Waddill, C.M. Aldao, C. Capasso, P.J. Benning, Y. Hu, T.J. Wagener, M.B. Jost and J.H. Weaver, Phys. Rev. B 41 (1990) 5960.
[21] A.B. McLean, R. Ludeke, M. Prietsch, D. Heskett, D. Tang and T.M. Wong, Phys. Rev. B 43 (1991) 7243.
[22] U. Resch, N. Esser and W. Richter, Surf. Sci. 251/252 (1991) 621.
[23] M.G. Betti, M. Pedio, U. del Pennino and C. Mariani, Phys. Rev. B 45 (1992) 14057.
[24] V. DeRenzi, M.G. Betti and D. Mariani, Surf. Sci. 287/288 (1993) 550.
[25] B. Kübler, W. Ranke and K. Jacobi, Surf. Sci. 92 (1980) 519.
[26] R.Z. Bachrach, R.S. Bauer, P. Chiaradia and G.V. Hansson, J. Vac. Sci. Technol. 19 (1981) 335.
[27] T.T. Chiang and W.E. Spicer, J. Vac. Sci. Technol. A 7 (1989) 724.
[28] J.E. Northrup, Phys. Rev. B 44 (1991) 1349.
[29] J. Zhou, Y. Huang, Y. Li and W.Y. Jia, J. Cryst. Growth 81 (1983) 221.
[30] L. Pfeiffer, K.W. West, H.L. Störmer, J.P. Eisenstein, K.W. Baldwin, D. Gershoni and J. Spector, Appl. Phys. Lett. 56 (1990) 1697.
[31] D. Gershoni, J.S. Weiner, S.N.G. Chu, G.A. Baraff, J.M. Vandenberg, L.N. Pfeiffer, K. West, R.A. Logan and T. Tanbun-Ek, Phys. Rev. Lett. 65 (1990) 1631.
[32] W. Wegschneider, L.N. Pfeiffer, M.M. Dignam, A. Pinczuk, K.W. West, S.C. McCall and R. Hull, Phys. Rev. Lett. 71 (1993) 4071.
[33] Z.Q. He, Y.O. Khazmi, J. Kanski, L. Ilver, P.O. Nilsson and U.O. Karlsson, Phys. Rev. B 52 (1995) 16602.
[34] P.V. Santos, B. Koopmans, N. Esser, W.G. Schmidt and F. Bechstedt, Phys. Rev. Lett. 77 (1996) 759.
[35] F. Schäffler, R. Ludeke, A. Taleb-Ibrahimi, G. Hughes and D. Rieger, Phys. Rev. B 36 (1987) 1328.
[36] M.G. Betti, C. Mariani, N. Jedrecy, R. Pinchaux, A. Ruocco and M. Sauvage-Simkin, Phys. Rev. B 50 (1994) 14336.
[37] C. Stringer, A. McKinley, G.J. Hughes and R.H. Williams, Vacuum 33 (1983) 597.
[38] C. Maani, A. McKinley and R.H. Williams, J. Phys. C 18 (1985) 4975.
[39] C.B. Duke, C. Mailhiot, A. Paton, K. Li, C. Bonapace and A. Kahn, Surf. Sci. 163 (1985) 391.
[40] W. Drube and F.J. Himpsel, Phys. Rev. B 37 (1988) 855.
[41] M. Hünermann, J. Geurts and W. Richter, Phys. Rev. Lett. 66 (1991) 640.
[42] R. Whittle, I.T. McGovern, D.R.T. Zahn, C. Müller, C. Nowak, A. Cafolla and W. Braun, Appl. Surf. Sci. 56–58 (1992) 218.
[43] W.K. Ford, T. Guo, K.-J. Wan and C.B. Duke, Phys. Rev. B 45 (1992) 11896.
[44] A. Tulke and H. Lüth, Surf. Sci. 178 (1986) 131.
[45] C. Nowak, J. Krujatz, A. Märkl, C. Meyne, A. Chassé, W. Braun, W. Richter and D.R.T. Zahn, Surf. Sci. 331–333 (1995) 619.
[46] M. Prietsch, A. Samsavar and R. Ludeke, Phys. Rev. B 43 (1991) 11850.
[47] K.E. Miyano, T. Kendelewicz, J.C. Woicik, P.L. Cowan, C.E. Bouldin, B.A. Karlin, P. Pianetta and W.E. Spicer, Phys. Rev. B 46 (1992) 6869.
[48] N. Esser, M. Reckzügel, R. Srama, U. Resch, D.R.T. Zahn, W. Richter, C. Stephens and M. Hünermann, J. Vac. Sci. Technol. B 8 (1990) 680.
[49] P.V. Santos, N. Esser, J. Groenen, M. Cardona, W.G. Schmidt and F. Bechstedt, Phys. Rev. B 52 (1995) 17379.
[50] A. Taleb-Ibrahimi, R. Ludeke, R.M. Feenstra and A.B. McLean, J. Vac. Sci. Technol. B 7 (1989) 936.
[51] R.M. Feenstra, P. Mårtensson and R. Ludeke, Mater. Res. Soc. Symp. Proc. 139 (1989) 15.
[52] W.K. Ford, T. Guo, S.L. Lantz, K. Wan, S.-L. Chang, C.B. Duke and D.L. Lessor, J. Vac. Sci. Technol. B 8 (1990) 940.
[53] J.J. Joyce, J. Anderson, M.M. Nelson, C. Yu and G.J. Lapeyre, J. Vac. Sci. Technol. A 7 (1989) 850.
[54] A.B. McLean and F.J. Himpsel, Phys. Rev. B 40 (1989) 8425.
[55] K.-H. Hellwege, Ed., Landolt–Börnstein, Vol. III/17a (Springer, Heidelberg, 1982).
[56] R. Whittle, E. Dudzik, I.T. McGovern, D.R.T. Zahn, C. Nowak, A. Cafolla and W. Braun, Surf. Sci. 287 (1993) 554.
[57] D.N. McIlroy, D. Heskett, D.M. Swanston, A.B. McLean, R. Ludeke, H. Munekata, M. Prietsch and N.J. DiNardo, Phys. Rev. B 47 (1993) 3751.
[58] T. van Gemmeren and R.L. Johnson, Surf. Sci. 331–333 (1995) 613.

[59] P. Casarini, L. Gavioli, M.G. Betti and C. Mariani, in: Proc. 4th Int. Conf. on the Formation of Semiconductor Interfaces, Ed. J. Pollmann (World Scientific, Singapore, 1994) pp. 231–234.
[60] L. Gavioli, M.G. Betti, P. Casarini and C. Mariani, Phys. Rev. B 51 (1995) 16822.
[61] A. Tulke and H. Lüth, Surf, Sci. 211/212 (1989) 1001.
[62] T. Chassé, G. Neuhold and K. Horn, Surf. Sci. 331–333 (1995) 511; T. Chassé, private communication.
[63] C. Mailhiot, C.B. Duke and D.J. Chadi, Phys. Rev. B 31 (1985) 2213.
[64] T. Kendelewicz, J.C. Woicik, K.E. Miyano, A. Herrera-Gómez, P.L. Cowan, B.A. Karlin, C.E. Bouldin, P. Pianetta and W.E. Spicer, Phys. Rev. B 46 (1992) 7276.
[65] A. Herrera-Gómez, T. Kendelewicz, J.C. Woicik, K.E. Miyano, P. Pianetta, S. Southworth, P.L. Cowan, B.A. Karlin and W.E. Spicer, J. Vac. Sci. Technol. A 11 (1993) 2345.
[66] A. Ruocco, N. Jedrecy, R. Pinchaux, M. Sauvage-Simkin and A. Waldhauer, Phys. Rev. B 50 (1994) 8004.
[67] R.M. Feenstra, P. Mårtensson and R. Ludeke, Mater. Res. Soc. Symp. Proc. 138 (1989) 305.
[68] C.K. Shih, R.M. Feenstra and P. Mårtensson, J. Vac. Sci. Technol. A 8 (1990) 3379.
[69] N. Esser, D.R.T. Zahn, C. Müller, W. Richter, C. Stephens, R. Whittle, I.T. McGovern, S. Kulkarni and W. Braun, Appl. Surf. Sci. 56–58 (1992) 169.
[70] D.R.T. Zahn, N. Esser, C. Müller, W. Richter, C. Stephens, R. Whittle, I.T. McGovern, S. Kulkarni and W. Braun, Appl. Surf. Sci. 56–58 (1992) 228.
[71] C. Nowak, A. Chassé, A. Hempelmann, W. Richter, E. Dudzik, R. Whittle, I.T. McGovern, W. Braun and D.R.T. Zahn, Surf. Sci. 307–309 (1994) 685.
[72] C. Nowak, PhD Thesis, Berlin University of Technology (Wissenschaft & Technik, 1996).
[73] C. Nowak, A. Hempelmann, A. Märkl, A. Chassé, E. Dudzik, C. Müller, I.T. McGovern, W. Braun, W. Richter and D.R.T. Zahn, Surf. Sci. 331–333 (1995) 564.
[74] C. Nowak, A. Chassé, W. Braun, W. Richter, I.T. McGovern and D.R.T. Zahn, J. Electron Spectrosc. Rel. Phen., in press.
[75] P. Skeath, C.Y. Su, I. Lindau and W.E. Spicer, Solid State Commun. 40 (1981) 873.
[76] F.J. Himpsel, W. Drube, A.B. McLean and A. Santoni, Appl. Surf. Sci. 56 (1992) 160.
[77] Y. Hu, T.J. Wagener, M.B. Jost and J.H. Weaver, Phys. Rev. B 40 (1989) 1146.
[78] Y. Hu, T.J. Wagener, M.B. Jost and J.H. Weaver, Phys. Rev. B 41 (1990) 5817.
[79] N. Esser, R. Hunger, J. Rumberg, W. Richter, R. Del Sole and A.I. Shkrebtii, Surf. Sci. 307–309 (1994) 1045.
[80] A.I. Shkrebtii, N. Esser, M. Köpp, P. Haier, W. Richter and R. Del Sole, Appl. Surf. Sci., to be published.
[81] N. Esser, M. Köpp, P. Haier and W. Richter, Phys. Status Solidi (b) 152 (1995) 191.
[82] M. Hünermann, W. Pletschen, U. Resch, U. Rettweiler, W. Richter, J. Geurts and P. Lautenschlager, Surf. Sci. 189/190 (1987) 322.
[83] W. Richter, N. Esser, A. Kelnberger and M. Köpp, Solid State Commun. 84 (1992) 165.
[84] N. Esser, M. Köpp, P. Haier and W. Richter, J. Electron Spectrosc. Rel. Phen. 64/65 (1993) 85.
[85] W. Pletschen, N. Esser, H. Münder, D. Zahn, J. Geurts and W. Richter, Surf. Sci. 178 (1986) 140.
[86] N. Esser, I. Benne, R. Srama and W. Richter, Surf. Sci. 269/270 (1992) 1037.
[87] G. Annovi, M.G. Betti, U. del Pennino and C. Mariani, Vacuum 41 (1990) 695.
[88] G. Annovi, M.G. Betti, U. del Pennino and C. Mariani, Phys. Rev. B 41 (1990) 11978.
[89] C. Mariani, V. DeRenzi and R. Compañó, Appl. Surf. Sci. 56–58 (1992) 247.
[90] J. Geurts, Festkörperprobleme 31 (1991) 177.
[91] N. Esser, PhD Thesis, Berlin University of Technology (Biesterfeld, Aachen, 1991).
[92] D.J. Chadi, Phys. Rev. Lett. 41 (1978) 1062; Phys. Rev. B 19 (1979) 2074.
[93] J.C. Slater and G.F. Koster, Phys. Rev. 94 (1954) 1498.
[94] P. Vogl, H-P. Hjalmarson and J.D. Dow, J. Phys. Chem. Solids 44 (1983) 365.
[95] J.P. LaFemina, C.B. Duke and C. Mailhiot, J. Vac. Sci. Technol. B 8 (1990) 888.
[96] J.M. McCoy and J.P. LaFemina, Phys. Rev. B 50 (1994) 17127.
[97] J.P. LaFemina, Surf. Sci. Rep. 16 (1992) 133.
[98] WA. Harrison, Electronic Structure and the Properties of Solids (Freeman, San Francisco, 1980).
[99] P. Hohenberg and W. Kohn, Phys. Rev. 136 (1964) B864.
[100] W. Kohn and L.J. Sham, Phys. Rev. 140 (1965) A1133.
[101] D.M. Ceperley and B.J. Alder, Phys. Rev. Lett. 45 (1980) 566.

[102] J.P. Perdew and A. Zunger, Phys. Rev. B 23 (1981) 5048.
[103] J.C. Slater, The Self-Consistent Field for Molecules and Solids, Vol. 4 (McGraw-Hill, New York, 1974)
[104] D.R. Hamann, M. Schlüter and C. Chiang, Phys. Rev. Lett. 43 (1979) 1494.
[105] G.B. Bachelet, D.R. Haman and M. Schlüter, Phys. Rev. B 26 (1982) 4199.
[106] N. Troullier and J.L. Martins, Phys. Rev. B 43 (1991) 1993.
[107] D. Vanderbilt, Phys. Rev. B 41 (1990) 7892.
[108] L. Kleinman and D.M. Bylander, Phys. Rev. Lett. 48 (1982) 1425.
[109] J.L.A. Alves, J. Hebenstreit and M. Scheffler, Phys. Rev. B 44 (1991) 6188.
[110] W.G. Schmidt, B. Wenzien and F. Bechstedt, Phys. Rev. B 49 (1994) 4731.
[111] J. Ihm, A. Zunger and M.L. Cohen, J. Phys. C 12 (1979) 4409.
[112] M.T. Yin and M.L. Cohen, Phys. Rev. B 26 (1982) 5668.
[113] G.P. Srivastava and D. Weaire, Adv. Phys. 36 (1987) 463.
[114] R.P. Feynman, Phys. Rev. 56 (1939) 340.
[115] A.A. Maradudin, E.W. Montroll, G.H. Weiss and I.P. Ipatova, Solid State Physics, Suppl. 3, Eds. Montroll et al. (Academic Press, New York, 1971).
[116] R.A. Evarestov and V.P. Smirnov, Phys. Status Solidi (b) 119 (1983) 9.
[117] W.G. Schmidt, A. Scholze and F. Bechstedt, Surf. Sci. 351 (1996) 183.
[118] W.E. Pickett, Comp. Phys. Rep. 9 (1989) 115.
[119] A. Umerski and G.P. Srivastava, Phys. Rev. B 48 (1993) 8450.
[120] A. Umerski and G.P. Srivastava, Phys. Rev. B 51 (1995) 2334.
[121] R. Car and M. Parrinello, Phys. Rev. Lett. 55 (1985) 2471.
[122] M.C. Payne, M.P. Teter, D.C. Allan, T.A. Arias and J.D. Joannopoulous, Rev. Mod. Phys. 64 (1992) 1045.
[123] M.C. Payne, J.D. Joannopoulous, D.C. Allan, M.P. Teter and D.H. Vanderbilt, Phys. Rev. Lett. 56 (1986) 2656.
[124] X. Gonze, P. Käckell and M. Scheffler, Phys. Rev. B 41 (1990) 12264; X. Gonze, R. Stumpf and M. Scheffler, Phys. Rev. B 44 (1991) 8503.
[125] R. Stumpf and M. Scheffler, Comp. Phys. Commun. 79 (1994) 447.
[126] L. Hedin, Phys. Rev. 139 (1965) A796.
[127] L. Hedin and S. Lundqvist, Solid State Physics, Vol. 23, Eds. F. Seitz, D. Turnbull and H. Ehrenreich (1969) p. 1.
[128] M.S. Hybertsen and S.G. Louie, Phys. Rev. B 34 (1986) 5390.
[129] X. Zhu, S.B. Zhang, S.G. Louie and M.L. Cohen, Phys. Rev. Lett. 63 (1989) 2112.
[130] R.W. Godby, M. Schlüter and L.J. Sham, Phys. Rev. B 37 (1988) 10159.
[131] F. Bechstedt, in: Festkörperprobleme/Advances in Solid State Physics, Vol. 32, Ed. U. Rössler (Vieweg, Braunschweig, 1992) p. 161.
[132] F. Bechstedt, R. Del Sole and F. Manghi, J. Phys: Condens. Matter 1 (1989) SB75.
[133] F. Bechstedt and R. Del Sole, Solid State Commun. 74 (1990) 41.
[134] S.J. Jenkins, G.P. Srivastava and J.C. Inkson, Phys. Rev. B 48 (1993) 4388.
[135] S.J. Jenkins, G.P. Srivastava and J.C. Inkson, Surf. Sci. 331—333 (1995) 1238.
[136] S. Gwo, A.R. Smith and C.K. Shih, J. Vac. Sci. Technol. A 11 (1993) 1644.
[137] C.J. Whitman, J.A. Stroscio, R.A. Dragoset and R.J. Celotta, Phys. Rev. Lett. 66 (1991) 1338.
[138] F. Bechstedt and M. Scheffler, Surf. Sci. Rep. 18 (1993) 145.
[139] J.-Y. Yi, J.-Y. Koo, S. Lee, J.S. Ha and E.-H. Lee, Phys. Rev. B 52 (1995) 10733.
[140] C.R. Bonapace, D.W. Tu, K. Li and A. Kahn, J. Vac. Sci. Technol. B 3 (1985) 1099.
[141] D.E. Savage and M.G. Lagally, Appl. Phys. Lett. 50 (1987) 1719.
[142] K. Li and A. Kahn, J. Vac. Sci. Technol. A 4 (1986) 958.
[143] N. Esser, H. Münder, M. Hünermann, W. Pletschen, W. Richter and D.R.T. Zahn, J. Vac. Sci. Technol. B 5 (1987) 1044.
[144] T. Kendelewicz, K.E. Miyano, R. Cao, I. Lindau and W.E. Spicer, J. Vac. Sci. Technol. B 7 (1989) 991.
[145] R.H. Williams, D.R.T. Zahn, N. Esser and W. Richter, J. Vac. Sci. Technol. B 7 (1989) 997.
[146] M. Pedio, M.G. Betti, C. Ottaviani, C. Quaresima and M. Capozi, Phys. Rev. B 43 (1991) 9070.
[147] K.E. Miyano, T. Kendelewicz, R. Cao, C.J. Spindt, I. Lindau, W.E. Spicer and J.C. Woicik, Phys. Rev. B 42 (1990) 3017.
[148] C. Stephens, D.R.T. Zahn, K. Fives, R. Cimino, W. Braun and I.T. McGovern, J. Vac. Sci. Technol. B 8 (1990) 674.

[149] C. Stephens, D.R.T. Zahn, R. Cimino, W. Braun, K. Fives and I.T. McGovern, Vacuum 41 (1990) 1021.
[150] K.M. Choudhary, P.S. Mangat, P. Seshradi, D. Kilday and G. Margaritondo, J. Vac. Sci. Technol. B 9 (1991) 2294.
[151] T. Guo, K.J. Wan and W.K. Ford, in: Atomic Scale Structure of Interfaces, Eds. R.D. Bringans, R.M. Feenstra and J.M. Gibson (Materials Research Society, Pittsburgh, PA, 1990) pp. 39–44.
[152] D.N. McIlroy, D. Heskett, A.B. McLean, R. Ludeke, H. Munekata and N.J. Di-Nardo, Phys. Rev. B 48 (1993) 11897.
[153] L. Gavioli, M.G. Betti, P. Casarini and C. Mariani, Phys. Rev. B 49 (1994) 2911.
[154] W.G. Schmidt, B. Wenzien and F. Bechstedt, Surf. Sci. 307–309 (1994) 235.
[155] F. Bechstedt, W.G. Schmidt and B. Wenzien, Europhys. Lett. 25 (1994) 357.
[156] J. Hebenstreit, M. Heinemann and M. Scheffler, Phys. Rev. Lett. 67 (1991) 1031.
[157] W.G. Schmidt and G.P. Srivastava, J. Phys.: Condens. Matter 5 (1993) 9025.
[158] W.G. Schmidt and F. Bechstedt, Phys. Rev. B 50 (1994) 17280.
[159] F. Flores, R. Saiz-Pardo, R. Rinón, J. Ortega, R. Pérez and F.J. García-Vidal, J. Phys.: Condens. Matter 5 (1993) A41.
[160] R. Saiz-Pardo, R. Rinón, R. Pérez and F. Flores, in: Proc. 4th Int. Conf. on the Formation of Semiconductor Interfaces, Ed. J. Pollmann (World Scientific, Singapore, 1994) pp. 301–304.
[161] R. Saiz-Pardo, R. Rinón, R. Pérez and F. Flores, Surf. Sci. 307–309 (1994) 309.
[162] R. Magri, Phys. Rev. B, in press.
[163] M. Mattern-Klosson and H. Lüth, Solid State Commun. 56 (1985) 1001.
[164] W.E. Spicer, I. Lindau, P.R. Skeath, C.Y. Su and P.W. Chye, Phys. Rev. Lett. 44 (1980) 420.
[165] W.E. Spicer, T. Kendelewicz, N. Newman, R. Cao, C. McCants, K. Miyana, I. Lindau, Z. Lilienthal-Weber and E.R. Weber, Appl. Surf. Sci. 33/34 (1988) 1009.
[166] R. Cao, K. Miyano, T. Kendelewicz, I. Lindau and W.E. Spicer, J. Vac. Sci. Technol. A 6 (1988) 1571.
[167] R.M. Feenstra and P. Mårtensson, in: Proc. 19th Int. Conf. on the Physics of Semiconductors, Ed. W. Zawadzki (Polish Institute of Physics, Warsaw, 1988).
[168] W. Mönch, J. Vac. Sci. Technol. B 6 (1988) 1270.
[169] W. Mönch, Semiconductor Surfaces and Interfaces (Springer, Berlin, 1993).
[170] M. Menon and R.E. Allen, Superlatt. Microstruct. 8 (1990) 387.
[171] F. Manghi and C. Calandra, Vacuum 41 (1990) 693.
[172] R. Magri, F. Maghi and C. Calandra, in: Proc. 22th Int. Conf. on the Physics of Semiconductors, Ed. D.J. Lockwood (World Scientific, Singapore, 1995) pp. 572–575.
[173] O. Pankratov and M. Scheffler, Phys. Rev. Lett. 70 (1993) 351.
[174] R.H. Williams, A. McKinley, G.J. Hughes, T.P. Humphreys and C. Maani, J. Vac. Sci. Technol. B 2 (1984) 561.
[175] C. Mailhiot, C.B. Duke and D.J. Chadi, Phys. Rev. Lett. 53 (1984) 2114.
[176] C. Mailhiot, C.B. Duke and D.J. Chadi, J. Vac. Sci. Technol. A 3 (1985) 915.
[177] J.P. LaFemina, C.B. Duke and C. Mailhiot, in: Atomic Scale Calculations of Structures in Materials, Eds. M.A. Daw and M.S. Schlüter (Materials Research Society, Pittsburgh, PA, 1990) pp. 41–46.
[178] W.K. Ford, T. Guo, D.L. Lessor and C.B. Duke, Phys. Rev. B 42 (1990) 8952.
[179] K.E. Miyano, J.C. Woicik, T. Kendelewicz, W.E. Spicer, M. Richter and P. Pianetta, Phys. Rev. B 47 (1993) 6444.
[180] G.P. Srivastava, Phys. Rev. B 46 (1992) 7300.
[181] G.P. Srivastava, Phys. Rev. B 47 (1993) 16616.
[182] G.P. Srivastava, Surf. Sci. 307–309 (1994) 328.
[183] P. Mårtensson, G.V. Hansson, M. Lähdeniemi, K.O. Magnusson, S. Wiklund and J.M. Nicholls, Phys. Rev. B 33 (1986) 7399.
[184] I.T. McGovern, R. Whittle, D.R.T. Zahn, C. Müller, C. Nowak, A. Cafolla and W. Braun, J. Phys.: Condens. Matter 3 (1991) SA367; I.T. McGovern et al., private communication.
[185] M.G. Betti, M. Pedio, U. del Pennino and C. Mariani, Phys. Rev. B 43 (1991) 14317.
[186] C. Goletti, P. Chiaradia, W. Jian and G. Chiarotti, Solid State Commun. 84 (1992) 421.
[187] W.G. Schmidt, B. Wenzien and F. Bechstedt, Czech. J. Phys. 43 (1993) 1003.
[188] W.G. Schmidt, and G.P. Srivastava, Solid State Commun. 89 (1994) 345.
[189] G.P. Srivastava, J. Phys.: Condens. Matter 5 (1993) 4695.
[190] W.G. Schmidt and G.P. Srivastava, Surf. Sci. 331–333 (1995) 540.

[191] C.B. Duke, D.L. Lessor, T. Guo and W.K. Ford, J. Vac. Sci. Technol. A 8 (1990) 3412.
[192] A. Umerski and G.P. Srivastava, Surf. Sci. 307–309 (1994) 680.
[193] A. Umerski and G.P. Srivastava, Surf. Sci. 307–309 (1994) 963.
[194] D.N. McIlroy, D. Heskett, D.M. Swanston, A.B. McLean, R. Ludeke, H. Munekata and N.J. DiNardo, J. Vac. Sci. Technol. B 11 (1993) 1786.
[195] T. van Gemmeren and R.L. Johnson, Hasylab Annu. Rep. (1994) 227; L. Gaviola, M.G. Betti, C. Mariani, M. Sauvage-Simkin, L. Lottermoser, T. van Gemmeren, R.L. Johnson, R. Feidenhans'l, M. Nielsen, D. Smilgies and E. Landemark, Hasylab Annu. Rep. (1994) 321; L. Lottermoser, T. van Gemmeren and R.L. Johnson, Hasylab Annu. Rep. (1994) 333.
[196] S. Schömann, K. Schmidt, H. Peisert and T. Chassé, Surf. Sci. 352–354 (1996) 855.
[197] G. Burns, Solid State Physics (Academic Press, New York, 1990).
[198] A. Garcia and M.L. Cohen, Phys. Rev. B 47 (1993) 4215.
[199] Table of Periodic Properties of the Elements (Sargent-Welch, Skokie, IL, 1980).
[200] X. Gonze, J.-P. Michenaud and J.-P. Vigneron, Phys. Rev. B 41 (1990) 11827.
[201] N. Esser, M. Köpp, P. Haier, A. Kelnberger and W. Richter, J. Vac. Sci. Technol. B 11 (1993) 1481.
[202] M. Hünermann, PhD Thesis, Aachen University of Technology, Germany (1990).
[203] M. Cardona, in: Light Scattering in Solids II, Eds. M. Cardona and G. Güntherodt, Topics in Applied Physics, Vol. 50 (Springer, Berlin, 1982).
[204] T.J. Godin, J.P. LaFemina and C.B. Duke, J. Vac. Sci. Technol. B 9 (1991) 2282.
[205] G.K. Schenter and J.P. LaFemina, J. Vac. Sci. Technol. A 10 (1991) 2429.
[206] W.G. Schmidt, F. Bechstedt and G.P. Srivastava, Phys. Rev. B 52 (1995) 2001; and references cited therein.
[207] U. Harten and J.P. Toennies, Europhys. Lett. 4 (1987) 833.
[208] U. del Pennino, M.G. Betti, C. Mariani and I. Abbati, Surf. Sci. 211/212 (1989) 557.
[209] H. Nienhaus and W. Mönch, Phys. Rev. B 50 (1994) 11750; Surf. Sci. 328 (1995) L561.
[210] C. Mariani, G. Annovi and U. del Pennino, J. Electron Spectrosc. Rel. Phen. 54/55 (1990) 1105.
[211] C. Mariani, G. Annovi and U. del Pennino, Surf. Sci. 251/252 (1991) 218.
[212] P.V. Santos, N. Esser, M. Cardona, W.G. Schmidt and F. Bechstedt, Phys. Rev. B 52 (1995) 12158.
[213] R.M. Feenstra, Appl. Surf. Sci. 56–58 (1992) 104.
[214] A. Tulke, M. Mattern-Klosson and H. Lüth, Solid State Commun. 59 (1986) 303.
[215] M. Yamada, A.K. Wahi, T. Kendelewicz and W.E. Spicer, Appl. Surf. Sci. 56–58 (1992) 325.
[216] M. Yamada, A.K. Wahi, T. Kendelewicz and W.E. Spicer, Phys. Rev. B 45 (1992) 3600.
[217] R. Whittle, E. Dudzik, I.T. McGovern, A. Hempelmann, C. Nowak, D.R.T. Zahn, A. Cafolla and W. Braun, J. Electron Spectrosc. Rel. Phen. 68 (1994) 399.
[218] A.B. McLean, D.M. Swanston, D.N. McIlroy, D. Heskett, R. Ludeke and H. Munekata, Phys. Rev. B 51 (1995) 14271.
[219] C.M. Bertoni, C. Calandra, F. Manghi and E. Molinari, Phys. Rev. B 27 (1983) 1251.
[220] F. Manghi, C. Calandra and E. Molinari, Surf. Sci. 184 (1987) 449.
[221] G.P. Srivastava and R.P. Martin, J. Phys.: Condens. Matter 4 (1992) 2009.
[222] A. Bödicker, W. Schattke, J. Henk and R. Feder, J. Phys.: Condens. Matter 6 (1994) 1927.
[223] R. Whittle, I.T. McGovern, A. Hughes, T.-H. Shen and C.C. Matthai, J. Phys.: Condens. Matter 5 (1993) 6555.
[224] R. Compañó, U. del Pennino and C. Mariani, Phys. Rev. Lett. 68 (1992) 986.
[225] G.Y. Guo, in: Proc. 21st Int. Conf. on the Physics of Semiconductors, Eds. P. Jiang and H.-Z. Zheng (World Scientific, Singapore, 1992) pp. 522–525.
[226] J.R. Myron, J. Anderson and G.J. Lapeyre, in: Proc. 17th Int. Conf. on the Physics of Semiconductors, Eds. J.D. Chadi and W.A. Harrison (Springer, New York, 1985) p. 133.
[227] J.R. Chelikowski and M.L. Cohen, Phys. Rev. B 20 (1979) 4150.
[228] P. Chiaradia, A.I. Shkrebtii, C. Goletti, W. Jiang and R. Del Sole, Solid State Commun. 85 (1993) 479; Solid State Commun. 89 (1994) 87.
[229] R.J. Voorhoeve, in: Treatise on Solid State Chemistry, Vol. 6A, Ed. N.B. Hannay (Plenum, New York, 1976) p. 293.
[230] J.C. Patrin, Y.Z. Li, M. Chander and J.H. Weaver, Phys. Rev. B 45 (1992) 3918.
[231] J.C. Patrin, Y.Z. Li, M. Chander and J.H. Weaver, Phys. Rev. B 46 (1992) 10221.
[232] N. Esser, U. Resch, U. Rettweiler, W. Richter, D.R.T. Zahn and R.H. Williams, Vacuum 38 (1988) 229.

[233] R.N. Zitter, in: The Physics of Semimetals and Narrow Gap Semiconductors, Eds. D.L. Carter and R.T. Bate (Pergamon, New York, 1971).
[234] J.S. Lannin, Phys. Rev. B 15 (1977) 3863.
[235] H. Lüth, Surfaces and Interfaces of Solids (Springer, Berlin, 1993).
[236] W. Ranke, Phys. Rev. B 27 (1983) 7807.
[237] F. Bechstedt and R. Enderlein, Semiconductor Surfaces and Interfaces (Akademie Verlag, Berlin, 1988).
[238] N. Esser, M. Hünermann, U. Resch, D. Spaltmann, J. Geurts, D.R.T. Zahn, W. Richter and R.H. Williams, Appl. Surf. Sci. 41/42 (1989) 169.
[239] R.H. Williams, V. Montgomery and R.R. Varma, J. Phys. C 11 (1978) L735.
[240] D.R.T. Zahn, A.B. McLean, R.H. Williams, N. Esser and W. Richter, Appl. Phys. Lett. 52 (1988) 739.
[241] D.R.T. Zahn, N. Esser, W. Richter, C. Stephens and R.H. Williams, J. Phys.: Condens. Matter 1 (1989) SB45.
[242] C. Tejedor, F. Flores and E. Louis, J. Phys. C 10 (1977) 2163.
[243] F. Flores and C. Tejedor, J. Phys. C 20 (1987) 145.
[244] V. Heine, Phys. Rev. 136 (1965) A1689.
[245] J. Bardeen, Phys. Rev. 71 (1947) 717.
[246] C.F. Fischer, At. Data 4 (1972) 301.
[247] T. Kendelewicz, R. Cao, K. Miyano, I. Lindau and W.E. Spicer, J. Vac. Sci. Technol. A 7 (1989) 765.
[248] T. Kendelewicz, K. Miyano, R. Cao, J.C. Woicik, I. Lindau and W.E. Spicer, Surf. Sci. 220 (1989) L726.
[249] C. Stephens, PhD Thesis, University of Dublin (1990).
[250] M.G. Betti, A. Campo, M. Capozi, M. Pedio, P. Perfetti and C. Quaresima, Vuoto XX (1990) 75.
[251] Y.F. Komik, B.I. Belevtsev and L.A. Yatsuk, Sov. Phys. JETP 36 (1973) 1177.